UNIVERSITY OF LONDON

IMPERIAL COLLEGE OF SCIENCE AND TECHNOLOGY

Department of Electrical Engineering

THE STEADY STATE STABILITY OF SYNCHRONOUS MACHINES AS AFFECTED BY DIRECT AND QUADRATURE AXIS EXCITATION REGULATORS

Thesis submitted for the degree of
Doctor of Philosophy in Engineering

by

Satish Chandra Kapoor, M. Tech.

December 1967

Page

INDEX 2

Abstract 8

Acknowledgements 10

List of Symbols 11

CHAPTER 1 INTRODUCTION 14

1.1 General 14

1.2 Investigation of Direct-axis Regulation 16

1.3 Investigation of Quadrature-axis Regulation 17

1.4 General Theoretical Methods 22

CHAPTER 2 THEORY OF THE DIRECT-AXIS REGULATOR WITH VOLTAGE AND FIELD CURRENT FEEDBACKS 27

2.1 General 27

2.2 The System Equations 29

2.2.1 The Machine Equations 29

2.2.2 Expressions for the Feedback Quantities 31

2.2.3 The Closed-loop Transfer Function and the Characteristic Equation 35

2.2.4 The Gain Constants 40

2.3 Application of the Analysis to determine Stability 40

2.3.1 The System and the Method of Analysis 40

2.3.2 The unregulated System 43

2.3.3 The System with Voltage Feedback 46

2.3.4 The System with Voltage and Field Current Feedbacks 57

2.3.5 Stability Limit Curves 67

Page

2.4 Convergence of the Direct-axis Regulated Power-var Characteristic Curve at Zero Power 69

CHAPTER 3 THEORY OF QUADRATURE-AXIS REGULATION 73

3.1 General 73

3.2 The System Equations 73

3.2.1 The Machine Equations 73

3.2.2 Feedback Quantities 77

3.2.3 The Open-loop Transfer Function and the Characteristic Equation 79

3.3 Quadrature-axis Regulation with Various Signals 79

3.3.1 The Unregulated System 80

3.3.2 Terminal Voltage Feedback at Zero Power 81

3.3.3 Resolved Component Feedback at Zero Power 82

3.3.3.1 Feedback of I_d 83

3.3.3.2 Feedback of I_q 83

3.3.3.3 Rotor Angle Feedback 84

3.4 Equilibrium Diagram with the Angle Regulator for the Quadrature Winding 85

3.5 Theoretical Determination of Stability for the Quadrature Angle Regulator 88

3.5.1 The Proportionate Regulator 89

3.5.1.1 With Ideal Angle Device 90

3.5.1.1.1 Application of the Nyquist Criterion for a Qualitative Assessment 90

3.5.1.1.2 Application of the Nyquist Criterion for Quantitative Assessment 93

Page

3.5.1.2 With a Practical Angle Device 99

3.5.2 Regulator with Derivative Feedback 102

3.5.2.1 Proportionate Regulator with First Derivative 102

3.5.2.2 Proportionate Regulator with First and Second Derivative -'Derivative Regulator' 107

3.5.3 Effect of Alternator Damping 114

3.5.4 Effect of Resistance 115

CHAPTER 4 EXPERIMENTAL EQUIPMENT 117

4.1 The Micro-machine and its Parameters 120

4.1.1 The Quadrature-axis Regulation Machine Parameters 120

4.1.1.1 Determination of X_d and X_q 121

4.1.1.2 Variable Frequency Response Static Impedance Test 122

4.2 Time Constant Regulator - T.C.R. 127

4.2.1 Conventional Time Constant Regulator 128

4.2.2 Modified Time Constant Regulator 131

4.2.3 Difficulties with the Modified T.C.R. 135

4.3 Feedback Circuits 138

4.3.1 Direct-axis Feedback Circuits 138

4.3.1.1 The Voltage Feedback Circuit 138

4.3.1.2 The Field Current Feedback Circuit 139

4.3.2 Quadrature-axis Feedback Circuit 143

4.3.2.1 A Conventional Phase Detection Circuit 143

Page

4.3.2.2 The Angle Device 146

4.3.2.3 The Angle Device Operation 148

4.3.2.4 The Filter Unit 152

4.4 The Regulator and Associated Circuitry 154

4.4.1 Direct-axis Regulator 154

4.4.2 Quadrature-axis Regulator 156

CHAPTER 5 DIRECT-AXIS STEADY STATE STABILITY EXPERIMENTAL RESULTS AND COMPARISON 159

5.1 The Stability 159

5.1.1 The Stability Code 159

5.1.2 Precautions Against Erratic Judgment 160

5.2 The Regulator Constants 161

5.2.1 The Regulator Gain R 161

5.2.2 The Current Feedback Gain M 162

5.3 The Steady State Stability Curves with the Direct-axis Regulator 162

5.3.1 With the Voltage Feedback Regulator 162

5.3.2 With the Regulator having both Voltage and Field Current Feedbacks 165

5.4 A Comparison of the Theoretical and the Experimental Curves 165

CHAPTER 6 QUADRATURE-AXIS REGULATION AND ASSOCIATED EXPERIMENTS, RESULTS AND COMPARISON 168

6.1 Voltage Feedback into the Quadrature-axis Excitation 169

Page

6.2 The Angle Device Output Characteristic and Zero Setting 172

6.3 Angle Device Frequency Response Test 175

6.4 The Regulator Gain 177

6.5 Starting of the System 179

6.6 Zero Angle Equilibrium 180

6.7 Steady State Stability Limit Curves for Proportionate Regulator 181

6.7.1 A Comparison of the Theoretical and Experimental Curves 187

6.8 The Steady State Limit Curve for the Derivative Regulator 190

6.8.1 A Comparison of the Theoretical and Experimental Curves 193

6.9 A Comparison between the Proportionate and the Derivative Regulator 194

6.10 Frequency Response of the Quadrature-axis Regulator 195

6.10.1 The Proportionate Regulator 195

6.10.2 The Derivative Regulator 196

6.11 Open-loop Frequency Response Test of the System 196

CHAPTER 7 EXTENSION OF THE LAPLACE APPROACH AND STATE VARIABLE METHODS 206

7.1 Extension of the Laplace Approach to Multivariable System 208

7.2 State Variable Methods 211

7.2.1 Eigen Value Approach 213

7.2.1.1 Eigen Values 213

Page

7.2.1.2 Eigen Values for the Voltage Regulator of Sect. 2.3.3 214

7.2.2 Lyapunov Technique 217

7.2.2.1 Lyapunov Stability Criterion 217

7.2.2.2 Lyapunov Function 218

CHAPTER 8 CONCLUSIONS 221

Appendix I 229

Appendix II 230

Appendix III 233

Appendix IV 236

Appendix V 240

Table I 256

Table II 257

References 259

ABSTRACT

With recent developments in power systems the demand on alternators to operate in the leading var region at light loads is increasing. With these developments in view, the effect of automatic direct and quadrature axis excitation regulators on the stability of an alternator connected to an infinite bus through a series reactance is investigated. The study is limited to small oscillations, and the stability analysis is done using conventional techniques, such as, the root-locus, the Nyquist, the Routh, and some consideration is also given to state variable methods.

A proportionate voltage regulator in conjunction with the field current feedback for the direct-axis excitation regulation is investigated. The limitations and the usefulness of the scheme are discussed.

It is mathematically shown that at zero power no direct-axis excitation regulation scheme can extend the steady state reactive absorption beyond a limit depending on the quadrature-axis synchronous reactance. On the other hand the quadrature-axis excitation regulation can extend the steady state reactive absorption limit.

Out of the various signals theoretically considered for the quadrature-axis excitation regulation the rotor angle signal proves to be the most effective.

A proportionate angle regulator on the quadrature-axis acts like a position control servo-system and ideally can extend the steady state reactive absorption limit depending on the transient reactance at all power levels, but the gain range of such a regulator is poor. A proportionate regulator with first and second derivative terms can however increase the reactive absorption limit and the gain range many times compared with a proportionate regulator.

Experiments were performed on a model machine in conjunction with simulated regulators to determine the steady state stability limit curves as a function of regulator gain. For some regulators the open-loop frequency response loci were determined from the closed-loop frequency response test for small oscillations.

All the experimental and theoretical results show reasonable agreement.

ACKNOWLEGEMENTS

The work presented in this thesis was carried out under the supervision of Dr. B. Adkins, M.A., D.Sc. (Eng), F.I.E.E., of the Electrical Engineering Department, Imperial College of Science and Technology. I wish to thank Dr. Adkins for his helpful guidance and constant encouragement.

I also wish to thank Dr. P.F. Blackman, Senior Lecturer in Electrical Engineering, Imperial College, and the research team in the Central Electricity Generating Board, South Eastern Region, for helpful discussions.

Finally I wish to express my gratitude to the British Council for a grant under the 'Colombo Plan' and to the Indian Institute of Technology, Delhi for sponsoring my candidature.

LIST OF SYMBOLS

The axis quantities are represented by small letters, whereas their corresponding R.M.S. values are represented by capital letters. The symbols represent the per unit values in accordance with reference 16, and a reasonable uniformity is also maintained with reference 1.

$v_d(V_d)$, $v_q(V_q)$	:	Direct and quadrature axis voltages
$i_d(I_d)$, $i_q(I_q)$	:	Direct and quadrature axis currents
v_{fd}, v_{fq}	:	Direct and quadrature axis field voltages
$v_t(V_t)$	:	Machine terminal voltage
V	:	Infinite bus voltage
V_o	:	Induced voltage in the machine
r_a	:	Armature resistance including that of the line reactance
r_{fd}, r_{fq}	:	Direct and quadrature axis field resistances
X_a	:	Machine leakage reactance
X_c	:	Transmission line reactance
X_{md}, X_{mq}	:	Direct and quadrature axis magnetising reactances
$X_d(p)$, $Y_d(p)$	:	Direct-axis operational reactance (admittance)
$X_q(p)$, $Y_q(p)$	:	Quadrature-axis operational reactance (admittance)

$X_d(Y_d)$, $X'_d(Y'_d)$, $X''_d(Y''_d)$	:	Direct-axis synchronous, transient and subtransient reactances (admittances)
$X_q(Y_q)$, $X'_q(Y'_q)$, $X''_q(Y''_q)$	:	Quadrature-axis synchronous, transient and subtransient reactances (admittances)
$T'_d(T'_q)$, $T''_d(T''_q)$	:	Direct (quadrature) axis short circuit transient and subtransient time constants
$T'_{do}(T'_{qo})$, $T''_{do}(T''_{qo})$	:	Direct (quadrature) axis open circuit transient and subtransient time constants
T_2, T_5	:	Time constants as in Ref. 16
S_o	:	Slope of Power-angle curve
S'_o	:	Slope of transient Power-angle curve
δ	:	Rotor angle with respect to infinite bus
δ_s	:	Peak of the Power-angle curve
δ'_s	:	Peak of the transient Power-angle curve
P	:	Power at the infinite bus
J	:	Moment of inertia
T_m, T_e, T_i	:	Turbine, electrical and inertia torques
$f(\omega)$	:	Frequency cycles per sec. (radians/sec.)
$R(p)$, $R_q(p)$	:	Direct and quadrature axis regulator transfer functions
$L(p)$, $L_q(p)$	:	Direct and quadrature axis open-loop transfer functions

$C(p)$	:	Closed-loop transfer function
R, R_q	:	Direct and quadrature axis regulator gains
M	:	Field current gain
R_e	:	Rectifier conversion constant
$R(min)$, $R(max)$	:	Minimum and maximum direct-axis regulator gains
$R_q(min)$, $R_q(max)$	:	Minimum and maximum quadrature-axis regulator gains
R.H.	:	Right half
L.H.	:	Left half
ω_n	:	Natural frequency of the closed-loop system
	:	Prefix to denote differential
o	:	Subscript to denote steady state value
$z_i(p_i)$	:	A zero (pole) in the complex plane of the open-loop transfer function
$Z(P)$	:	Number of zeros (poles) in the right half complex plane.

1 INTRODUCTION

1.1 General

With increasing grid voltages and growth of cable network feeding large load centres the synchronous generators supplying a power system are required to operate at lightly loaded conditions with large reactive obsorption. It is well known[1-10] that increased reactive absorption is possible when continuously acting regulators are used in the direct-axis excitation circuit. The common type of feedback signal is one depending on the terminal voltage[1-9]. Other important signals are the load angle[8,10] and the current[8]. It is proved mathematically in the present thesis that the reactive absorption at zero power cannot be increased by any type of regulator acting on the direct-axis field winding. It can however be increased by using a regulator acting on the quadrature-axis field winding. Fig. 1.1 gives typical curves on a diagram of active power P (Watts) against reactive power Q (Vars).

This thesis is concerned with two main lines of work.

1. An extension of the study of methods of direct-axis regulation.

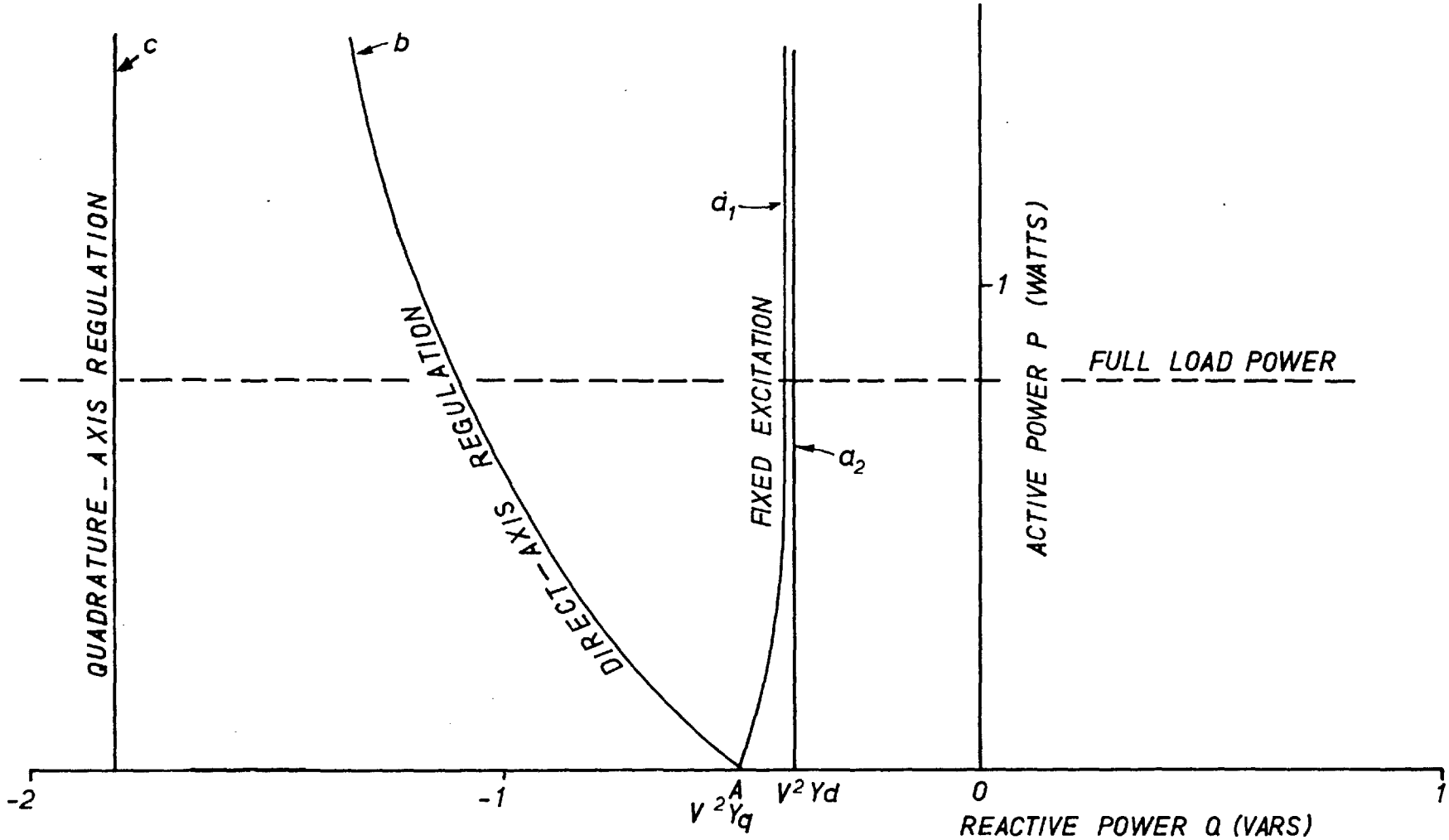

FIG. 1.1. POWER–VAR CHART SHOWING STABILITY LIMIT CURVES

2. An investigation of some methods of quadrature-axis regulation.

In each case experiments were carried out on the micro-machine equipment, and methods of theoretical analysis were developed to obtain theoretical curves for comparison with the experimental results .

1.2 Investigation of Direct-axis Regulation

The steady state operation range of an alternator supplying a power system can be extended by using a voltage regulator,[1-9] in which a signal depending on the terminal voltage is fed through a suitable regulator to the field winding. An earlier investigation[1] showed how the range of steady state stability depends on the type of regulator which may have proportionate or more complicated feedbacks. The characteristics of the regulator are expressed by its transfer function.

It has been proposed[2] that it would be advantageous to use, in conjunction with a direct voltage feedback, an auxiliary signal derived from the field current. Some analogue computer studies[3], using derivative of the field current as an auxiliary signal showed a marked effect on the steady state stability of the system. This scheme is investigated in some details in the following pages.

One point of interest which emerges from the analysis of direct-axis regulation is that the automatic voltage regulator (a.v.r.) behaves as if it decreases the direct-axis reactance X_d to transient reactance level X_d', but it does not affect X_q. This explains why the steady state stability curve for the direct-axis regulation converges at $-V^2Y_q$ at zero power (Fig. 1.1 point 'A') irrespective of the nature of the feedback. The above explanation is rather simple, but a rigorous proof for the convergence of the regulated steady state stability curve at 'A', is developed in Sect. 2.4.

In Fig. 1.2 is shown the schematic diagram of the system in which a direct-axis regulator is used. The alternator is connected through a reactance to a fixed supply, and has a main regulating feedback in which the regulator output depends on the terminal voltage V_t. An auxiliary signal proportional to the derivative of the field current I_f is added to the main signal and the total actuates a regulator system with transfer function $R(p)$. The output of the regulator affects the excitation in the direct-axis.

1.3 Investigation of Quadrature-axis Regulator

To improve transient stability it has been proposed[11]

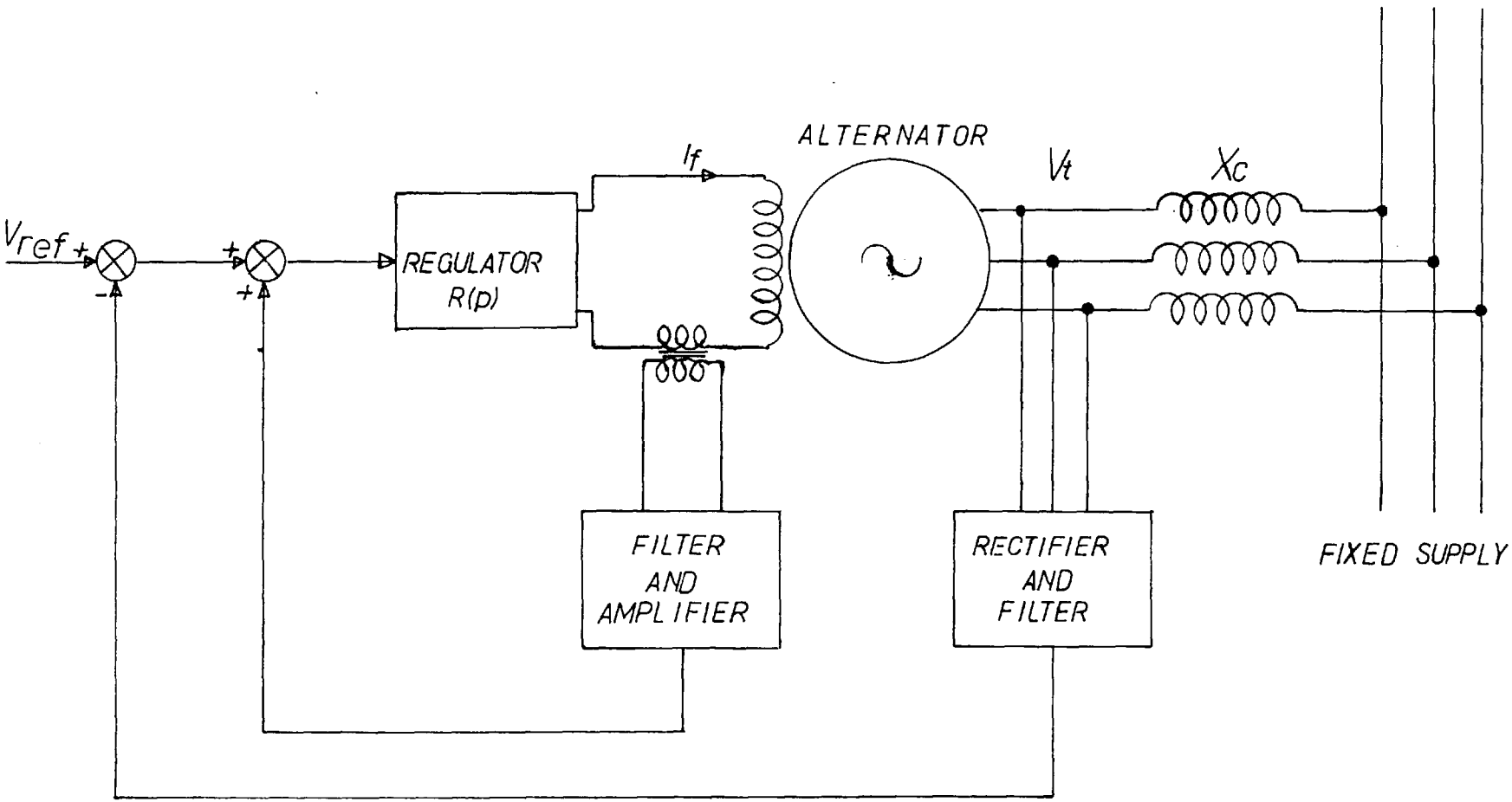

FIG. 1.2_ THE SCHEMATIC DIAGRAM FOR DIRECT_AXIS REGULATOR

to excite a field winding in quadrature to the direct-axis field winding. The original idea was to build up quadrature excitation during any transient disturbance and let the rotor advance, but to keep the magnetic-axis within limits in order to pull in when the fault was cleared. In a digital study[12] of an integrated control of a turbo-alternator for transient disturbances, a signal related to the swing of the rotor during the disturbance fed into the quadrature-axis field winding has been shown to be useful in extending the transient stability, thus in general supporting Ref. 11. In a C.E.G.B. report[13] a divided winding scheme is suggested in which the axes of the two parts of the winding are separated by 60° instead of by 90°. In physical terms the divided winding arrangement makes the quadrature component of m.m.f. available without having to arrange the field winding on the pole faces which would be impracticable on a large turbo-alternator. The leading winding supplies the excitation which determines the torque and is actuated by a rotor angle feedback. Reference 13 gives m.m.f. diagrams for increased reactive absorption at steady state operation, but no limits are defined and there is no analysis explaining why the improved stability is obtained. Model tests demonstrated

the practicability of the scheme.

A range of signals for controlling the quadrature-axis are considered, namely, the voltage, the direct and quadrature current and the rotor angle. Out of these only the rotor angle effectively increases the steady state reactive absorption limit at zero power as well as under loaded conditions (see Fig. 1.1 curve 'C'). The steady state stability limit of reactive absorption depends upon the regulator gain and its transfer function.

In Fig. 1.3 is shown the schematic diagram of the quadrature-axis angle regulator. The arrangement of the alternator and the fixed supply is the same as in the direct-axis regulation scheme, shown in Fig. 1.2. In a practical installation the direct axis field would have its own regulator, but for the purposes of the present investigation it is adjustable but unregulated. The quadrature-axis excitation is actuated through a regulator system with transfer function $R_q(p)$, fed from a device giving an output proportional to the angle between the fixed supply treated as reference, and the rotor direct-axis position. For a system with no steady state error between the reference and the rotor position the quadrature-axis excitation is proportional to the power delivered.

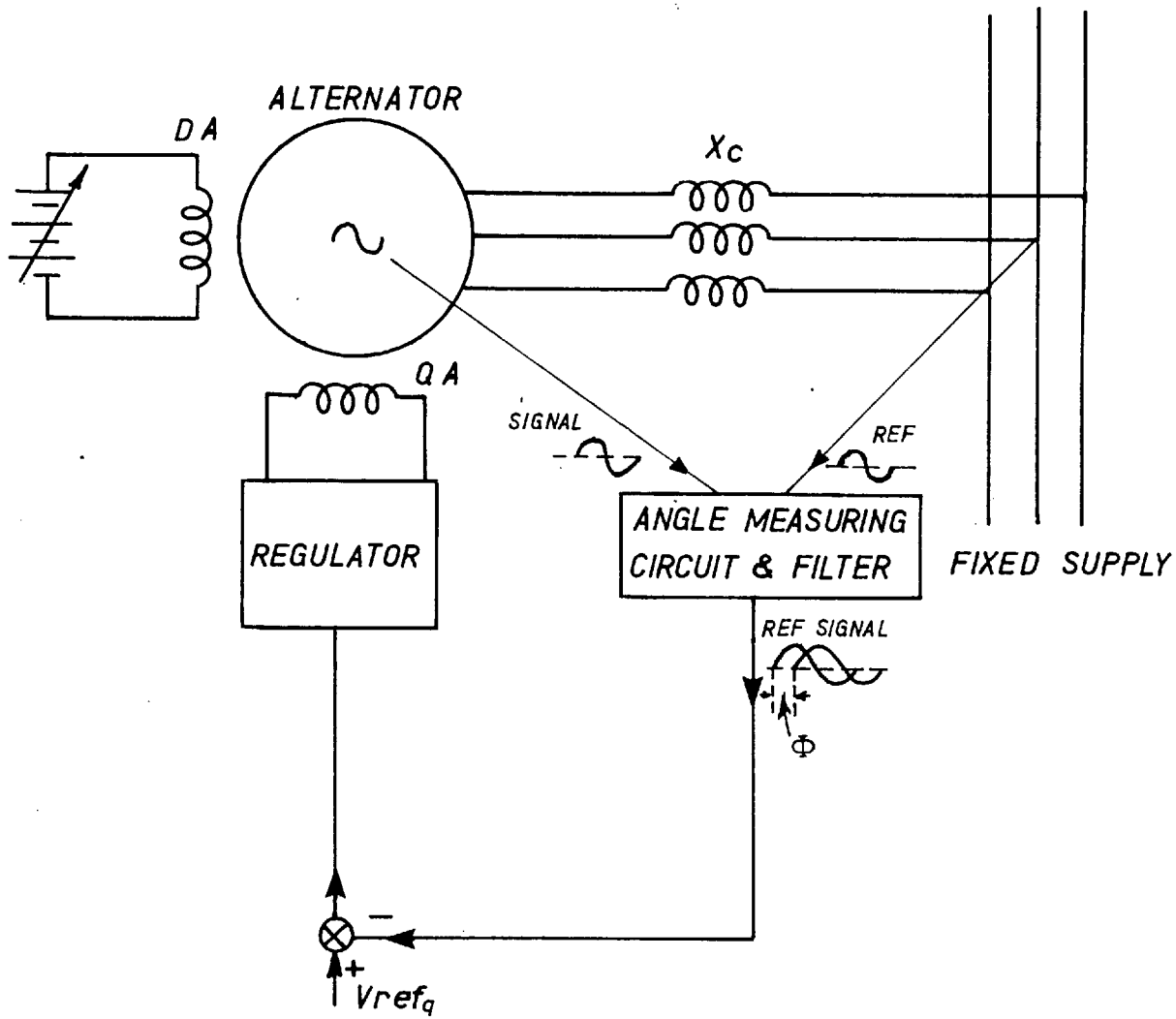

FIG. 1.3. THE SCHEMATIC DIAGRAM OF THE QUADRATURE−AXIS ANGLE REGULATOR.

1.4 General Theoretical Methods

The problem of steady state stability analysis of any control system is essentially the problem of small perturbation equations about the point of equilibrium. This technique is extensively used in the analysis of regulator system. Whether it is the direct-axis or the quadrature-axis regulation or both, the basic problem is to develop small perturbation equations either as differential equations relating the system variables[12,14] or in the form of Laplace transforms.[1,3-10] For the state variable methods using differential equations, matrix algebra can readily be applied with the aid of digital computers. This technique can usefully be applied to large systems like a multi-machine problem[14] or an integrated system of turbine, alternator and the rest of the system[12]. The Laplace transform method on the other hand yields transfer functions between input and output quantities and allows for greater detail to be included for a smaller system, which can be analysed using the established literature of conventional control theory. The Laplace approach can be reasonably extended to a multi input-output system though it becomes cumbersome for a large system. This thesis uses the Laplace approach, although, the state variable approach is

discussed.

With the system equations in the form of transfer functions the steady state stability limits can be determined by the application of conventional stability criteria, e.g., the Routh-criteria, the Root-locus technique, the Nyquist criterion. In the literature on voltage regulators the Nyquist or Routh criteria or both are used extensively.[1,3-9] The Root-locus technique[9,15] is cumbersome for detailed studies but under simplifying assumptions can give insight into the system and yield useful results. For the direct-axis regulation stability problem, the Root-locus technique was used neglecting damping, resistance and filter delays, thus keeping the order of roots low, but nevertheless obtaining reasonable results. Some results were also obtained by applying the Routh criteria. However, for the quadrature-axis regulation it was preferred to apply the Nyquist criterion making use of the frequency response plots, thus including without difficulty the filtering and the regulator transfer function details.

Alternatively, if the system equations were expressed in terms of state variables the Lyapunov function or Eigen value approach could be used. It is of interest to note that for linear systems the Lyapunov

function gives the same condition of stability as the Routh criteria and the eigen values are the poles of the system's closed-loop transfer function. The later point is demonstrated by taking the example of a proportionate voltage regulator. The Lyapunov function and Eigen value approach are briefly discussed.

Some important new formulations and conclusions, most of which have been confirmed experimentally, are summarized as follows.

a) The system equations are arranged so that a mathematical model of the system could be set-up. Any type of feedback from within or outside the alternator is formulated from the alternator output quantities.

b) The theoretical formulation of the field current feedback is obtained in a general form. The limitations of this method are demonstrated.

c) It is proved that irrespective of the nature of the feedback and the regulator transfer function the steady state reactive absorption limit at zero power remains unchanged for direct-axis excitation regulation.

d) It is shown that the voltage feedback with any regulator transfer function as a feedback into

the quadrature-axis excitation has no useful effect in altering the steady state reactive absorption limit at zero power.

e) It is shown that a signal derived from the direct-axis current cannot make any useful contribution in improving the reactive absorption limit at zero power.

f) A signal derived from the quadrature-axis current is not of the right polarity for stabilisation in the negative var region and moreover changes sign from positive to negative vars. By itself it is not a desirable signal but can be used in combination with other signals.

g) The rotor angle is a positive signal which does not change sign from positive to negative vars and, depending on the regulator transfer function, can be used to modify the steady state reactive absorption limits.

h) It is shown that by proportional angle feedback into the quadrature-axis winding the steady state limit of reactive absorption can be increased from $-V^2Y_q$ to a maximum of $-V^2Y_q'$ at all power levels.

i) It is shown that the steady state reactive absorption limit can be increased beyond $-V^2Y_q$ by

including a suitable proportion of first and second derivative terms in the proportional regulator. The optimum increase in reactive absorption and the permissible regulator gain depend on the regulator transfer function.

CHAPTER 2

2. Theory of the Direct-axis Regulator with Voltage and Field Current Feedbacks

2.1 General

The System for the direct-axis excitation control is shown in Fig. 1.2. It can be presented by the block diagram for small oscillations in Fig. 2.1, where the prefix Δ indicates that small variations are being considered. Feedbacks are derived from v_t , the terminal voltage and i_f , the field current. For convenience v_t is taken as the value after the rectifier conversion. All quantities are expressed in per unit. The linearized system equations around the point of equilibrium give the operational relations, i.e., the transfer function between the input and output quantities. Using such relations the multifeedbacks are reduced to an equivalent single loop configuration and the system is analysed with the aid of conventional control systems theory.

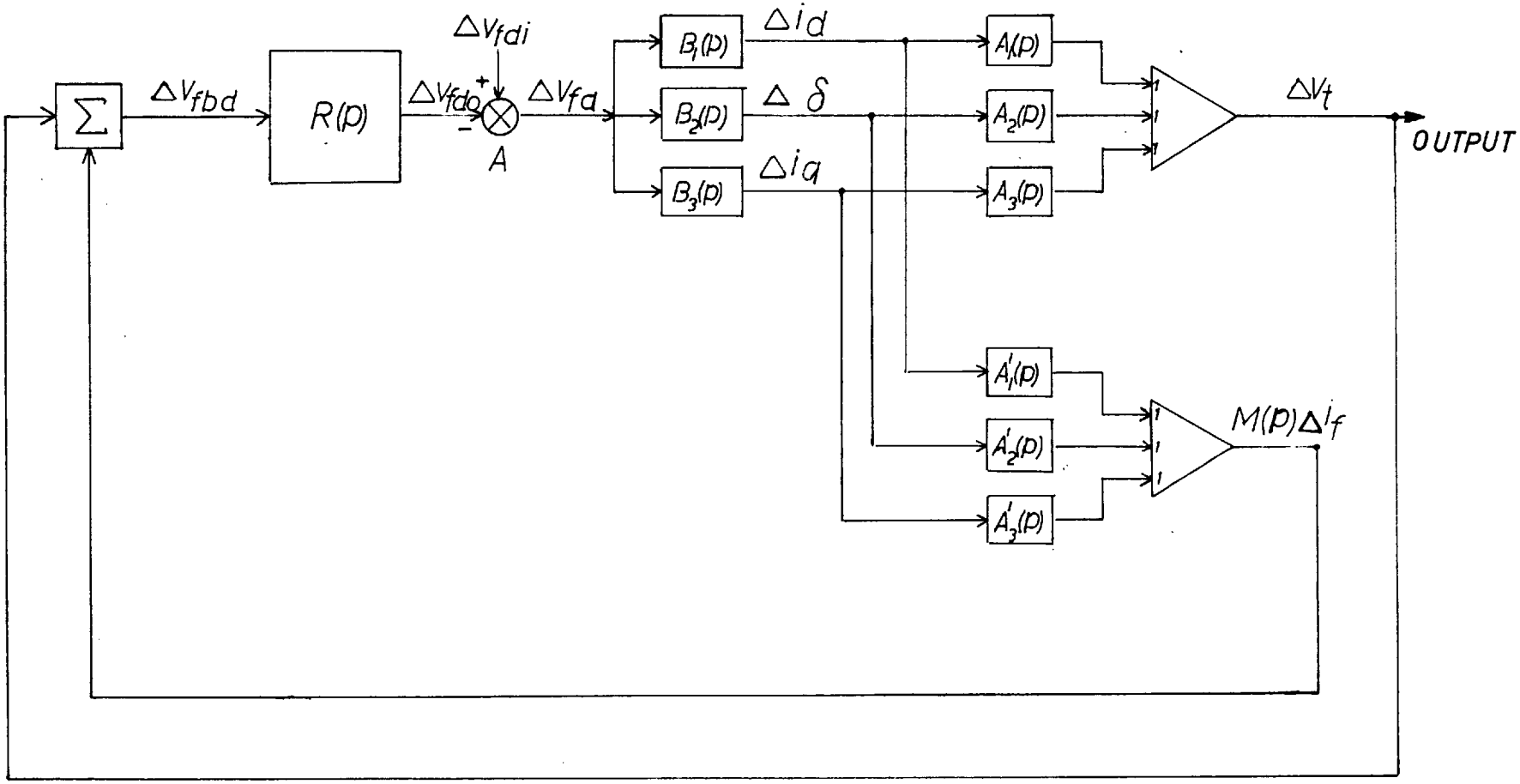

FIG.2.1_ BLOCK DIAGRAM FOR DIRECT_AXIS EXCITATION CONTROL

2.2 System Equations

2.2.1 The Machine Equations

The machine equations are those derived in Ref. 1 and allow for armature resistance and damping. The principal assumptions are: no saturation, sinusoidal air-gap fluxes and no slot effects. Also, since the frequency of oscillations in the system is quite low, the frequency dependent terms $p\psi_d, p\psi_q$ and $p\delta$ in the machine voltage equations are justifiably neglected. The parameters are those of an equivalent machine in which the external reactance is combined with the generator. There is no quadrature field winding and it is assumed that the prime mover torque T_m does not vary with the angle δ. A summary of equations[1,16] is given in Appendix I from which the following small oscillation equations are deduced.

$$\begin{bmatrix} G(p)\ \Delta v_{fd} \\ 0 \\ 0 \end{bmatrix} = \begin{bmatrix} -X_d(p) & v_{do} & r_a \\ -\frac{1}{2}v_{do}+r_a i_{do} & -(Q_o+Jp^2) & -\frac{1}{2}v_{qo}+r_a i_{qo} \\ -r_a & v_{qo} & -X_q(p) \end{bmatrix} \times \begin{bmatrix} \Delta i_d \\ \Delta\delta \\ \Delta i_q \end{bmatrix} \qquad (2.1)$$

The suffix o denotes the steady state conditions, and

$$Q_o = \frac{1}{2}(v_{qo}i_{do} - v_{do}i_{qo}) = V_{qo}\, I_{do} - V_{qo}I_{qo} \ldots\ldots \quad (2.2)$$

There are three out-put quantities Δid, $\Delta\delta$, Δiq but only one input quantity Δv_{fd} for the system considered. Inversion of the matrix (2.1) gives operational relations between the output and the input quantities. The transfer functions of the alternator $B_1(p)$, $B_2(p)$ and $B_3(p)$ which are indicated on Fig. 2.1, are given by the following expressions

$$B_1(p) = \frac{\Delta i_d}{\Delta v_{fd}} = [Q_o+Jp^2+V_{qo}{}^2Y_q(p)-2r_aV_{qo}I_{qo}Y_q(p)\,] \cdot \frac{G(p).Y_d(p)}{D'(p)}$$

$$B_2(p) = \frac{\Delta \delta}{\Delta v_{fd}} =$$

$$\frac{1}{\sqrt{2}}[-V_{do}+r_a(2I_{do}+V_{qo}Y_q(p))-2r_a{}^2I_{qo}Y_q(p)] \; \frac{G(p).Y_d(p)}{D'(p)}$$

$$B_3(p) = \frac{\Delta i_q}{\Delta v_{fd}} = [-V_{qo}V_{do}Y_q(p)-r_a(2V_{do}I_{do}+Q_o+Jp^2)] \cdot \frac{G(p).Y_d(p)}{D'(p)}$$

(2.3)

where

$$D'(p) = -[Q_o+Jp^2+V_{qo}{}^2Y_q(p)+V_{do}{}^2Y_d(p)-2r_a(V_{qo}I_{qo}Y_q(p)+$$

$$V_{do}I_{do}Y_d(p)) + r_a{}^2(V_{do}I_{qo}-V_{qo}I_{do}+Jp^2)] \quad (2.4)$$

and

$$G(p).Y_d(p) = \frac{X_{md}}{r_{fd}} \frac{(1+T_{kd}\,p)}{(1+T'_d p)(1+T''_d p)}\, Y_d \qquad (2.5)$$

When substituting $G(p)Y_d(p)$ from Eqn. (2.5) in Eqn. (2.3) for later use of expressions $B_r(p)$, (r=1,2,3)

1. the constant $\frac{X_{md}}{r_{fd}}$ is ignored and is later considered to be merged with the regulator gain, (see Sect. 5.2).

2. the denominator terms are merged, i.e.,

$$D(p) = D'(p)(1+T'_d p)(1+T''_d p)$$

3. the minus sign of $D'(p)$ is ignored and later instead of assigning negative numerical values in the sign convention to the regulator gain R that is also taken as positive.

2.2.2 Expressions for the Feedback Quantities

The feedback signals are definite functions of the three alternator output quantities. The small changes of terminal voltage and field current are related to the output quantities as follows

$$\Delta v_t = A_1(p)\Delta i_d + A_2(p)\Delta \delta + A_3(p)\Delta i_q \qquad (2.4a)$$

$$\Delta i_f = \alpha_1(p)\Delta i_d + \alpha_2(p)\Delta \delta + \alpha_3(p)\Delta i_q \qquad (2.4b)$$

where

$$\left.\begin{aligned} A_1(p) &= (X_c I_{do} + V_{qo})\frac{X_c R_e}{V_{to}} \\ A_2(p) &= -\sqrt{2}\, P_o \frac{X_c R_e}{V_{to}} \\ A_3(p) &= -(V_{do} - I_{qo} X_c)\frac{X_c R_e}{V_{to}} \end{aligned}\right\} \qquad (2.5)$$

and

$$\left.\begin{aligned} \alpha_1(p) &= \frac{-X_{d1}(p)}{G_1(p)} \\ \alpha_2(p) &= \frac{v_{do}}{G_1(p)} \\ \alpha_3(p) &= \frac{r_a}{G_1(p)} \end{aligned}\right\} \qquad (2.6)$$

In these equations

$$P_o = V_{do} I_{do} + V_{qo} I_{qo} \qquad (2.7)$$

R_e = rectifier constant.

The transfer functions $A_r(p)$, $\alpha_r(p)$ (r=1,2,3) and the expressions for $G_1(p)$ and $X_{d1}(p)$ are derived in Appendix II.

The voltage feedback is taken direct but the field current feedback is operated on by a transfer function $M(p)$ before the two feedbacks are added. The feedback from the field current is therefore

$$M(p)\ \Delta i_f = A'_1(p)\ \Delta i_d + A'_2(p)\ \Delta\ \delta + A'_3(p)\Delta i_q \quad (2.8)$$

where

$$A'_r(p) = \alpha_r(p) \times M(p) \text{ for } r=1,2,3 \quad (2.8a)$$

The transfer functions $A'_r(p)$, (r=1,2,3) are indicated on Fig. 2.1.

Substituting the relations of Eqn. (2.3) in Eqn. (2.4a) and Eqn.(2.8) the following relations are obtained.

$$F_1(p) = \frac{\Delta\ v_t}{\Delta\ v_{fd}}$$

$$= \sum_{r=1}^{3} A_r(p)\ \ B_r(p)$$

$$= [\ (V_{qo}Y_q(p)+I_{do}-r_aY_q(p)I_{qo})\ .\ (V^2-2r_aP_c+X_cQ_o)\ +$$

$$Jp^2\ ((V_{qo}+X_cI_{do})+r_a(V_{do}-X_cI_{qo})Y_q(p))\ ]\ \frac{X_cR_e}{V_{to}}.\frac{(1+T_{kd}p)Y_d}{D(p)}$$

(2.9)

and

$$F_2(p) = \frac{M(p).\Delta\ i_f}{\Delta\ v_{fd}}$$

$$= \sum_{r=1}^{3} A'_r(p)B_r(p)$$

$$= [-\ (Q_o+V_{qo}{}^2Y_q(p)+V_{do}{}^2Y_{d1}(p)+Jp^2)\ X_{d1}(p)\ +$$

$$r_a\ (2V_{qo}I_{qo}X_{d1}(p)+2V_{do}I_{qo}X_q(p)-V_{qo}V_{do})\ Y_q(p)$$

$$-r_a{}^2\ (I_{qo}V_{do}-V_{do}I_{do}+Jp^2)\ ]\ \frac{M(p)}{G_1(p)}.\frac{(1+T_{kd}\ p)Y_d}{D(p)} \qquad (2.10)$$

The derivation of the expressions for $F_1(p)$ and $F_2(p)$ is given in Appendix III.

Eqn. (2.9) and Eqn. (2.10) are added to give the operational relation for the feedback voltage Δv_{fbd} and the error signal Δv_{fd} ,

$$\frac{\Delta v_{fbd}}{\Delta v_{fd}} = F_1(p) + F_2(p) \qquad (2.11)$$

The feedback voltage Δv_{fbd} is operated on by the regulator transfer function $R(p)$ before being fed to the direct-axis field winding. If the loop is considered opened at A (see Fig.2.1), the open-loop transfer function becomes

$$L(p) = \frac{\Delta v_{fdo}}{\Delta v_{fd}} = R(p)\,[F_1(p) + F_2(p)] \qquad (2.12)$$

2.2.3 The Closed-loop Transfer Function and the Characteristic Equation

For the system shown in Fig. 2.1, the synchronous machine in between the field voltage Δv_{fd} and Δv_t is considered to form the forward-loop, i.e. Δv_t is taken as the output. The reference input is Δv_{fdi} which is related to Δv_{fdo} and Δv_{fd} by

$$\Delta v_{fdi} - \Delta v_{fdo} = \Delta v_{fd} \qquad (2.13)$$

Eliminating Δv_{fdo} from Eqns. (2.12) and (2.13) we have

$$\frac{\Delta v_{fd}}{\Delta v_{fdi}} = 1 + L(p) \qquad (2.14)$$

The closed-loop transfer function $C(p)(=\frac{\Delta v_t}{\Delta v_{fdi}})$ is obtained by eliminating Δv_{fd} from Eqns. (2.9) and Eqn. (2.14), thus we have

$$C(p) = \frac{F_1(p)}{1+L(p)} \qquad (2.15)$$

For the system represented by Eqn. (2.15) the characteristic equation is:

$$\text{Numerator of } [1+L(p)] = 0 \qquad (2.16)$$

To develop the characteristic equation (2.16) in the polynomial form the functions $R(p)$ and $M(p)$ associated with $L(p)$ must be defined; till now these have been treated in general as ratio of polynomials in 'p'. Since we are interested to study a feedback regulator using the derivative of the field current in conjunction with a proportionate voltage signal, we take

$R(p) = R$, and

$M(p) = M\,p$

where R and M are adjustable constants, later referred to as the regulator and field current gains respectively, see Sect. 2.2.4. In the characteristic equation (2.16) it is preferred to write the open-loop transfer function $L(p)$ in the form below:

$$L(p) = R\ \frac{N(p)}{D(p)}$$

thus, Eqn. (2.16) becomes

$$D(p) + R\,N(p) = 0 \qquad (2.17)$$

This form of Eqn. (2.17) is later referred to as the original characteristic equation. In Appendix IV, Eqn. (2.17) is expanded in the polynomial form as below

$$C_4p^4 + C_3p^3 + C_2p^2 + C_1p + C_o = 0 \qquad (2.18)$$

where

$$C_4 = J[(T'_dT''_{do}+T'_{do}T''_{do}r_a{}^2Y_dY_q)-(T_5+T_2r_a{}^2Y_dY_q)\frac{R.M}{R_eX_{md}}]$$

$$C_3 = J[T'_d+T''_d+r_a{}^2Y_dY_q(T'_{do}+T''_{do})+T_{kd}\frac{Y_dX_c}{V_{to}}\{(V_{qo}+X_cI_{do}) +$$

$$r_a(V_{do}-X_cI_{qo})Y_q\}R-(1-r_a{}^2Y_dY_q).\frac{R.M}{R_eX_{md}}]$$

$$C_2 = J+T'_dT''_d(Q_o+V_{qo}{}^2Y_q)+T'_{do}T''_{do}V_{do}{}^2Y_d-2r_a(T'_dT''_dV_{qo}I_{qo}Y_q +$$

$$T'_{do}T''_{do}V_{do}I_{do}Y_d)+r_a{}^2Y_dY_q\ [T'_{do}T''_{do}(V_{do}I_{qo}-V_{qo}I_{do})+J] +$$

$$J.\frac{X_cY_d}{V_{to}}\ [(V_{qo}+X_cI_{do})+r_aY_q(V_{do}-X_cI_{qo})]\ .R+Y_d[-\{T_5(Q_o+V_{qo}Y_q)$$

$$+T_2V_{do}{}^2Y_d\}X_d+r_aY_q(2V_{qo}I_{qo}X_dT_5+2V_{do}I_{do}X_qT_2-V_{do}V_{qo}T_2)$$

$$-r_a{}^2Y_qT_2(I_{qo}V_{do}-V_{qo}I_{do})]\frac{M.\ R}{X_{md}R_e}$$

$$C_1 = T'_dS'_o+(Q_o+V_{qo}{}^2Y_q)T''_d\ +V_{do}{}^2Y_dT''_{do}-2r_a\ [V_{qo}I_{qo}Y_q(T'_d+T''_d)$$

$$+V_{do}I_{do}Y_d(T'_{do}+T''_{do})]\ +r_a{}^2Y_qY_d\ [(V_{do}I_{qo}-V_{qo}I_{do})(T'_{do}+T''_{do})]+$$

$$T_{kd}\frac{X_cY_d}{V_{to}}\ [(V_{qo}Y_q+I_{do}-r_aI_{qo}Y_q)(V^2-2r_aP_o+X_cQ_o)]\ +Y_d\ [-S_oX_d\ +$$

$$r_aY_q(2V_{qo}I_{qo}X_d+2V_{do}I_{do}X_q-V_{do}V_{qo})-r_a{}^2(I_{qo}V_{do}-V_{qo}I_{do})]\ \frac{R.M}{R_eX_{md}}$$

$$C_o = S_o-2r_a(V_{qo}I_{qo}Y_q+V_{do}I_{do}Y_d)+r_a{}^2Y_dY_q(V_{do}I_{qo}-V_{qo}I_{do})\ +$$

$$\frac{X_cY_d}{V_{to}}\ (V_{qo}Y_q+I_{do}-r_aY_qI_{qo})(V^2-2rP_o+X_cQ_o).R \qquad (2.19)$$

The expressions[1,17] for S_o and S'_o are as follows

$$S_o = Q_o+V_{qo}{}^2Y_q+V_{do}{}^2Y_d = VV_oY_d\cos\delta_o+V^2(Y_q-Y_d)\cos2\delta_o$$

$$S'_o = Q_o+V_{qo}{}^2Y_q+V_{do}{}^2Y'_d = VV'_oY'_d\cos\delta_o+V^2(Y_q-Y'_d)\cos2\delta_o$$

(2.20)

S_o and S'_o are the slopes of the power-angle and transient power-angle curves respectively V_o is the voltage behind the synchronous reactance and V'_o is the q-axis component of the voltage behind the transient reactance. The expressions on the extreme right of Eqn. (2.20) are standard formulae. The left hand side in each Eqn. (2.20) can be shown to be equal to the righ hand side by substituting for Q_o, V_{qo}, V_{do} in terms of V and δ.

In a theoretical study in Ref.4 the derivative of the field current is incorporated by modifying the expressions for $G(p)$ and $X_d(p)$, using the deductions made by the same authors in a paper Ref. 3 with simplifying assumptions of no damping and resistance and making approximations with time constants. The theoretical formulations in the present treatment can allow for any transfer function $M(p)$ for the field current feedback

and $R(p)$ for the regulator transfer function. However, the characteristic Eqn. (2.18) is a particular case deduced from the general formulation represented by Eqn. (2.16).

2.2.4 The Gain Constants

In Eqn. (2.12) the rectifier conversion factor R_e and the field current gain M are associated with $F_1(p)$ and $F_2(p)$ respectively. In the development of the characteristic Eqn. (2.18) R_e is merged with R and the field current constant is modified to M/R_e, although, when referring to the field current gain, only M is mentioned.

2.3 Application of the Analysis to determine Stability

2.3.1 The System and the Method of Analysis

In Ref. 1 the study of a system using voltage regulators of different types was carried out by means of the Nyquist criterion. Calculations were made alternatively allowing for alternator damping and resistance and neglecting them. It was found that although damping and resistance had a noticeable effect, a useful approximation was obtained when they were neglected and some important general deductions could be made.

For the direct-axis excitation control this thesis described an investigation of a system in which the voltage feedback is supplemented by a feedback from the field current. It was decided to make the calculations with damping and resistance neglected. With the simpler equations then obtained, the root-locus method proved to lead to useful deductions, as explained below. Some results using the Routh criteria were also obtained.

The root-locus method uses the characteristic equation derived from the open-loop transfer function as in Eqn. (2.17). Conventionally the loci of roots of the characteristic equation (2.18) as the gain is varied from zero to infinity, are obtained from the poles and zeros of the open-loop transfer function $L(p)$. As applied here the root-loci are obtained by computing directly the roots of the polynomial characteristic equation (2.18) for gains from zero upwards. The Routh criteria uses a function of coefficients of the characteristic Eqn. (2.18) to predict the stability of the system. It should be noted that the Nyquist method is also in effect an indirect method of determining the roots with positive real parts of the characteristic equation. All three methods[18-20] are discussed briefly in Appendix V.

The results given in this section relate to a simple system in which the voltage feedback is proportional without delay (i.e., $R(p) = R$), and the field current feedback is a simple derivative (i.e., $M(p) = M.p$). The characteristic equation for such a system is given by Eqn. (2.18). When resistance and damping are neglected Eqn. (2.18) is simplified, its order is reduced from 4th to 3rd. With the coefficient

$$C_4 = 0$$

the simplified characteristic equation becomes:

$$C_3 p^3 + C_2 p^2 + C_1 p + C_o = 0 \qquad (2.21)$$

where

$$\left.\begin{aligned}
C_3 &= J[T'_d - R.\frac{M}{R_e}.\frac{1}{X_{md}}.] \\
C_2 &= J + J\frac{X_c.Y_d}{V_{to}}(V_{qo}+X_c I_{do}).R \\
C_1 &= T'_d S'_o - S_o R.\frac{M}{R_e}.X_{md} \\
C_o &= S_o + \frac{X_c Y_d}{V_{to}}(V_{qo}Y_q+I_d)(V^2+X_c Q_o).R
\end{aligned}\right\} \quad -- \quad (2.22)$$

From the consideration of the feedbacks three alternative cases arise:

1. the unregulated system, i.e. when $R = 0$,
2. the system with only the voltage feedback, i.e. when R is an adjustable constant,
3. the system with the main voltage feedback and the auxiliary field current feedback, i.e. when R and M are both adjustable constants.

The characteristic equation for any of the above mentioned systems can be derived from Eqn. (2.21). With the above classification the system study is carried out in the following sections.

2.3.2 The Unregulated System

As mentioned in Sect. 2.3.1 the unregulated system corresponds to zero regulator gain and therefore both of the feedbacks of the system are rendered inoperative. The characteristic equation for the unregulated system is obtained by putting the regulator gain to zero in the general characteristic equation (2.21) and is as given below

$$D(p) = J\,T'_d p^3 + Jp^2 + T'_d S'_o p + S_o = 0 \qquad (2.23)$$

Since the general characteristic equation (2.21) is derived from Eqn. (4.17), Eqn. (2.23) is simply $D(p) = 0$, of which the roots are the poles of the open-loop transfer function $R\frac{N(p)}{D(p)}$. $N(p) = 0$ gives the zeros of the open-loop transfer function. The following sections are concerned with root-loci of the characteristic equation, on which the open-loop transfer function poles and zeros are marked respectively by crosses and encircled dots.

In the following analysis power is considered constant at 0.8 p.u. and the rotor angle is varied. For every value of the rotor angle δ, Eqn. (2.23) gives a pair of complex conjugate roots in the left half (L.H.) of the complex plane, referred to later as p-plane, and a root on the real-axis. In Fig. 2.2 are shown the roots of the characteristic Eqn. (2.23) at various rotor angles. Let δ_s be the limiting rotor angle for the steady state operation of the unregulated system (84^o for the machine considered). For the rotor angle $\delta < \delta_s$ the real root of the characteristic Eqn. (2.23) is negative, whereas, for $\delta > \delta_s$ it is positive. The positive real root contributes to an exponent term with a positive exponent in the time domain and causes instability of the drifting type. The limiting condition ($\delta = \delta_s$) arises when the real root is at the origin.

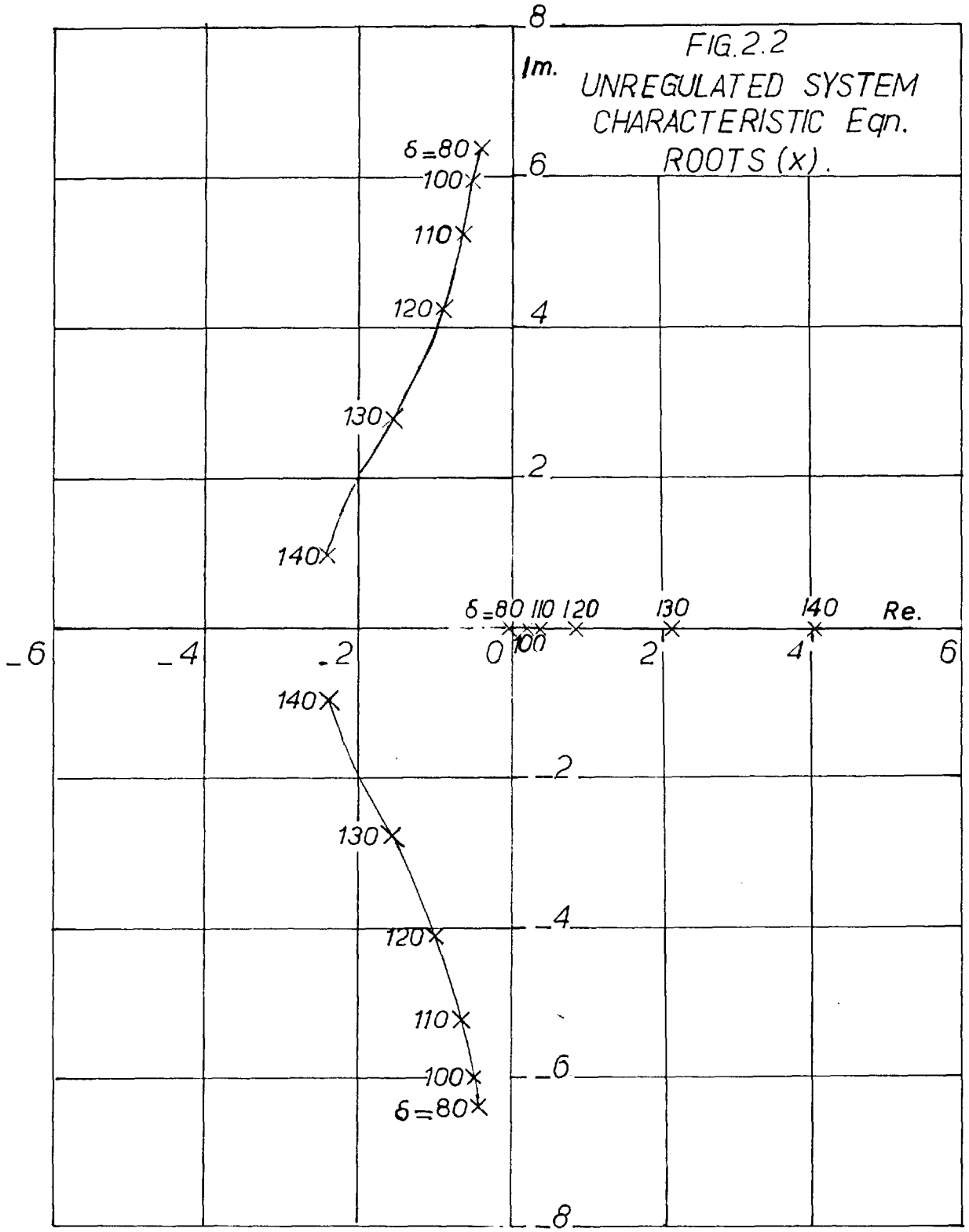
FIG. 2.2
UNREGULATED SYSTEM
CHARACTERISTIC Eqn.
ROOTS (x).
Im.
Re.
8
6
4
2
-2
-4
-6
δ=80
100
110
120
130
140
0

This occurs when the term S_o in the characteristic Eqn. (2.23) is zero, i.e., when the slope of the power-angle curve is zero. For an unregulated machine this is the well known steady state limit. The full line of Fig. 2.3 shows how S_o varies with δ. For the micro-machine under study S_o is zero when δ is 84^o.

2.3.3 The System With Voltage Feedback

When a voltage feedback is used, stable operation is possible at angles greater than δ_s because the feedback modifies the characteristic equation (2.23) of the unregulated system.

With no auxiliary field current feedback the gain factor M is zero and the characteristic equation (2.21) becomes

$$J\,T'_d p^3 + J\left[1+\frac{R.X_c.Y_d}{V_{to}}(V_{qo}+X_c I_{do})\right]p^2 + T'_d S'_o p + \left[S_o + \frac{X_c.Y_d}{V_{to}}(V_{qo}Y_q+I_{do})(V^2+X_c Q_o).R\right] = 0 \quad (2.24)$$

Returning to the original form of the characteristic equation

$$D(p) + R\,N(p) = 0 \quad (2.17)$$

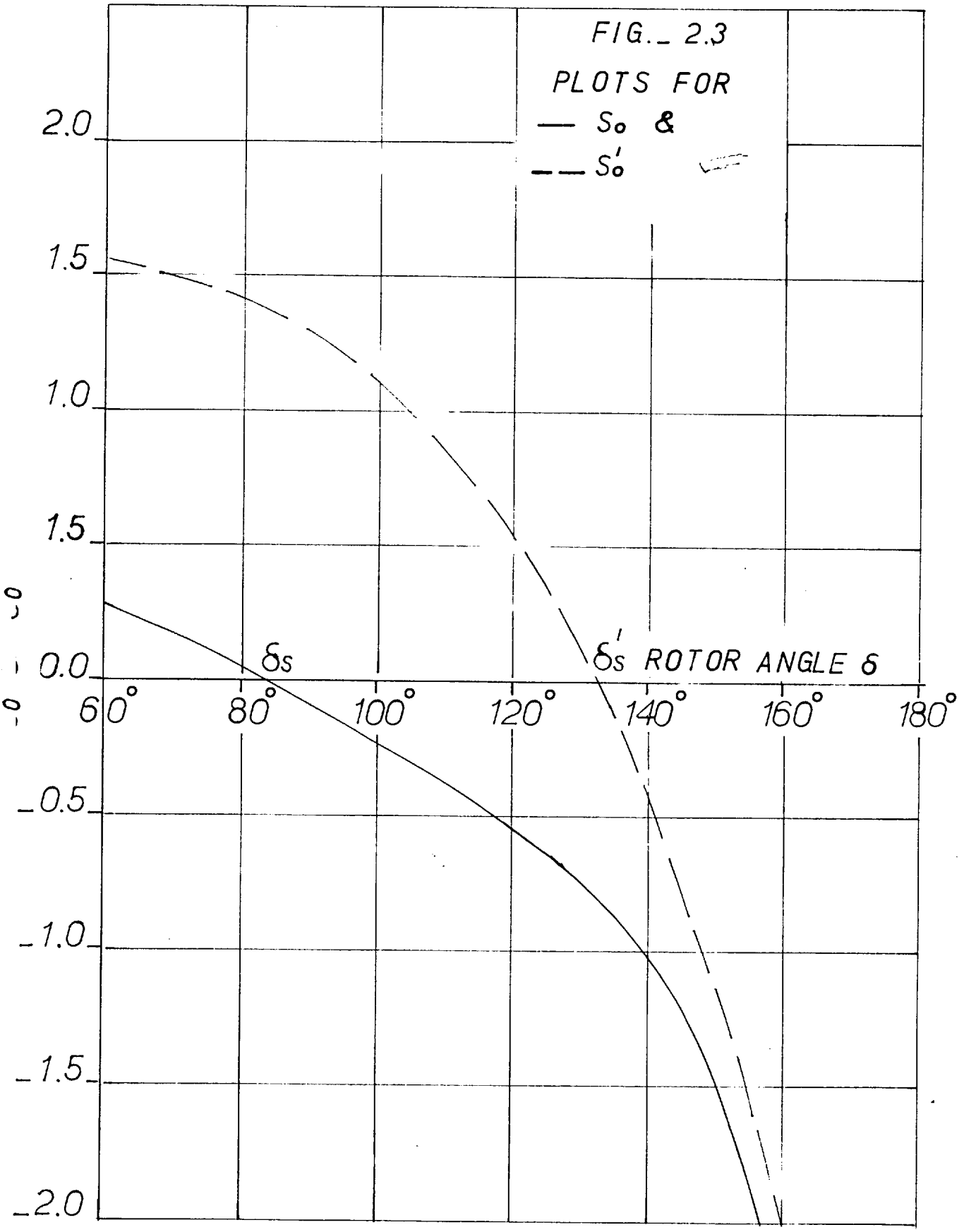
FIG._ 2.3
PLOTS FOR
— S_o &
-- S_o'
2.0
1.5
1.0
1.5
0.0
δ_s
δ_s' ROTOR ANGLE δ
60°
80°
100°
120°
140°
160°
180°
_0.5
_1.0
_1.5
_2.0

$D(p)$ has the values given by Eqn. (2.23) and

$$N(p) = [(V_{qo}+X_c I_{do})p^2 + (V_{qo}Y_q+I_{do})(V^2+X_c Q_o)] \frac{X_c . Y_d}{V_{to}} \quad (2.25)$$

$D(p) = 0$ and $N(p) = 0$ give the poles and zeros respectively of the open-loop transfer function $R \frac{N(p)}{D(p)}$

When R is zero the roots of the characteristic equation (2.24) are the poles of the open-loop transfer function, and when R is infinity the roots are the zeros, with the remaining roots at infinity as explained in Appendix V.1.3.3.

Consider the condition when $\delta = 100^o$ illustrated by Fig. 2.4a and b, where the root loci are mapped on different scales. Along the length of each root-locus discrete gain values are marked. When $R = 0$ the roots are the same as on Fig. 2.2, but as R increases the position of the roots changes. The real root moves into the L.H. p-plane at $R = 2.2$ while the complex conjugate pair of roots move towards the R.H. p-plane and at $R = 16$ cross the $j\omega$-axis. Hence the system is stable for a limited range $2.2<R<16$.

The root-loci as plotted here and for all the subsequent cases are computed from the characteristic equation using a digital computer upto $R = 20$. For

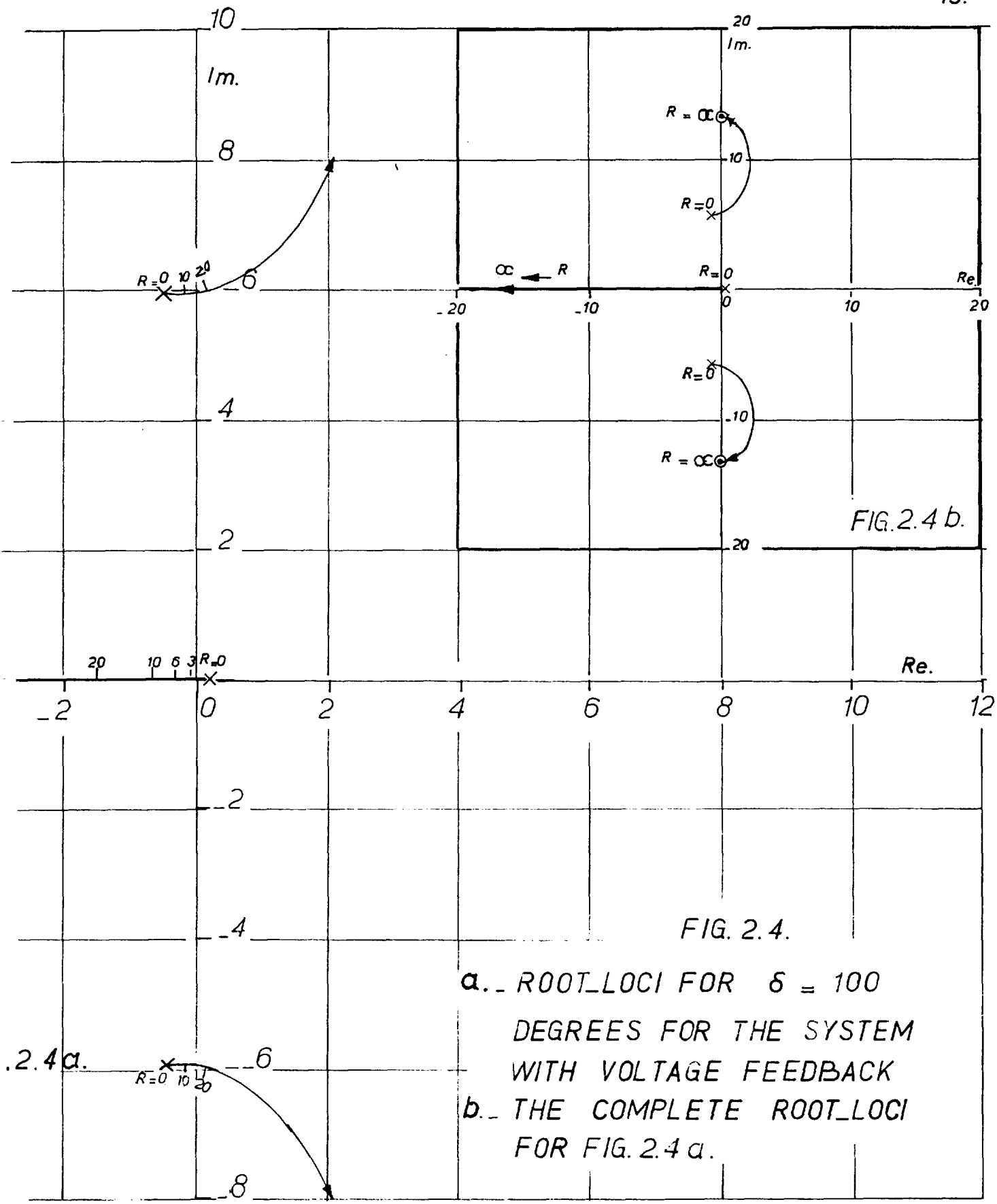

FIG. 2.4.

a.- ROOT-LOCI FOR δ = 100 DEGREES FOR THE SYSTEM WITH VOLTAGE FEEDBACK

b.- THE COMPLETE ROOT-LOCI FOR FIG. 2.4 a.

.2.4 a.

R>20 the loci are plotted graphically using the open-loop pole-zero configuration as explained in Appendix V.1.3. Accordingly in Fig. 2.4b are plotted the complete root-loci for $\delta = 100^{0}$, on a smaller scale. At $R = \infty$ the real root is at infinity and the complex conjugate pair of roots close on the two zeros on the imaginary axis given by $N(p) = 0$.

The algebraic expressions for R(min) , the minimum gain R required to stabilise the system and R(max), the maximum gain R limit for the stable operation are derived below from the characteristic equation (2.24) using the root-locus concepts. R(min) is the value at which the real root crosses the (0,0) point and enters the L.H. p-plane; this occurs when C_o in Eqn. (2.24) is zero, i.e.

$$S_o + \frac{X_c Y_d}{V_{to}} (V_{qo}Y_q + I_{do})(V^2 + X_c Q_o).R = 0$$

giving

$$R(\min) = \frac{-S_o}{(V_{qo}Y_q + I_{do})(V^2 + X_c Q_o)} . \frac{V_{to}}{X_c Y_d} \qquad (2.26)$$

R = R(max) when the complex conjugate pair of roots are on the imaginary axis. For a third order characteristic equation (2.24) to give two equal and opposite imaginary

roots, the condition is (see Appendix V.2.1)

$$C_3C_0 = C_2C_1$$

Using the above relation R(max) is given by

$$R(max) = \frac{(S'_o-S_o)V_{to}}{[(V_{qo}Y_q+I_{do})(V^2+Q_oX_c)-S'_o(V_{qo}+X_cI_{do})]X_cY_d} \qquad (2.27)$$

The point of intersection of the complex conjugate roots with the $j\omega$-axis gives the natural frequency ω_n of the closed-loop. By substituting R(max) in the auxiliary equation (see Appendix V.2.1)

$$C_2p^2 + C_o = 0$$

we have

$$\omega_n = \sqrt{\frac{C_o}{C_2}} = \sqrt{\frac{S'_o}{J}} \qquad (2.28)$$

The instability for $R<R(min)$ is of the drifting type, because the real root is positive, whereas, at $R>R(max)$ it is of an oscillatory nature, because the complex conjugate roots have positive real parts.

Fig. 2.5a shows the root-loci upto $R = 20$ for $\delta = 120^o$, and Fig. 2.5b shows the complete root-loci.

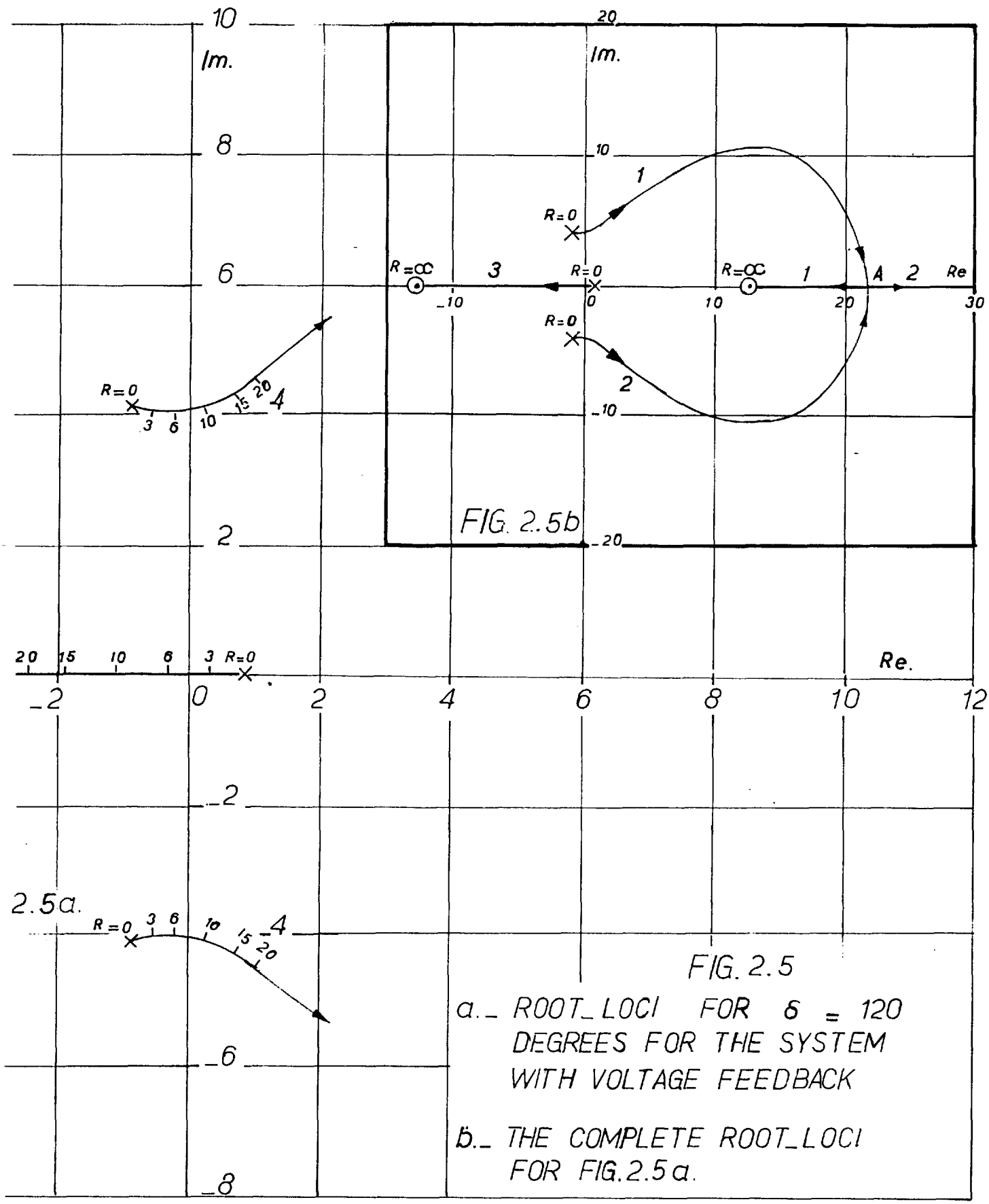

FIG. 2.5

a._ ROOT_LOCI FOR δ = 120 DEGREES FOR THE SYSTEM WITH VOLTAGE FEEDBACK

b._ THE COMPLETE ROOT_LOCI FOR FIG. 2.5 a.

The pattern of the root-loci in Fig. 2.5a is very similar to that of Fig. 2.4a ($\delta = 100^{\circ}$, showing the root-loci upto $R = 20$) and so the description for Fig. 2.5a is omitted. To explain the complete pattern of root-loci in Fig. 2.5b the complex conjugate roots and the real root are labelled 1, 2 and 3 respectively. All the subsequent root-loci plots are similarly labelled as in Fig. 2.5b. At $R = 20$ the roots 1 and 2 are in the R.H. p-plane and root 3 is in the L.H. p-plane. As R increases the roots 1 and 2 follow an elliptical path in the R.H. p-plane and converge at 'A' on the real-axis, later root 1 turns leftwards and root 2 rightwards. Whenever the complex conjugate roots 1 and 2 close on the real-axis, one turning right and the other left the labelling is arbitrary and interchangeable. This is applicable to all the subsequent root-loci plots for a similar condition. Root 3 moves along the real-axis in the L.H. p-plane. At $R = \infty$ root 2 is at infinity and the roots 1 and 3 close on the open-loop transfer function zeros in the right and left half p-plane respectively. The pattern in Fig. 2.5b differs from that in Fig. 2.4b, because at $\delta = 120^{\circ}$ the open-loop transfer function zeros given by $N(p) = 0$ [Eqn. (2.25)], are real, wheras the zeros at $\delta = 100^{\circ}$ are imaginary. The

zeros are real because the $(V_{qo}+I_{do}X_c)$ term in the expression for $N(p)$ [Eqn. (2.25)] changes its sign from positive to negative. This changes the right hand side of Eqn. (V.8) from $\pi+2\pi\lambda$ to $0+2\pi\lambda$, as explained in Appendix V.1.2.5. For $120^\circ>\delta>100^\circ$, when the term $(V_{qo}+I_{do}X_c)$ is zero, the three roots of the characteristic equation approach infinity as $R\longrightarrow\infty$ as explained in Appendix V.1.2.3.

For $\delta = 140^\circ$ Fig. 2.6a shows the root-loci for the important range of gain R and Fig. 2.6b shows the complete root-loci on a smaller scale. The pattern of the root-loci for $\delta = 140^\circ$ is very different from those for $\delta = 100^\circ$ and 120° in Figs. 2.4 and 2.5. At $R = 0$ the roots are the same as given on Fig. 2.2. As R increases the complex conjugate roots 1 and 2 meet at 'A' on the real-axis, root 1 turning left and root 2 turning right. The real root 3 moves towards the origin. At R about 6.3 root 2 crosses from the L.H. into the R.H. p-plane and meets roots 3 at 'B', and for higher values of R they break off and become complex conjugate. Root 2 moves towards C and root 3 towards D. The root labelling for the BC and BD part of the root-loci is interchangeable, although the movement of the roots 2 and 3 is specified above. Under similar conditions for

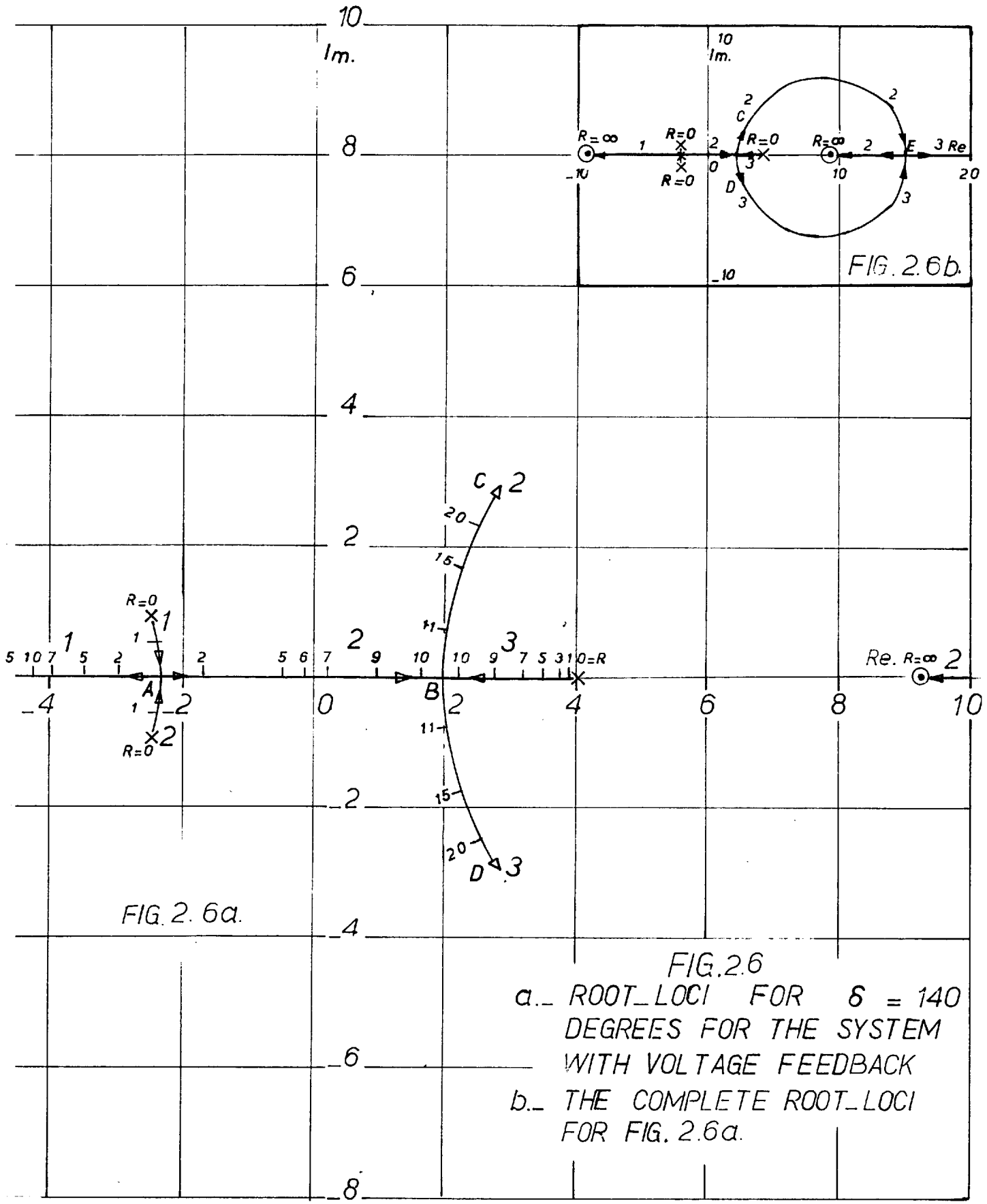

FIG. 2.6

a.- ROOT_LOCI FOR δ = 140 DEGREES FOR THE SYSTEM WITH VOLTAGE FEEDBACK

b.- THE COMPLETE ROOT_LOCI FOR FIG. 2.6a.

the subsequent root-loci plotting the interchangeability of the roots is understood, however not mentioned. Root 1 moves towards infinity in the L.H. p-plane. As R increases from zero root 3 remains in the R.H. p-plane and never becomes negative, for that reason the system is always unstable. Fig. 2.6b shows the complete root-loci. As R increases the roots 2 and 3 follow an elliptical path in the R.H. p-plane and converge at E , root 2 turns leftwards and root 3 rightwards. Root 1 continues moving in the L.H. p-plane. For $R = \infty$ the roots 1 and 2 close on the real open-loop transfer function zeros given by Eqn. (2.25) in the left and right half p-plane respectively and root 3 is at infinity in the R.H. p-plane.

This illustration demonstrates the limitation of the proportionate regulator, which arises because $T'_d S'_o$ the coefficient of p in the characteristic Eqn. (2.24), becomes negative with increasing δ , and is not affected by the feedback. Thus, the maximum steady state δ limit, for the proportionate regulator is given by $S'_o = 0$, i.e. when the slope of the transient power angle curve is zero. In Fig. 2.3 the broken line is the curve relating S'_o and δ indicating that $\delta = \delta'_s = 134^o$ is the limit for the machine investigated. The limit δ'_s is known in the literature on voltage regulators[1].

2.3.4 The System with Voltage and Field Current Feedbacks

With both the feedbacks in action, Eqn. (2.21) is the characteristic equation. The coefficients C_3, C_1 contain the field current feedback terms and C_2, C_o contain the voltage feedback terms.

Returning to the original characteristic equations (2.17), $D(p)$ is given by Eqn. (2.23), and $N(p)$ by

$$N(p) = -\frac{JM}{R_e.X_{md}} p^3 + \frac{JX_cY_d}{V_{to}}(V_{qo}+X_cI_{do})p^2 - \frac{M}{R_eX_{md}}.S_o p$$

$$+ \frac{X_cY_d}{V_{to}} (V_{qo}Y_q+I_{do})(V^2+X_cQ_o) \qquad (2.29)$$

The open-loop transfer function poles given by $D(p)$ reamin unchanged, but the zeros now depend on M. For $M = 0$ the expression for $N(p)$ becomes that of the proportional voltage regulator given by Eqn. (2.25).

In Fig. 2.7 are shown the root-loci for $\delta = 140^o$ and $M = .002$. For zero R the roots are the same as on Figs. 2.2 and 2.6. As R increases the complex conjugate roots 1 and 2 meet at A on the real axis and follow exactly the same pattern as that of $\delta = 140^o$ with only the voltage feedback in Fig. 2.6a. The points A, B, C and D similar to those of Fig. 2.6a are shown

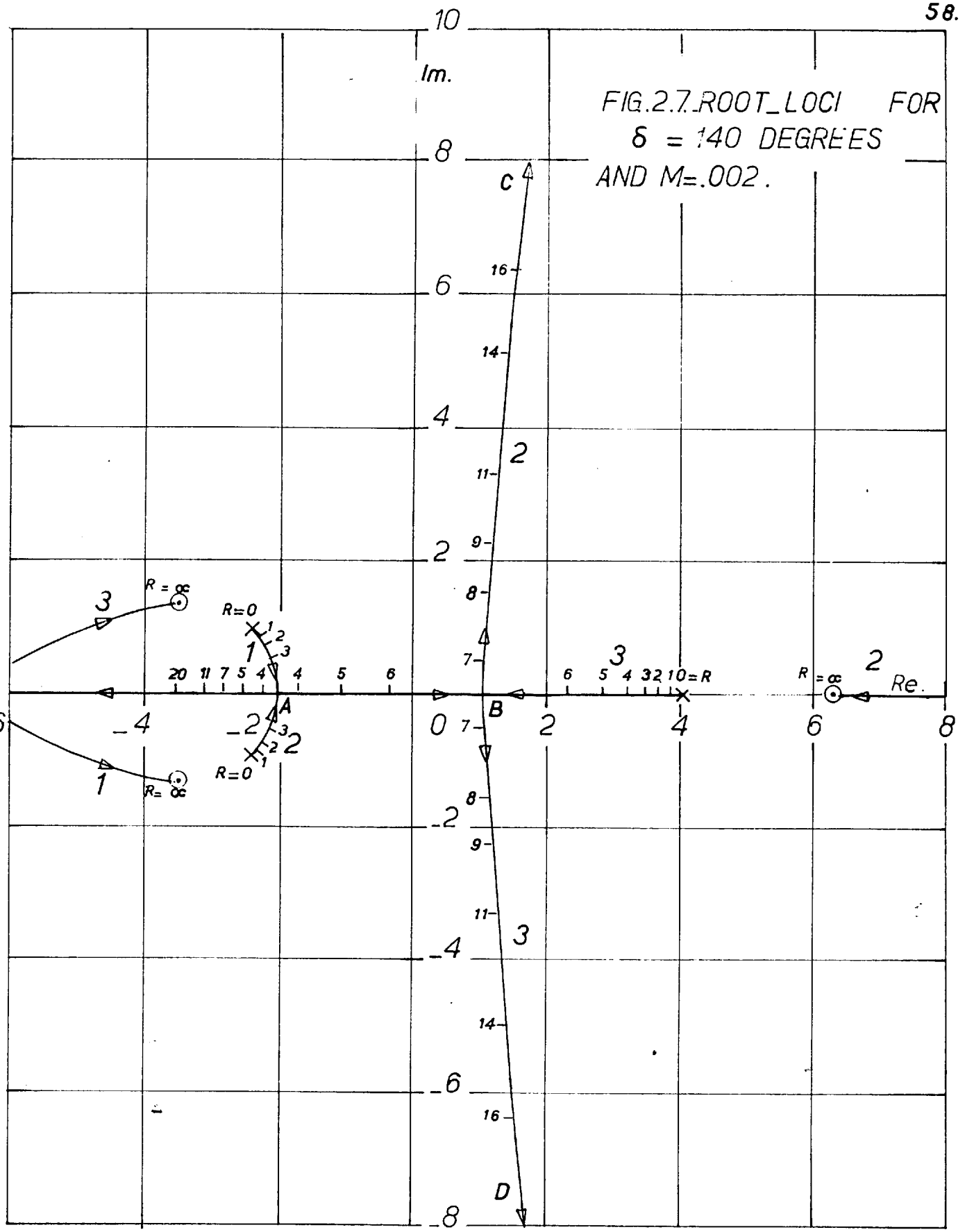

FIG.2.7.ROOT_LOCI FOR δ = 140 DEGREES AND M=.002.

and the various roots are labelled. The detailed root-loci plotting is shown up to R = 16 . The system is always unstable because for any gain R there is always one or more roots in the R.H. p-plane. The complete root-loci plotting is omitted, however, closing of the root-loci at R = ∞ on the open-loop transfer function zeros is shown and explained briefly here. As R increases the roots 2 and 3 move on a large elliptical path (not shown in Fig. 2.7) in the R.H. p-plane and eventually converge on a point very far from the origin, after which root 2 moves towards the origin and root 3 towards infinity. At infinity root 3 is established in the L.H. p-plane, from there it moves towards the origin and meets Root 1 at a point, after which both break off and become complex conjugate (partly shown in Fig. 2.7). At R = ∞ the roots 1 and 3 close on the complex conjugate pair of the open-loop transfer function zeros in the L.H. p-plane and root 2 closes on the real zero in the R.H. p-plane, (see Fig. 2.7).

At higher values of M the open-loop transfer function zeros cause a further modification of the pattern of the root-loci, In Fig. 2.8 are shown the root-loci for $\delta = 140^{\circ}$ and M = .004. All the three zeros become real, two being in the L.H. p-plane and

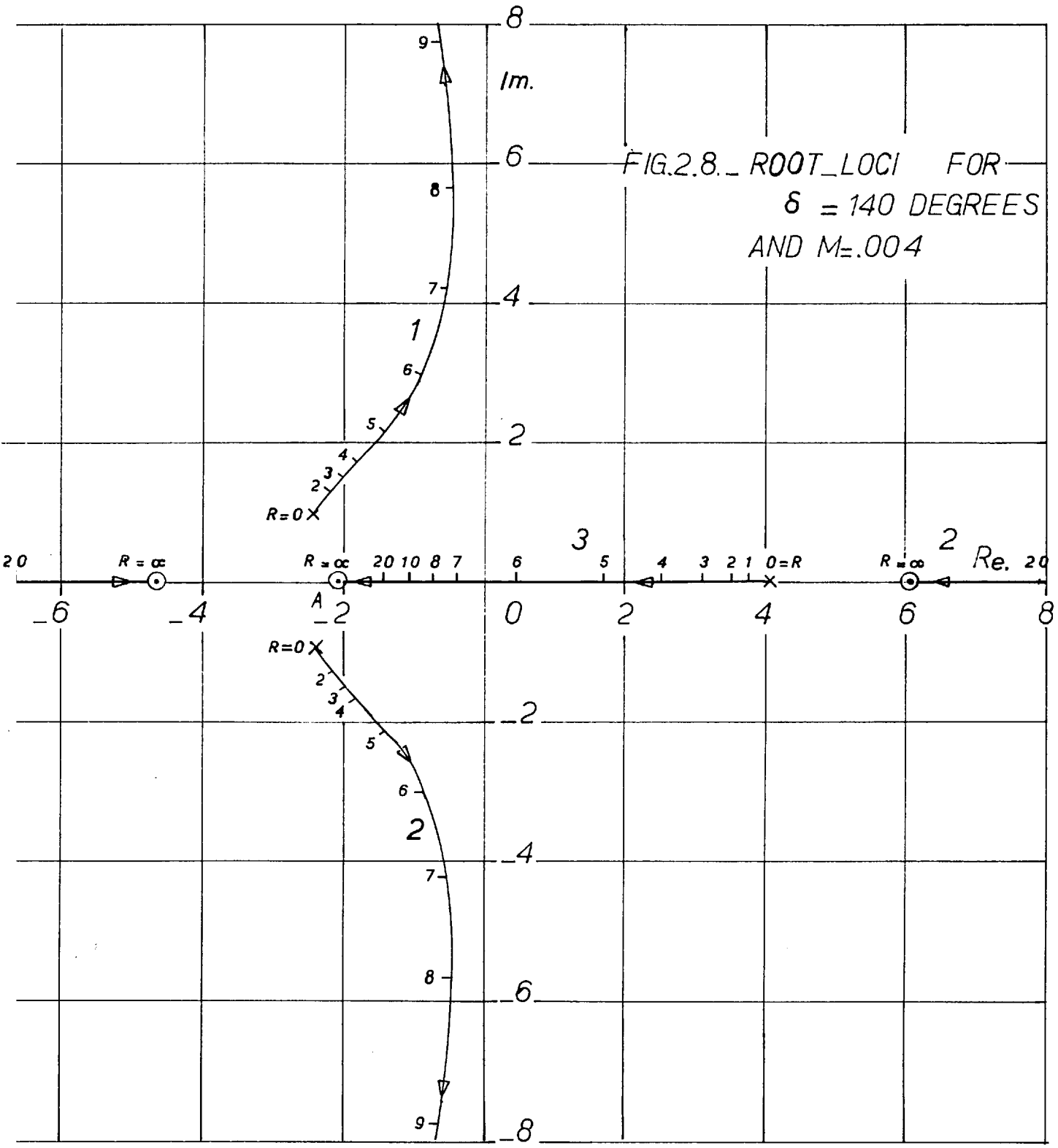

FIG.2.8._ ROOT_LOCI FOR δ = 140 DEGREES AND M=.004

one in the R.H. p-plane. The real negative zero at A is of great importance, because it assists in stabilising the system as will be seen later. At $R = 0$ the complex conjugate roots 1 and 2 and the real root 3 are the same as in Fig. 2.2. As R increases the roots 1 and 2 advance along the $j\omega$-axis in the L.H. p-plane and the real root 3 moves towards the L.H. p-plane, which crosses the origin at R about 6.6 (that is R_{min}) and becomes negative. With all the roots in the L.H. p-plane the system is stable. To obtain the upper limit for R from Fig. 2.8 is difficult, because the roots 1 and 2 move so rapidly that their mapping is a problem, for this reason the inverse root-locus technique is adopted which is dealt with in the following paragraph. However, at $R = \infty$ the closing points for the root-loci are shown in Fig. 2.8, the roots 3 and 1 close on the real open-loop transfer function zeros in the L.H. p-plane and root 2 on the real zero in the R.H. p-plane. How root 2 gets into the R.H. p-plane is clearly seen from the inverse root-loci plot.

In the inverse root-locus technique the root-loci are mapped in the W -plane using the transformation $W = \frac{1}{p}$ as explained in Appendix V.1.4. The main advantage is that infinity is brought to the origin so

that the behaviour of roots with large magnitude can be studied.

The characteristic equation (2.21) in the W-plane becomes

$$C_3 + C_2W + C_1W^2 + C_oW^3 = 0 \qquad (2.30)$$

Using Eqn. (2.30) the root-loci in the W-plane are shown in Fig. 2.9 for $\delta = 140^o$ and $M = .004$. Each root in Fig. 2.9 is the inverse of the root in Fig. 2.8 for the corresponding value of R . For $R = 0$ Eqn. (2.30) gives a pair of complex conjugate roots 1 and 2 in the L.H. W-plane and the real root 3 in the R.H. W-plane. When R is increased root 3 tends to infinity (which in the p-plane means the origin) and is established in the L.H. W-plane for $R = R(\min)$. From the characteristic Eqn. (2.30) this limiting value is obtained when $C_o = 0$, and is given by Eqn. (2.26). With R increasing the roots 1 and 2 move on an elliptical path converging on the real-axis at 'A' in the L.H. W-plane, after which root 1 turns leftwards and root 2 turns rightwards. Root 2 croses the origin at R about 11.5 giving the limiting value $R(\max)$. The characteristic equation (2.30) gives one root at the origin when

FIG.2.9_ INVERSE ROOT_LOCI
FOR δ = 140 DEGREES
AND M=.004

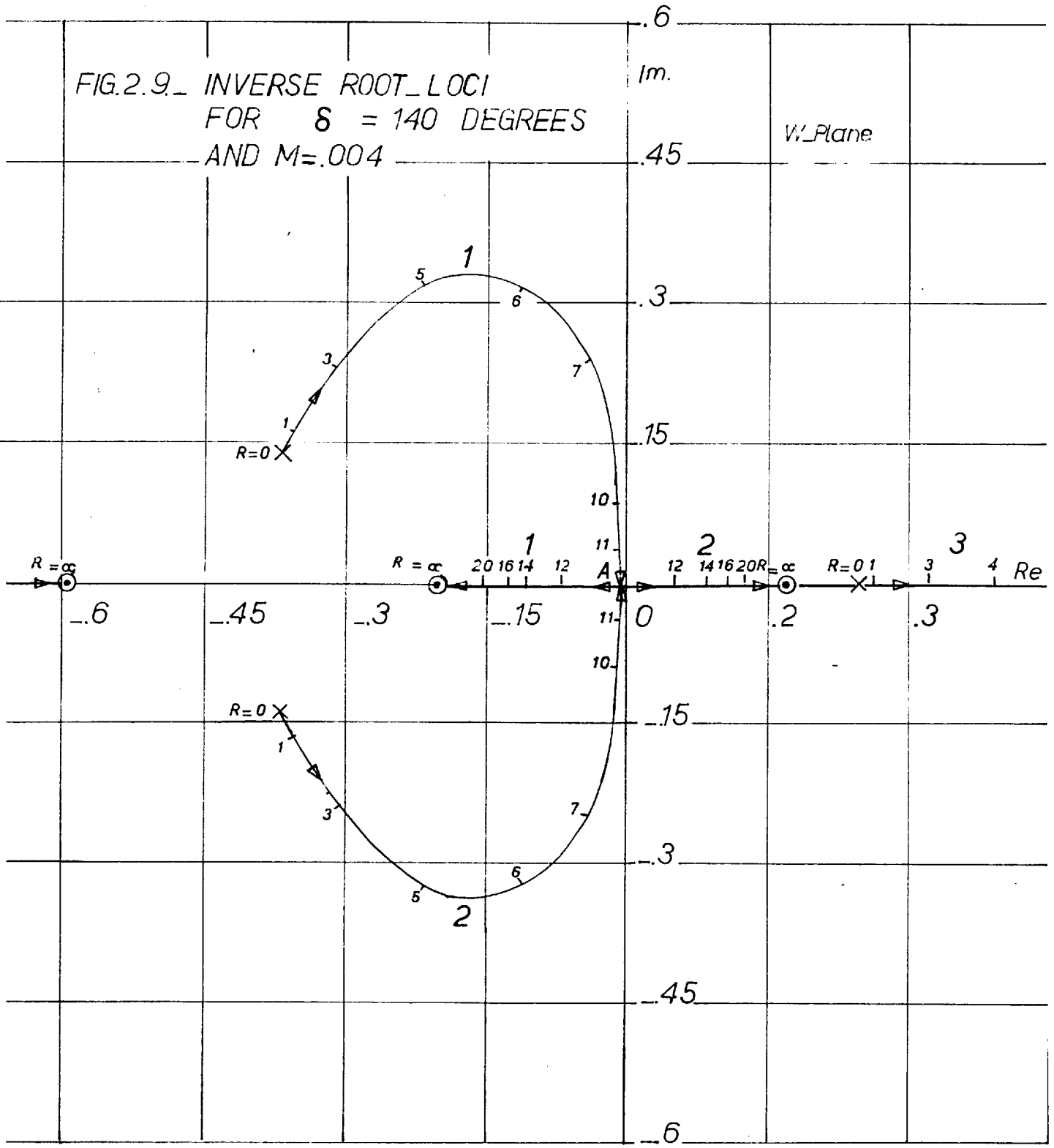

$C_3 = 0$, i.e.

$$T'_d - \frac{R.M}{R_e X_{md}} = 0 \qquad (2.31)$$

yielding,

$$R(max) = T'_d \frac{R_e}{M}.X_{md} \qquad (2.32)$$

Eqn. (2.31) suggests that the derivative of the field current has the effect of reducing the short-circuit transient time constant T'_d , and the system becomes unstable, irrespective of the load angle δ , at values of R and M such that Eqn. (2.31) is satisfied. However, depending on δ and M the system $R(max)$ may be less than the value given by Eqn. (2.32) if the complex conjugate pair of roots 1 and 2 in Fig. 2.9 cross over to the R.H. W-plane instead of converging on the real-axis. In algebraic terms it means that $R(max)$ is the value of R which satisfies

$$C_2 C_1 = C_3 C_0$$

In Appendix V.2 the graphical form of the Routh criterion is discussed. The coefficients C_3 , C_2 ,

C_1 , C_o of Eqn. (2.21) are functions of the regulator gain R treating M as a constant. For the third order system the necessary and sufficient condition for stability are:

$$C_3>0 \ , \ C_2>0 \ , \ C_1>0 \ , \ C_o> \ , \ C_2C_1-C_3C_o>0 \qquad (2.33)$$

The Routh coefficient $C_2C_1-C_3C_o$ is referred to as C_4 . For plotting all the coefficients C_4, C_3, ...C_o are referred to as the 'Routh Coefficients', In Fig. 2.10 the Routh Coefficients are plotted against the regulator gain R for $\delta = 130^o$ and M = .003. The stable and unstable zones are demarcated on the figure. R(min) is given by $C_o = 0$ and R(max) by $C_3 = 0$. However, depending upon δ and M R(max) may be given by $C_4 = 0$.

The Routh Coefficient plotting emphasises the importance of the coefficients of the characteristic equation and gives the precise limits, but cannot give details like the oscillatory modes of the system at any gain R .

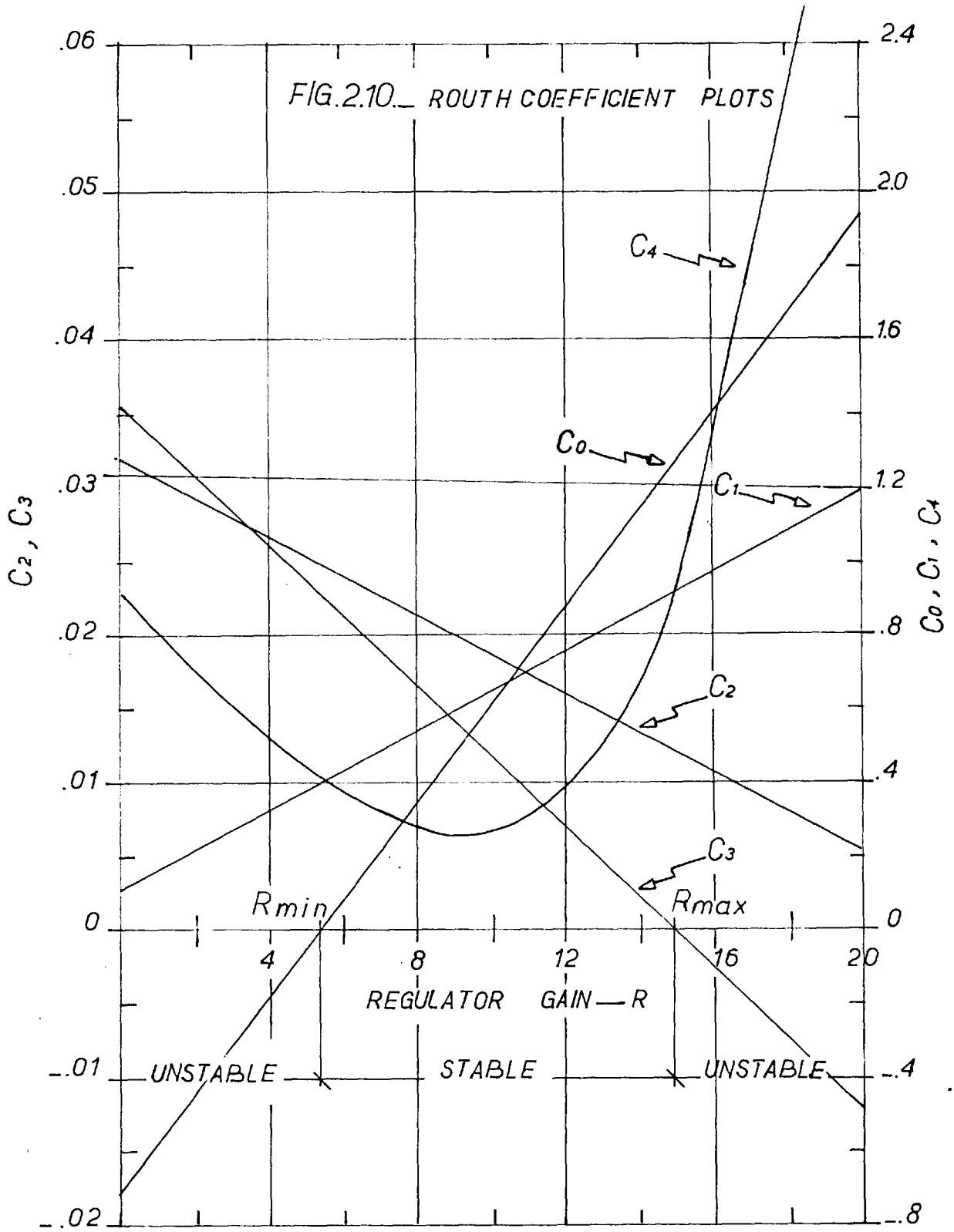
FIG. 2.10 — ROUTH COEFFICIENT PLOTS
.06
.05
.04
.03
.02
.01
0
-.01
-.02
2.4
2.0
1.6
1.2
.8
.4
0
-.4
-.8
C2, C3
Co, C1, C4
C4
Co
C1
C2
C3
Rmin
Rmax
4
8
12
16
20
REGULATOR GAIN — R
UNSTABLE
STABLE
UNSTABLE

2.3.5 Stability Limit Curves

Fig. 2.11 shows the theoretical curves for the steady state stability limit of the rotor angle against the regulator gain. These curves are marked 1, 2, 3, 4, 5 and correspond respectively to the field current gain M of 0.00, .001, .002, .003, .004. The curve for M = 0 applies to the condition with voltage feedback only.

The bounded region of these curves corresponds to stable operation. The distinct regions of the stability curves are marked AB, BB, BC, etc. AB is the common region for all the curves and correspond to R(min) . BB is a small region for curves 4 and 5, that is the small extension in stability beyond δ'_s . BC and CD are regions associated with R(max). The CD region is at the greatest value R(max) can have by virtue of the relation in Eqn. (3.32).

A comparative study of the theoretical curves indicate that

1. The BB region can be introduced at the cost of limiting R(max)
2. Curve 2 for M = .001 is an improvement on curve 1 in the BC region, but cannot increase the maximum steady state limit beyond δ'_s.

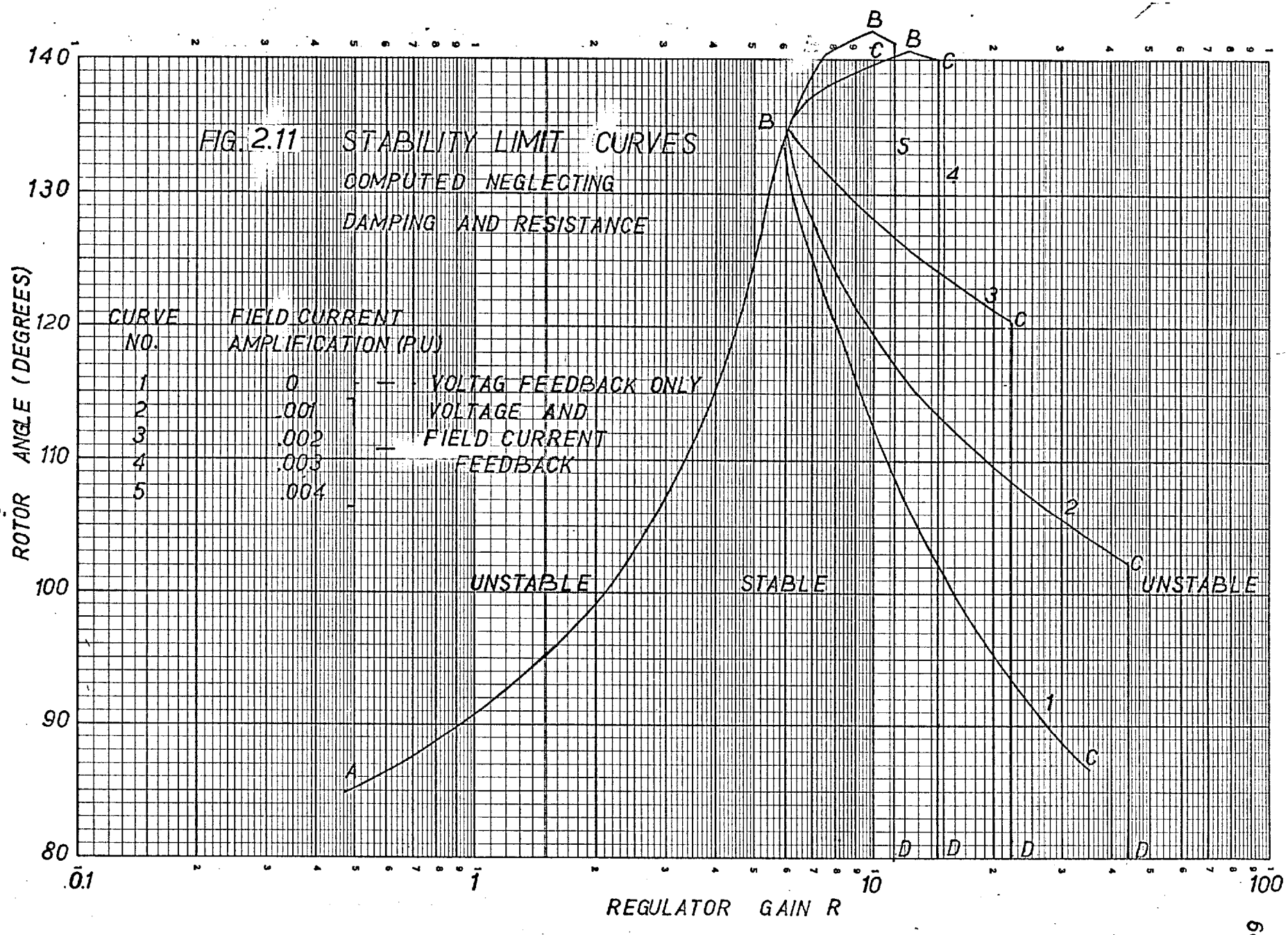
FIG. 2.11 STABILITY LIMIT CURVES
COMPUTED NEGLECTING
DAMPING AND RESISTANCE
CURVE NO.
FIELD CURRENT AMPLIFICATION (P.U)
1 0 — VOLTAG FEEDBACK ONLY
2 .001 VOLTAGE AND
3 .002 — FIELD CURRENT
4 .003 FEEDBACK
5 .004
UNSTABLE
STABLE
UNSTABLE
ROTOR ANGLE (DEGREES)
140
130
120
110
100
90
80
.01
1
10
100
REGULATOR GAIN R

3. Curve 3 for $M = .002$ can give greater limiting δ for the same gain than to curves 1 and 2, but the gain range is decreased. For $M > .002$ the gain range is considerably reduced.

2.4 Convergence of the Direct-axis Regulated Power-var Characteristic Curve at Zero Power

In Fig. 1.1 curve b shows the steady state stability limit relation between Power and Vars for a direct-axis regulated system in general. It is shown to converge at point A at zero power, thus implying that the steady state reactive absorption limit is $-V^2Y_q$ irrespective of the direct-axis excitation regulation. The proof of this is given below.

Let $R(p)$ be the general regulator transfer function acting on any number of feedbacks originated in any manner from the system. The basis for formulation of the system in general terms is laid in Sect. 2.2. Fig. 2.1 shows only two feedbacks, but using different sets of $A_r(p)$, $(r=1,2,3)$ transfer functions any number of feedbacks can be represented on the same figure. Using the transfer functions $B_r(p)$ and $A_r(p)$, ..., $(r=1,2,3)$, the characteristic Eqn. (2.16) in general

terms becomes

$$\text{Numerator of } [1+R(p) \sum_{r=1}^{3} (A_r(p)+A'_r(p)+A''_r(p)+---)B_r(p) \ ] = 0 \qquad (2.34)$$

Two typical sets of transfer functions $A_r(p)$ and $A'_r(p)$ for the voltage and field current feedbacks are given by Eqns. (2.5) and (2.8a) respectively. The alternator transfer functions $B_r(p)$ are given by Eqn. (2.3).

For zero power the steady state value of δ_o, I_{qo} and V_{do} are zero and $V_{qo} = V$. In order to reach a conclusion of practical significance resistance and damping are neglected. The transfer functions $B_r(p)$ given by Eqn. (2.3) then reduce to:

$$\left.\begin{aligned} B_1(p) &= (Q_o+V_{qo}{}^2Y_q+Jp^2)\ \frac{Y_d}{D(p)} \\ B_2(p) &= 0 \\ B_3(p) &= 0 \end{aligned}\right\} \quad - - - \quad (2.35)$$

In general the coefficients of $D(p)$ are given in Eqn. (IV.5). Under the simplified assumptions mentioned above and zero power condition the coefficients d_4, d_3, d_2, d_1, d_o associated with p^4, p^3, p^2, p^1, p^o respectively are:

$$d_4=0\ ,\ d_3=T'_d J\ ,\ d_2=J\ ,\ d_1=T'_d(Q_o+V_{qo}{}^2Y_q)\ \text{and}\ d_o=(Q_o+V_{qo}{}^2Y_q) \tag{2.36}$$

yielding, $D(p) = d_3p^3+d_2p^2+d_1p+d_o$. Substituting the expressions for $B_r(p)$, $(r=1,2,3)$, given by Eqn. (2.35) in Eqn. (2.34), the characteristic equation reduces to

$$\text{Numerator of } [1+R(p)\ (\frac{(Q_o+V_{qo}Y_q+Jp^2).Y_d}{D(p)}.(A_1(p)+A'_1(p)+A''_1(p)+ \ldots\ldots)) \ ] \tag{2.37}$$

In Eqn. (2.37) let

$$R(p)[A_1(p)+A'_1(p)+A''_1(p)+\ldots]Y_d = \frac{a_np^n+a_{n-1}p^{n-1}+\ldots\ldots a_2p^2+a_1p+a_o}{b_mp^m+b_{m-1}p^{m-1}+\ldots\ldots b_2p^2+b_1p+b_o} \tag{2.38}$$

where m and n are integers.

This formulation could cover any transfer function of R(p) and any feedback transfer functions $A_1(p)$, $A'_1(p)$, $A''(p)$ ..... Thus the characteristic equation (2.37) becomes

$$[d_3p^3+d_2p^2+d_1p+d_o][b_mp^m+b_{m-1}p^{m-1}+\ldots\ldots b_1p+b_o] +$$

$$[Q_o+V_{qo}{}^2Y_q+Jp^2][a_np^n+a_{n-1}p^{n-1}+\ldots\ldots a_1p+a_o] = 0 \tag{2.39}$$

Substituting the values of the coefficients d_2 , d_1 , d_o from Eqn. (2.36) in Eqn. (2.39), the three lowest order terms are

$$---- + [J(b_o+a_o)+(b_1T'_d+b_2+a_2)(Q_o+V_{qo}{}^2Y_q)]p^2 + (b_oT'_d+b_1+a_1)(Q_o+V_{qo}{}^2Y_q)p + (a_o+b_o)(Q_o+V_{qo}{}^2Y_q) = 0 \quad (2.40)$$

Eqn. (2.40) reveals that the reactive absorption term $(Q_o+V_{qo}{}^2Y_q)$ appears in product form with the coefficients of p^o and p . This factor changes sign from +ve to -ve when the reactive absorption (Q_o) is increased, thus, making the characteristic equation (2.40) unstable at the limiting value of $Q_o+V_{qo}{}^2Y_q = 0$, i.e. at the reactive absorption limit of $-V_{qo}{}^2Y_q$ (which is the same as $-V^2Y_q$ because $V_{qo} = V$). The above deduction can be generalised as follows.

The steady state limit of reactive absorption cannot be increased beyond $-V^2Y_q$ $(-V_{qo}{}^2Y_q)$ at zero power by direct-axis regulation whatever the regulator transfer function, or the nature of the feedback or feedbacks used.

CHAPTER 3

3. THEORY OF QUADRATURE-AXIS REGULATION

3.1 General

In Sect. 2.4 it is shown that at zero power the direct-axis regulation cannot extend the steady state reactive absorption limit beyond $-V^2Y_q$ irrespective of the regulator transfer function. The direct-axis regulator effectively reduces the direct-axis synchronous reactance, and the question arises whether the quadrature-axis regulation can similarly reduce the effective quadrature-axis synchronous reactance and provide reactive absorption beyond $-V^2Y_q$ at zero power. A theoretical investigation using various signals to regulate the quadrature-axis excitation, is explained in the present chapter.

3.2 The System Equations

3.2.1 The Machine Equations

The addition of a quadrature-axis field winding does not alter the basic structure of the machine equations (see Appendix I), but only the expression for the quadrature-axis flux linkages ψ_q is modified by

adding a term with v_{fq}.

$$\psi_q = \frac{X_q(p)}{\omega} i_q + \frac{G_q(p)}{\omega} v_{fq} \qquad \text{(I-6)}$$

where

$$G_q(p) = \frac{(1+T_{kq}\ p)}{(1+T'_{qo}\ p)(1+T''_{qo}\ p)} \cdot \frac{X_{mq}}{r_{fq}}$$

and corresponds to $G(p)$ in Eqn. (I-5) for the direct-axis field winding. Due to the extra rotor circuit on the quadrature-axis the operational impedance is modified by introducing extra time constants T'_{qo} and T'_{q}. Hence

$$x_q(p) = \frac{(1+T'_q\ p)(1+T''_q\ p)}{(1+T'_{qo}p)(1+T''_{qo}p)} \cdot X_q$$

Making the same assumptions as for the direct-axis field winding machine in Sect. 2.2.1. but allowing for variations of the quadrature-axis field voltage the following small oscillation equations are deduced. The direct axis field voltage is constant and $\Delta v_{fd} = 0$.

$$\begin{bmatrix} 0 \\ 0 \\ G_q(p)\,\Delta v_{fq} \end{bmatrix} = \begin{bmatrix} -X_d(p) & v_{do} & r_a \\ -\frac{1}{2}v_{do}+r_a i_{do} & -(Q_o+Jp^2) & -v_{qo}+r_a i_q \\ -r_a & -v_{qo} & X_q(p) \end{bmatrix} \begin{bmatrix} \Delta i_d \\ \Delta\delta \\ \Delta i_q \end{bmatrix} \tag{3.1}$$

For the one input Δv_{fq} considered there are three outputs Δi_d , $\Delta\delta$ and Δi_q . Inversion of the matrix (3.1) gives the following operational relations between the input and output quantities.

$$B_{q1}(p) = \frac{\Delta i_d}{\Delta v_{fq}} = \frac{G_q(p)Y_q(p)}{D'(p)} \left[-V_{do}V_{qo}+r_a(Q_o+Jp^2+2V_{do}I_{qo})Y_d(p)\right]$$

$$B_{q2}(p) = \frac{\Delta\delta}{\Delta v_{fq}} = \frac{G_q(p)Y_q(p)}{D'(p)} \left[\frac{1}{2}\left(V_{qo}-r_a(2I_{qo}-V_{do}Y_d(p)+2I_{do}Y_d(p))\right)\right] \tag{3.2}$$

$$B_{q3}(p) = \frac{\Delta i_q}{\Delta v_{fq}} = \frac{G_q(p)Y_q(p)}{D'(p)} \left[Q_o+Jp^2+V_{do}{}^2Y_d(p)-2r_a I_{do}V_{do}Y_d(p)\right]$$

where

$$D'(p) = -[Q_o+Jp^2+V_{qo}{}^2Y_q(p)+V_{do}{}^2Y_d(p)-2r_a(V_{qo}I_{qo}Y_q(p) + V_{do}I_{do}Y_d(p))+r_a{}^2(V_{do}I_{qo}-V_{qo}I_{do}+Jp^2)] \qquad (2.4)$$

and

$$G_q(p)Y_q(p) = \frac{X_{mq}}{r_{fq}} \frac{(1+T_{kq}p)}{(1+T'_{qo}p)(1+T''_{qo}p)}$$

When the expression of $G_q(p)Y_q$ is substituted in Eqn. (3.2) for later use of the expression $B_{qr}(p)$, (r = 1,2,3),

1. the constant term $\frac{X_{mq}}{r_{fq}}$ is ignored and is later treated merged with the regulator gain.
2. the denominator terms are merged, i.e.

$$D_q(p) = D'(p)(1+T'_qp)(1+T''_qp) \qquad (3.33)$$

3. the negative sign associated with $D'(p)$ is omitted and later, instead of assigning negative numerical values because of the sign convention to the regulator gain R_q , that is also taken positive, (See also Sect. 2.2).

The operational relations $B_{qr}(p)$, $(r=1,2,3)$, are referred to as the alternator transfer functions and are indicated on the block diagram in Fig. 3.1.

3.2.2 Feedback Quantities

Any feedback from within the system has a definite relation with the alternator output quantities. Any feedback signal Δv_{fbq} for small changes in the quadrature-axis is given by the following relation, which has the same form as in Eqn. (2.4a) or (2.4b) for the direct-axis.

$$\frac{\Delta v_{fbq}}{\Delta v_{fq}} = F_{q1}(p) = \sum_{r=1}^{3} B_{qr}(p).A_r(p) \qquad (3.4)$$

The transfer functions $A_r(p)$, $(r = 1,2,3)$, are indicated on Fig. 3.1. Eqn. (3.4) indicates only one feedback quantity, but to maintain generality any number of feedbacks are included in the following equation

$$\frac{\Delta v_{fbq}}{\Delta v_{fq}} = F_{q1}(p) + F_{q2}(p) + \ldots \qquad (3.5)$$

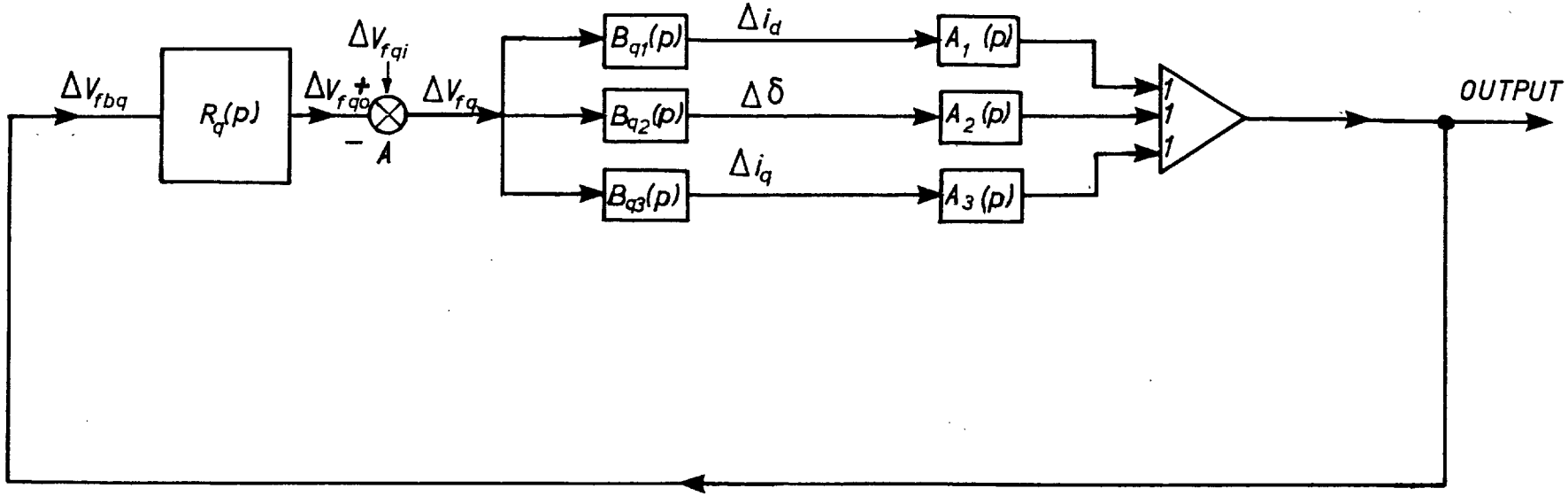

FIG. 3.1. BLOCK DIAGRAM FOR QUADRATURE—AXIS EXCITATION CONTROL

3.2.3. The Open-Loop Transfer Function and the Characteristic Equation

The total feedback signal Δv_{fbq} is operated on by the regulator function $R_q(p)$ before being fed to the quadrature-axis field winding. If the loop were open at A (see Fig. 3.1), then open-loop transfer function $L_q(p)$ would be

$$L_q(p) = \frac{\Delta v_{fqo}}{\Delta v_{fq}} = R_q(p)[F_{q1}(p) + F_{q2}(p) + \ldots] \quad (3.6)$$

For the system represented by Eqn.(3.6) the characteristic equation is

$$\text{Numerator of } [1 + L_q(p)] = 0 \quad (3.7)$$

3.3 Quadrature-axis Regulation with Various Signals

The idea here is to try various signals for regulating the quadrature excitation and theoretically examine whether they help in increasing the steady state limit of reactive absorption at light load. The usefulness of any signal can most easily be examined at zero load, since the system equations are simplified because the steady state values of the variables δ_o , I_{qo} , V_{do}

become zero and $V_{qo} = V$. In order to get simplified conclusions of practical significance the equations are further simplified by neglecting resistance and damping. The conclusion as to the usefulness of a signal is reached by studying the contribution of the feedback to the coefficients of the characteristic equation.

3.3.1 The Unregulated System

For the unregulated system $R_q(p) = 0$ and the characteristic equation (3.7) for zero power condition in the expanded form becomes:

$$D_q(p) = T'_q J\, p^3 + Jp^2 + T'_q(Q_o+V_{qo}{}^2Y'_q)p + Q_o+V_{qo}{}^2Y_q = 0 \qquad (3.8)$$

When the reactive absorption is increased the term $Q_o+V_{qo}{}^2Y_q$ in Eqn. (3.8) will eventually become negative and will establish the unstable mode. Thus Eqn. (3.8) gives $Q_o = -V_{qo}{}^2Y_q$ $(= -V^2Y_q)$ as the limiting value of negative vars. This is a well known condition. For the experimental machine this limit of negative vars is 0.517 p.u.

3.3.2 Terminal Voltage Feedback at Zero Power

The terminal voltage feedback in conjunction with the regulator of general transfer function $R_q(p)$ is considered. The transfer functions $A_r(p)$, (r=1,2,3), for the small changes of terminal voltage are given by Eqn. (2.5). For the zero power condition they become:

$$\left.\begin{aligned} A_1(p) &= (X_c I_{do} + V_{qo}) \frac{X_c R_e}{V_{to}} \\ A_2(p) &= 0 \\ A_3(p) &= 0 \end{aligned}\right\} \qquad (3.9)$$

The alternator transfer function $B_{q1}(p)$, $B_{q2}(p)$ and $B_{q3}(p)$ given by Eqn.(3.2) become:

$$\left.\begin{aligned} B_{q1}(p) &= 0 \\ B_{q2}(p) &= \frac{V_{qo} Y_q}{\sqrt{2}\, D_q(p)} \\ B_{q3}(p) &= \frac{Q_o + Jp^2 Y_q}{D_q(p)} \end{aligned}\right\} \qquad (3,10)$$

Using Eqns. (3.4), (3.6) and (3.7) the characteristic equation in the expanded form becomes

$$\text{Numerator of } [1+R_q(p)\ \{B_{q1}(p).A_1(p) + B_{q2}(p)A_2(p) + B_{q3}(p).A_3(p)\}\ ] = 0 \qquad (3.11)$$

Substituting the expressions of $B_{qr}(p)$ and $A_r(p)$, (r=1,2,3), from Eqns. (3.9) and (3.10), the characteristic Eqn. (3.11) yields

$$D_q(p) = 0$$

which is the characteristic equation (3.8) for the unregulated system, whatever the regulator transfer ... function may be. Thus the terminal voltage feedback cannot increase the steady state reactive absorption limit beyond that of the unregulated system, irrespective of the regulator transfer function.

3.3.3 Resolved Component Feedback at Zero Power

Instead of making composite feedback quantities out of the fundamental alternator output quantities, which are the resolved components in the two axis theory, the effect of individual component feedback in conjunction with a general regulator function $R_q(p)$ is investigated in the following sections.

3.3.3.1. Feedback of I_d

From the substitution of Eqns. (3.9) and (3.10) in Eqn. (3.11) one can deduce that an effective signal must be such that $A_2(p)$ and $A_3(p)$ are not both zero. For a straight feedback of signal I_d the transfer functions $A_r(p)$, (r=1,2,3) , are:

$$\left.\begin{aligned} A_1(p) &= 1 \\ A_2(p) &= 0 \\ A_3(p) &= 0 \end{aligned}\right\} \qquad (3.12)$$

Hence a signal I_d is ineffective.

3.3.3.2 Feedback of I_q

If the feedback depends on I_q the transfer function $A_r(p)$, (r=1,2,3) , are

$$\left.\begin{aligned} A_1(p) &= 0 \\ A_2(p) &= 0 \\ A_3(p) &= 1 \end{aligned}\right\} \qquad (3.13)$$

Substituting the transfer functions $A_r(p)$ and $B_r(p)$,

(r=1,2,3) from Eqns. (3.13) and (3.10) in the characteristic Eqn. (3.11) we have

$$D_q(p) + R_q(p)[(Q_o+Jp^2)Y_q] = 0 \qquad (3.14)$$

Depending on the regulator transfer function $R_q(p)$ Δi_q feedback causes the characteristic equation to differ from the unregulated value, $D_q(p)$. However, since the term Q_oY_q is negative when the vars are negative it is not a stabilising signal, and also it changes sign from positive to negative vars, which makes it undesirable. However it could be mixed with other feedbacks for special purposes.

3.3.3.3 Rotor Angle Feedback

For the rotor angle feedback the transfer function $A_r(p)$, (r=1,2,3), are as follows

$$\left.\begin{aligned} A_1(p) &= 0 \\ A_2(p) &= 1 \\ A_3(p) &= 0 \end{aligned}\right\} \qquad (3.15)$$

Substituting $A_r(p)$ and $B_{qr}(p)$, (r=1,2,3) , from

Eqn. (3.15) and Eqn. (3.10) respectively in Eqn. (3.11) the characteristic equation for the rotor angle feedback is

$$D_q(p) + R_q(p).(\tfrac{1}{\sqrt{2}}\, V_{qo}\, Y_q) = 0 \qquad (3.16)$$

This is the most effective feedback signal because $V_{qo}\, Y_q$ is always positive and, depending on the design of $R_q(p)$, the feedback term $R_q(p)\, \frac{1}{\sqrt{2}} V_{qo} Y_q$ can stabilise the system by modifying the various coefficients of $D_q(p)$. It can be concluded that the system represented by $D_q(p) = 0$ which is, unstable for reactive absorption greater than $-V^2 Y_q$ when there is no regulator, can now be stabilised by the feedback term $R_q(p)\, \frac{1}{\sqrt{2}}\, V_{qo} Y_q$. The detailed investigation is carried out in the subsequent sections.

3.4 Equilibrium Diagram With the Angle Regulator for the Quadrature Winding

For any possible operating condition, that is, any point on the Power-Var chart of Fig. 1.1, a vector diagram referred to as an 'equilibrium diagram' can be drawn but the system may or may not be stable. With a

fixed direct-axis field the system is stable at lagging power factor but is unstable at negative values of Q beyond the steady state limit line 'a_1' or 'a_2' on Fig. 1.1. Stable operation beyond the limit line 'a' can however be obtained by using a signal derived from the rotor angle for regulating the quadrature field winding, see Sect. 3.3.3.3.

Fig. 3.2a shows the equilibrium diagram of a conventional synchronous machine with direct-axis field and connected to a fixed supply. To maintain equilibrium the rotor angle δ swings round to an appropriate value. When a quadrature field winding is used as in Fig. 3.2b, the angle can be held at zero if a suitable control is used, because the quadrature field winding can provide the component of excitation required for equilibrium. Fig. 3.2b indicates a condition at leading power factor.

The salient features of the equilibrium condition shown in Fig. 3.2b are:

1. the rotor angle δ is zero
2. the infinite bus (reference) voltage is always in the quadrature-axis, and from Eqns. (I-1) and (I-2) we have

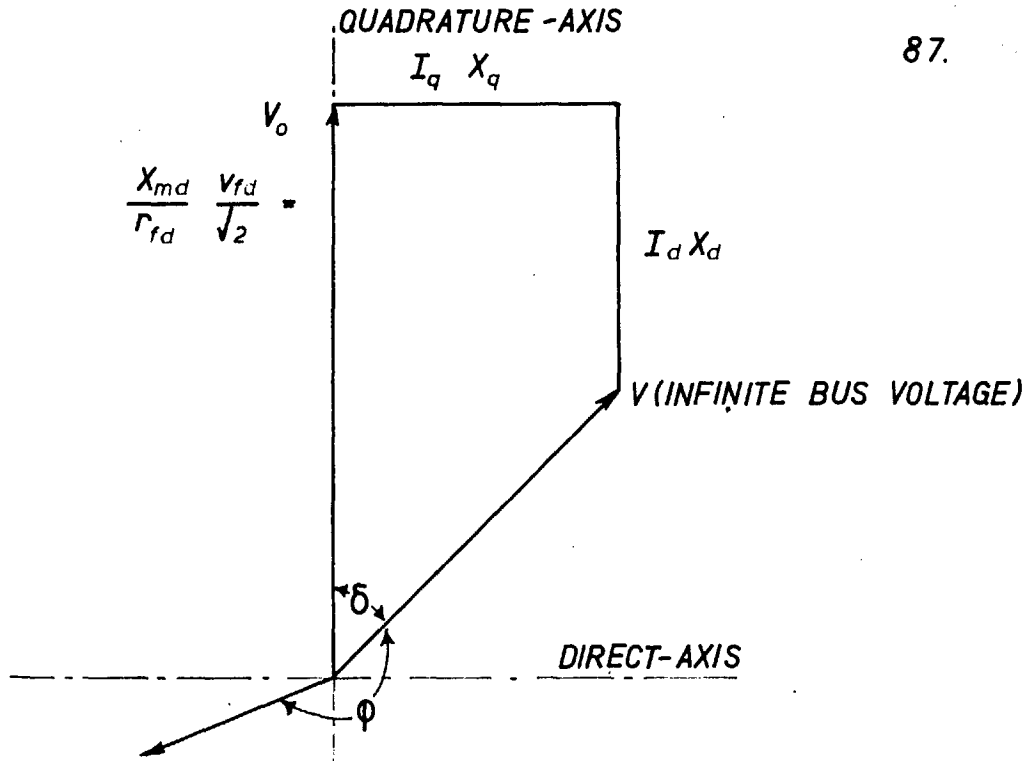

FIG. 3.2a

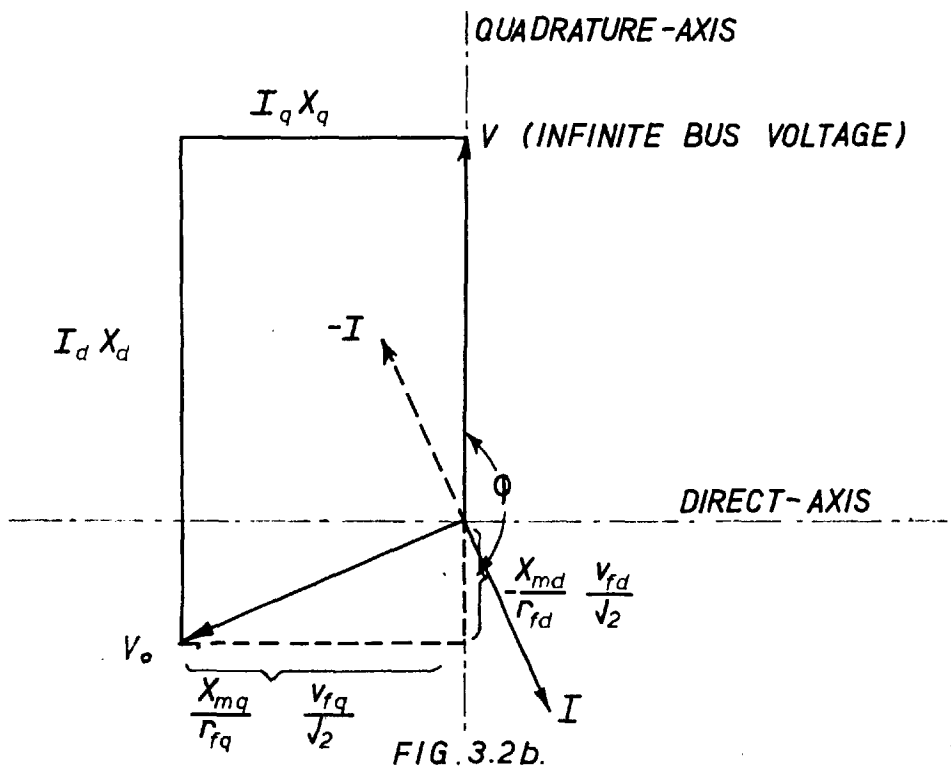

FIG. 3.2b.

FIG. 3.2 EQUILIBRIUM DIAGRAMS FOR A SYNCHRONOUS MACHINE.

a with conventional Direct-axis excitation

b with Direct and quadrature excitations.

$$\left.\begin{aligned} V_{do} &= 0 \\ V_{qo} &= V \end{aligned}\right\} \qquad (3.17)$$

3. Using Eqn. (I-1) and Eqn. (I-6) we have

$$I_{qo}X_q = \frac{X_{mq}}{r_{fq}} \cdot \frac{v_{fq}}{\sqrt{2}} \qquad (3.18)$$

4.
$$\left.\begin{aligned} P_o &= V_{qo}I_{qo} = VI_{qo} \\ Q_o &= V_{qo}I_{do} = VI_{do} \end{aligned}\right\} \qquad (3.19)$$

5. Using Eqns. (3.18) and (3.19) we have

$$P_o \propto \frac{v_{fq}}{r_{fq}} \propto I_{fq} \qquad (3.20)$$

3.5 Theoretical Determination of Stability for the Quadrature Angle Regulator

In this section a detailed analysis is carried out to determine the steady state reactive absorption limits for different types of regulators. The steady state stability limits are determined by application of the Nyquist criterion using the frequency response values of the system open-loop transfer function calculated by an IBM computer. For detailed analysis the Nyquist criterion is preferred to the root-locus technique as used in Sect. 2 for reasons given in Sect. 1.1, however, the

coefficients of simplified characteristic equations are used at times to make some general deductions. It was found that a regulator using first and second derivatives along with the proportionate term can be used to extend considerably the steady state reactive absorption limit as well as to extend the range of regulator gain. The question of the effect of damping and resistance on the steady state limits is also given some consideration.

3.5.1 The Proportionate Regulator

This section gives the analysis of the system with a proportionate regulator, the transfer function of which is an adjustable constant R_q . Throughout the analysis R_q is referred to as the regulator gain, although some constant terms of the open-loop transfer function are considered merged with R_q , Sect. 6.4.

The filter circuits used with the angle signal introduce some delay but this is ignored in the first instance. The proportionate regulator analysis is first made with the angle device transfer function as a constant in order to make some simple deductions. Later the complete angle device transfer function is used in a detailed analysis. The angle device with a constant transfer function 'k_1' is referred to as an 'ideal

angle device' and with its proper transfer function as a 'practical angle device'. The constant k_1 is merged with R_q as explained in Sect. 6.4.

3.5.1.1 With Ideal Angle Device

Under the ideal condition considered the open-loop transfer function of the system (see Fig. 1.3) is

$$L_q(p) = R_q(p).B_{q2}(p)$$

$$= \frac{R_q \frac{1}{\sqrt{2}} V_{qo} Y_q}{JT'_q p^3 + Jp^2 + T'_q(Q_o+V_{qo}^2 Y'_q)p+Q_o+V_{qo}^2 Y_q} \quad (3.21)$$

For a given value of Q_o the transfer function given by Eqn. (3.21) remains unchanged for any power, because it does not contain any terms dependent on I_{qo} (see Eqn. (3.19)) or P_o . Therefore, the steady state stability limit curves obtained in the following sections are valid for any power level.

3.5.1.1.1 Application of the Nyquist Criterion for a Qualitative Assessment

In Fig. 3.3 are shown diagramatic Nyquist plots for $L_q(j\omega)$ given by Eqn. (3.21) with p replaced by

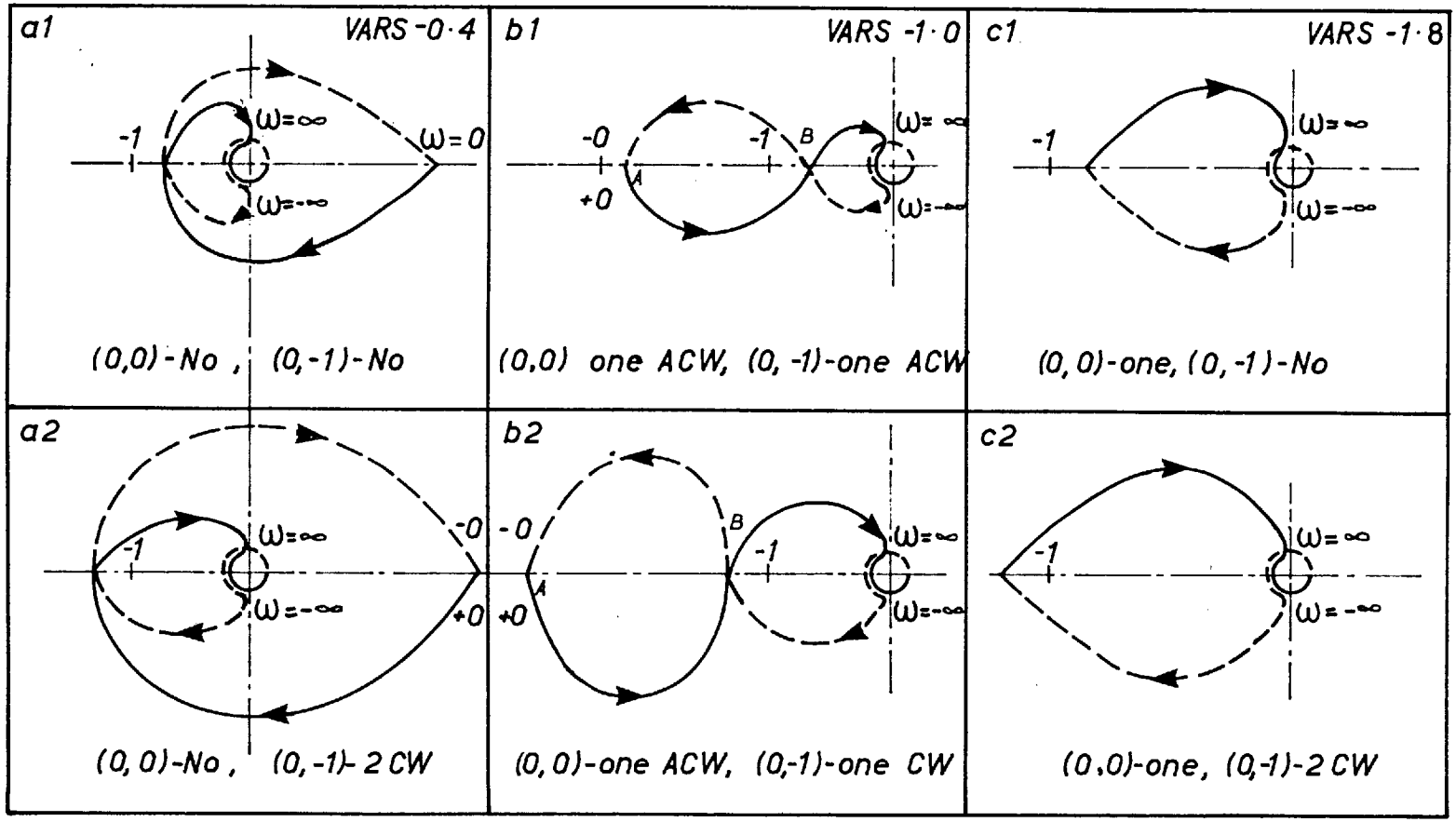

CW ⇒ Clockwise ACW ⇒ Anticlockwise

(0,0)-one ACW, etc. ⇒ Encirclement around (0,0) one time etc.

FIG. 3.3 DIAGRAMATIC NYQUIST PLOTS FOR $L_q(p)$, EQN. (3.21)

$j\omega$, plotted as explained in Appendix V.3. Figs. 3.3a, 3.3b, 3.3c are for -0.4, -1.0, -1.8 p.u. vars respectively. Fig. 3.3a1 for $R_q = 1$ indicates no-net encirclement around (0,0), since there is no zero of $L_q(p)$ in the R.H. p-plane. At -0.4 p.u. vars it is true because $Q_o + V_{qo}^2 Y_q > 0$. However, if the gain R_q is increased as in Fig. 3.3a2 the Nyquist plot encircles the (0,-1) point twice clockwise indicating two roots of the characteristic equation in the R.H. p-plane. Thus at high gains the system is rendered unstable when it would be stable without regulation. Vars = -0.4 p.u. is a typical case such that $Q_o + V_{qo}^2 Y_q > 0$.

Fig. 3.3b1 for vars = -1.0 p.u. shows one net encirclement of (0,0) indicating one pole of $L_q(p)$ in the R.H. p-plane. This is because $Q_o + V_{qo}^2 Y_q < 0$, in this respect Fig. 3.3b1 is representative of cases where $Q_o \leq - V_{qo}^2 Y_q$. The gain R_q in Fig. 3.3b is such that (0,-1) is also enclosed once anticlockwise, thus representing a stable system according to the Nyquist criterion (Appendix V.3). In Fig. 3.3b2 the regulator gain is large and the Nyquist plot encircles the (0,-1) point once clockwise disclosing the existence of two roots of the characteristic equation in the R.H.

p-plane. There are two roots in the R.H. p-plane for one net clockwise encirclement of (0,-1) because there is already a pole of $L_q(p)$ in the R.H. p-plane. According to the Nyquist criterion the system is unstable. The regulator, therefore, stabilises the system over a finite range of gain. For vars = -1.8, R_q = 1 Fig. 3.3c1 shows one net anticlockwise encirclement around (0,0) as expected because of $Q_o < -V_{qo}{}^2 Y_q$. In Fig. 3.3c2 when R_q is sufficiently increased to enclose the (0,-1) point, the plot encloses the (0,-1) point once, the system according to the Nyquist criterion is unstable and the adjustment of gain cannot make the plot encircle (0,-1) anticlockwise once to stabilise it. The diagram shows the limitation of proportionate regulation.

3.5.1.1.2 Application of the Nyquist Criterion for Quantitative Assessment

The Nyquist plots for $L_q(j\omega)$ obtained from Eqn. (3.21) with unity regulator gain for -0.4, -1.0, -1.6, -1.8 p.u. vars are shown in Fig. 3.4. The plots show only the curves for positive frequencies. The zero frequency point is marked 'A' and the point where the Nyquist plot cuts the negative real axis is marked

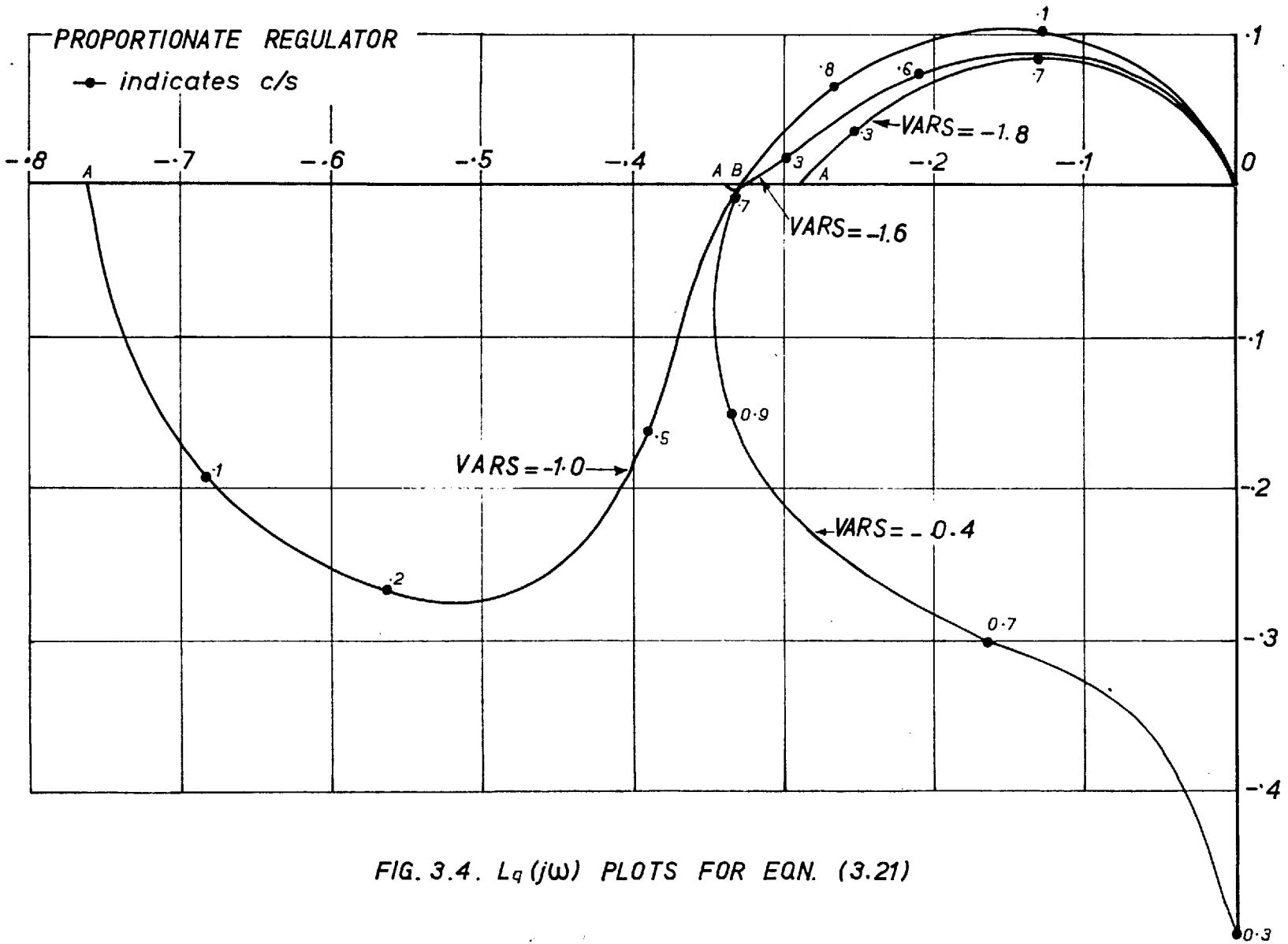

FIG. 3.4. $L_q(j\omega)$ PLOTS FOR EQN. (3.21)

'B'. The zero frequency point for -0.4 p.u. vars is off the diagram in the R.H. p-plane.

For reactive absorption greater than $V_{qo}^2 Y_q$ the minimum regulator gain $R_q(\min)$ required to stabilise the system is given when the zero frequency point 'A' just crosses the (0,-1) point (see Sect. 3.5.1.1.). Substituting these conditions in Eqn. (3.21) we have

$$-1 = \frac{\frac{1}{\sqrt{2}} V_{qo} R_q(\min)}{Q_o + V_{qo}^2 Y_q}$$

or

$$R_q(\min) = - \frac{Q_o + V_{qo}^2 Y_q}{\frac{1}{\sqrt{2}} V_{qo} Y_q} \qquad (3.22)$$

For $Q_o > - V_{qo}^2 Y_q$, $R_q(\min) = 0$, because the system is stable without feedback.

The maximum permissible regulator gain $R_q(\max)$ limit is reached when point B just crosses the (0,-1) point, see Sect. 3.5.1.1.1. To satisfy this condition the imaginary part of the denominator of $L_q(j\omega)$ (Eqn. (3.21)) should be zero and amplitude equal to 1. Equating the imaginary part to zero also yields the natural mode of oscillation (see also Appendix V. 2.1). Using the above condition and Eqn. (3.21) we have

$$-jJ\,T'_q\omega_n^3 + j\,\omega_n T'_q(Q_o+V_{qo}^2 Y'_q) = 0$$

or

$$\omega_n = \sqrt{\frac{Q_o+V_{qo}^2 Y'_q}{J}} \tag{3.23}$$

Substituting $j\omega_n$ $(=p)$ in Eqn. (3.21) and satisfying the amplitude condition we have

$$R_q(\max) = \frac{\frac{1}{\sqrt{2}} V_{qo}(Y'_q - Y_q)}{Y_q} \tag{3.24}$$

Eqn. (3.24) indicates that $R_q(\max)$ is independent of vars and that is why all the Nyquist plots in Fig. 3.4 cross over the negative real-axis at the same point.

If $R_q \leq R_q(\min)$ the unstable mode is of zero frequency resulting in drifting instability and for $R_q \geq R_q(\max)$ the unstable mode has complex frequency, and the instability is oscillatory at the natural frequency ω_n. This statement is generally valid for any $R_q(p)$.

The maximum steady state reactive absorption limit is reached when

$$R_q(\min) = R_q(\max)$$

Using Eqn. (3.22) and Eqn. (3.24) we have

$$Q_o(\max) = -V_{qo}{}^2 Y'_q \qquad (3.25)$$

This limiting point is illustrated in Fig. 3.4 for vars = -1.6 at which the points A and B almost converge into each other. The maximum steady state reactive absorption limit calculated for the practical system is -1.625 p.u. which is an ideal limit. The Nyquist plot at vars = -1.8 p.u. is always unstable, because $Q_o > Q_o(\max)$, (see also Sect. 3.5.1.1.1).

Fig. 3.5 curve is a steady state limit curve showing the reactive absorption against the regulator gain. The system is stable within the bounded region of the curve and is unstable outside it. A similar curve is obtained with any regulator transfer function $R_q(p)$. The curve has two distinct regions marked AB and BC. The region AB is associated with the zero frequency point 'A' and BC with the Nyquist plot cross over point 'B' (see Fig. 3.4). The BC region is a vertical straight line because the point B on the

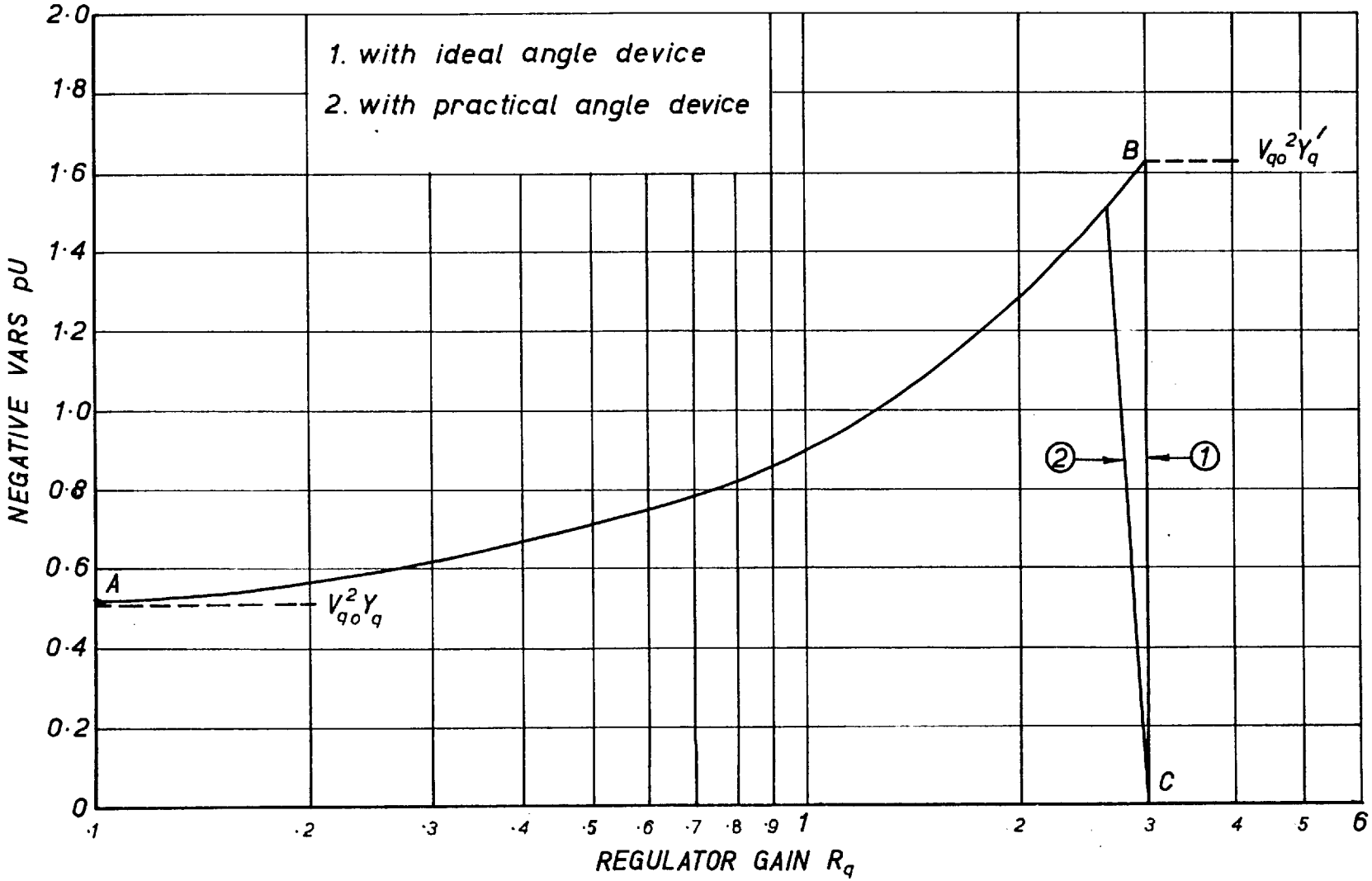

FIG. 3.5. STEADY STATE STABILITY LIMIT CURVES FOR PROPORTIONATE REGULATOR

Nyquist plot does not change its position with vars (see also Eqn. 3.24). If a linear scale was used for R_q the region AB would be a straight line because of the linear relation of $R_q(\min)$ and Q_o in Eqn. (3.22).

3.5.1.2 With a Practical Angle Device

In the previous section the angle device considered was an ideal one transmitting the signal without attenuation or delay. In this section a practical angle device defined by a transfer function is taken. The transfer function of the angle device used is

$$\frac{K_1(1+\tau^2 p^2)}{(Ap^2+Bp+C)(\tau^2 p^2+4\tau p+1)}$$

Numerical values of coefficients A,B,C,τ are given in Sect. 4.3.2.4. For later use of the above expression the constant K_1 is ignored, since it is taken care of by R_q as stated in Sect. 3.5.1 (see also Sect. 6.4). The open-loop transfer function $L_q(p)$ in Eqn. (3.21) becomes

$$L_q(p) = \frac{R_q\left(\frac{1}{2} V_{qo} Y_q\right)}{[J T'_q p^3+Jp^2+T'_q(Q_o+V_{qo}^2 Y'_q)p+(Q_o+V_{qo}^2 Y_q)]} \cdot \frac{(1+\tau^2 p^2)}{(Ap^2+Bp+C)(\tau^2 p^2+4\tau p+1)} \quad (3.26$$

In Fig. 3.6 curves 1 and 2 are typical Nyquist plots for vars = -1.0 p.u. and $L_q(j\omega)$ given by Eqn. (3.21) and Eqn. (3.26). The inclusion of the angle device transfer function modifies the Nyquist plot of $L(p)$ from 1 to 2. The zero frequency point A remains unchanged because at zero frequency the angle device transfer function is unity. However, attenuation and lag is introduced at higher frequencies and the negative axis cross over point B is shifted to B' . In Fig. 3.5 curve 2 shows the steady state stability limit curve along with curve 1 for the regulator with the ideal angle device. The portion AB is common to curves 1 and 2 because the point A on the Nyquist plots does not change. The line BC of curve 2 is no longer vertical and is shifted so that $R_q(max)$ is reduced because point B on the Nyquist plots is shifted to B' . (See Fig. 3.6). The maximum permissible limit is reduced because of the delays of the angle device transfer function and for the system considered the reduced limit $Q_o(max) = -1.53$ p.u.

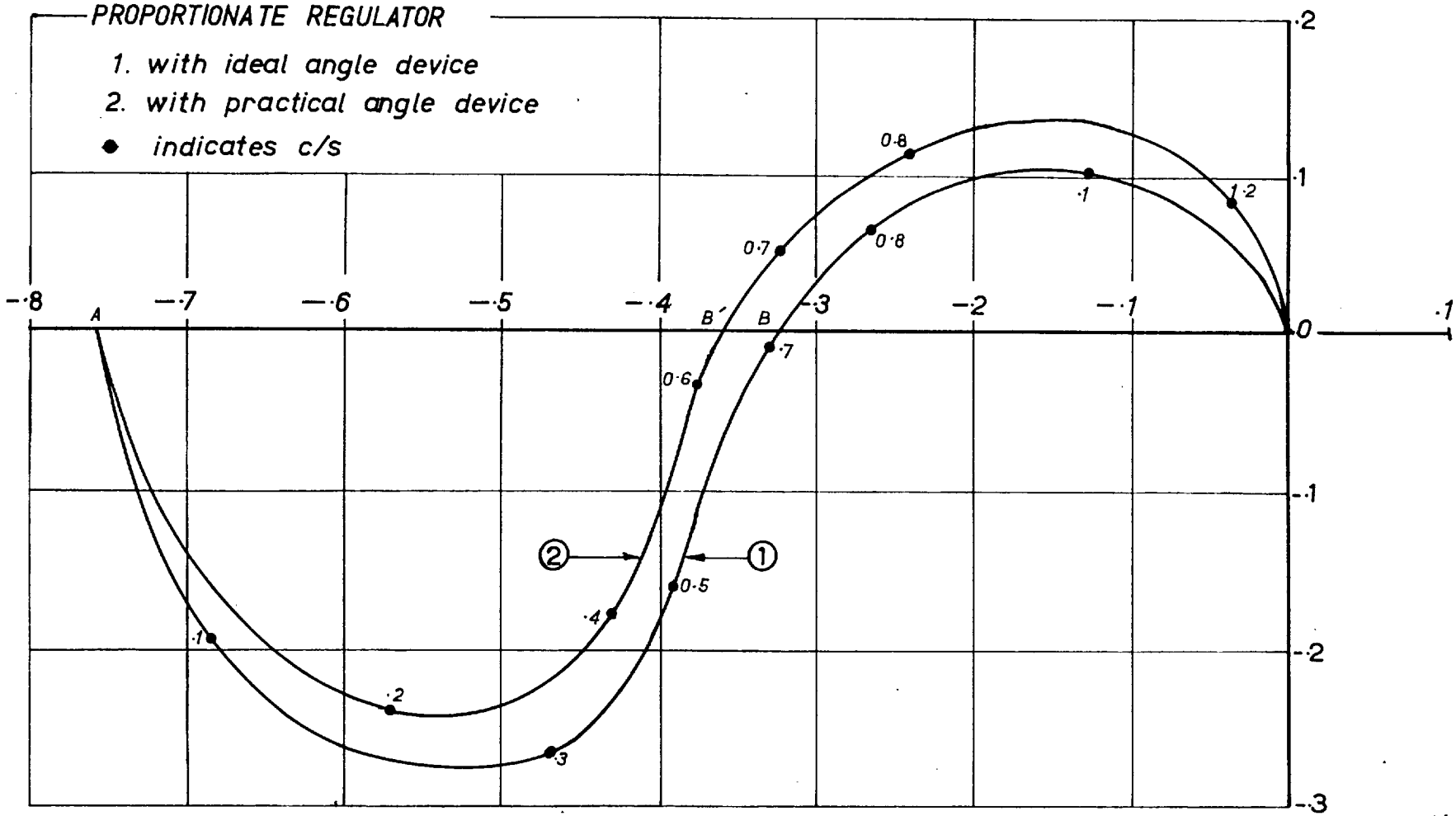

FIG. 3·6. $L_q(j\omega)$ PLOTS AT VARS = -1·0 FOR EQNS. (3.21) AND (3.26)

3.5.2 Regulator with Derivative Feedback

In the previous section the proportionate regulator is shown to increase the steady state reactive absorption to about 1.5 p.u. but the regulator gain margin is poor and leaves a great scope for improvement. The first and second derivative compensations are used in the following sections to increase the steady state limit of reactive absorption further and increase the gain range.

3.5.2.1 Proportionate Regulator with First Derivative

The idea of lead compensation can better be understood by studying the coefficients of the characteristic equation for the proportionate regulator with an ideal angle device. The simplified characteristic equation corresponding to Eqn. (3.21) is

$$\text{Numerator of } [1 + L_q(p)] = 0$$

or

$$T'_q J p^3 + J p^2 + T'_q (Q_o + V_{qo}{}^2 Y'_q) p + Q_o + V_{qo}{}^2 Y_q + R_q (\tfrac{1}{2} V_{qo} Y_q) = 0 \qquad (3.27)$$

As R_q varies the term $Q_o+V_{qo}^2 Y_q+R_q(\frac{1}{\sqrt{2}}V_{qo}Y_q)$ is kept >0 so that all the roots of the characteristic Eqn. (3.27) are in the L.H. p-plane, but when $(Q_o+V_{qo}^2 Y'_q) \leq 0$ the system is unstable regardless of R_q and the limit is set at $-V_{qo}^2 Y'_q$. However, by including a first derivative term $(Q_o+V_{qo}^2 Y'_q)$ in Eqn. (3.27) can be compensated and the system can be stabilized.

The transfer function of the practical regulator considered is:

$$R_q(p) = R_q \left[1 + \frac{.1\,p}{(1+.01p)(1+.01p)}\right] \qquad (3.28)$$

The open-loop transfer function in Eqn. (3.26) is modified to:

$$L_q(p) = \frac{R_q\,(\frac{1}{\sqrt{2}}V_{qo}Y_q)}{J\,T'_q p^3 + Jp^2 + T'_q(Q_o+V_{qo}^2 Y'_q)p+(Q_o+V_{qo}^2 Y_q)} \times \frac{(1+\tau^2 p^2)}{(\tau^2 p^2+4\tau p+1)(Ap^2+Bp+C)} \times \left[1 + \frac{.1p}{(1+.01p)(1+.01p)}\right] \qquad (3.29)$$

In Fig. 3.7 are shown some typical Nyquist plots for $L_q(j\omega)$ given by Eqn. (3.29) and a corresponding curve

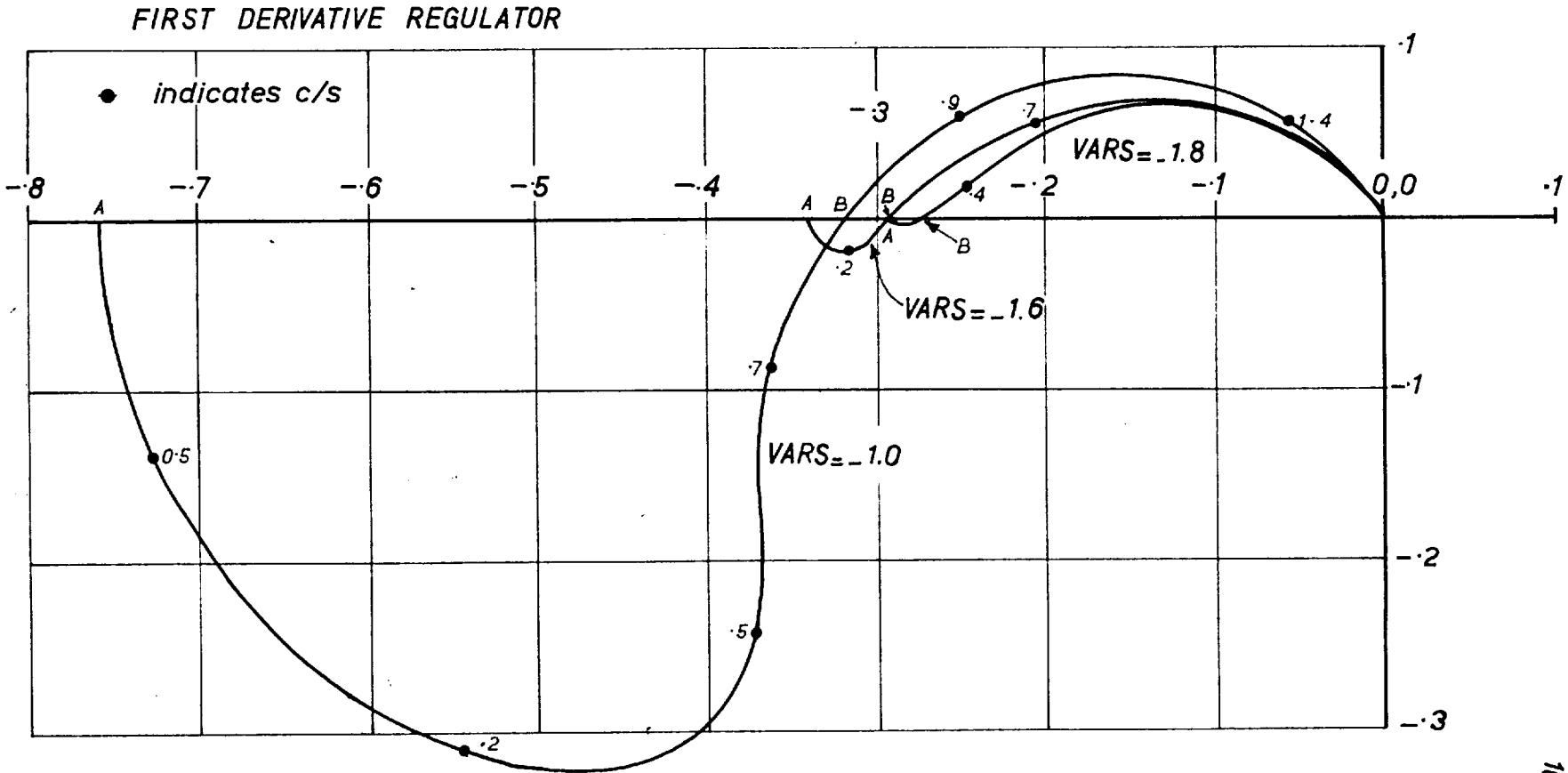

FIG. 3·7. L(jω) PLOTS FOR EQN. (3·29)

showing the steady state limiting value of reactive absorption against the regulator gain is plotted in Fig. 3.8. A study of the Nyquist plots reveals that the first derivative term of the regulator transfer function $R_q(p)$ tries to generate a portion of the curve in between points A and B , for example vars = -1.6, such that for a range of regulator gain it could enclose the (0,-1) point anticlockwise once (see Sect. 3.5.1.1.1.) and thus represent a stable operation; the range of operation is narrow and for the example considered is $2.85 \leq R_q \leq 3.55$. At vars = -1.8 p.u., the points A and B on the Nyquist plot almost converge and represent a case near the maximum reactive absorption limit for this first derivative regulator. In Fig. (3.8) (dotted line) for comparison the steady state reactive absorption limit curve is plotted against the regulator gain for the proportionate regulator with the practical angle device. The maximum reactive absorption limit is raised from -1.52 p.u. to -1.82 p.u. and the maximum permissible gain $R_q(max)$ is raised from 2.65 to 3.6. The line marked BC slopes inwards and hence there is very little increase in the gain margin at values of reactive absorption numerically greater than -1.0 p.u.

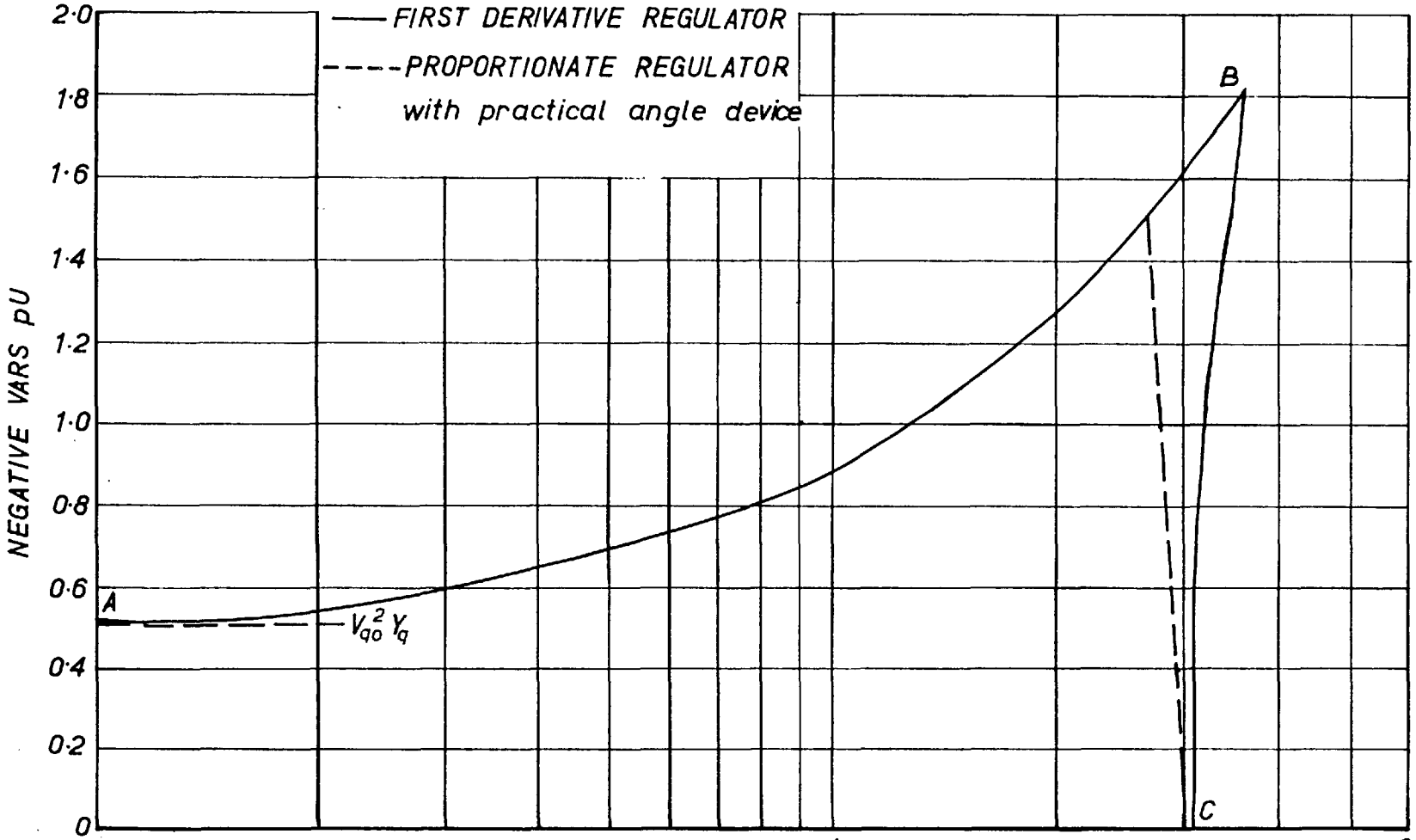

FIG. 3·8. STEADY STATE STABILITY LIMIT CURVES

3.5.2.2 Proportionate Regulator with First and Second Derivative - 'Derivative Regulator'

A regulator with first and second derivative elements is referred to as a 'derivative regulator' in this thesis.

It has been shown in Sect. 3.5.2.1 that the first derivative term helps to improve stability and it would be expected that the inclusion of second derivative would improve it further. The way in which the second derivative increases the stability range can be seen by studying the coefficients of the simplified characteristic equation. In obtaining the simplified characteristic equation for the first derivative only the angle device is assumed to be ideal and $R_q(p)$ of Eqn. (3.8) is taken as $R_q(1+.1p)$, thus we have

$$J\,T'_q p^3 + Jp^2 + [T'_q(Q_o+V_{qo}{}^2Y'_q) + .1(\tfrac{1}{\sqrt{2}}V_{qo}Y_q).R_q]\,p +$$

$$Q_o+V_{qo}{}^2Y_q + (\tfrac{1}{\sqrt{2}}V_{qo}Y_q)R_q = 0 \qquad (3.30)$$

For stability in addition to the requirement that all coefficients of Eqn. (3.30) must be >0 the following product inequality must be satisfied (see Appendix V.2)

$$J.\ [T'_q(Q_o+V_{qo}{}^2Y'_q) + .1(\tfrac{1}{\sqrt{2}}V_{qo}{}^2Y_q)R_q] >$$

$$J\ T'_q\ [Q_o+V_{qo}{}^2Y_q+R_q(\tfrac{1}{\sqrt{2}}V_{qo}{}^2Y_q)] \qquad (3.31a)$$

$R_q(\max)$ is established as the limiting value of R_q in the above inequality.

A simplified second derivative term $\tau_1 p^2$ in the regulator transfer function changes its simplified transfer function considered above to:

$$R_q(p) = R_q(1 + .1p + \tau_1 p^2)$$

Consequently the coefficient J associated with p^2 in the characteristic equation (3.30) is modified to

$$J + R_q\ \tau_1(\tfrac{1}{\sqrt{2}}V_{qo}Y_q)\ ,$$

and the new product inequality becomes

$$[J+R_q\tau_1(\tfrac{1}{\sqrt{2}}V_{qo}Y_q)][\ T'_q(Q_o+V_{qo}{}^2Y'_q) + .1(\tfrac{1}{\sqrt{2}}V_{qo}{}^2Y_q)R_q] >$$

$$J.T'_q\ [Q_o+V_{qo}{}^2Y_q+R_q(\tfrac{1}{\sqrt{2}}V_{qo}Y_q)] \qquad (3.31b)$$

In the inequality Eqn. (3.31b) the L.H.S. is modified compared to inequality Eqn. (3.31a) while the R.H.S. remains unchanged. The additional term $R_q\tau_1(\frac{1}{\sqrt{2}}V_{qo}Y_q)$ in the L.H.S. of inequality equation (3.31b) helps to maintain inequality for a longer R_q range and for increased reactive absorption than permissible by the inequality Eqn. (3.31a).

The practical regulator transfer function considered for detailed analysis is as follows

$$R_q(p) = R_q \left[1+ \frac{0.1\,p}{(1+.01p)(1+.01p)} + \frac{.02p^2}{(1+.01p)(1+.01p)(1+.02p)(1+.01p)}\right] \quad (3.32)$$

In the derivative regulator transfer function above, the second derivative is achieved from the first derivative term and the denominator terms are intentionally provided to keep the high frequency noise associated with the angle device output to a reasonable level (see Sect. 4.4.2). The open-loop transfer function allowing for the practical angle device becomes:

$$L_q(p) = \frac{R_q \frac{1}{\sqrt{2}} V_{qo} Y_q}{[J\,T'_q p^3 + Jp^2 + T'_q(Q_o + V_{qo}{}^2 Y'_q)p + (Q_o + V_{qo}{}^2 Y_q)]} \times$$

$$\frac{(1+\tau^2 p^2)}{[\tau^2 p^2 + 4\tau p + 1][Ap^2 + Bp + C]} \times R_q\left[1 + \frac{0.1p}{(1+.01p)(1+.01p)} + \right.$$

$$\left. \frac{.02p^2}{(1+.01p)(1+.01p)(1+.02p)(1+.01p)}\right] \qquad (3.33)$$

In Fig. 3.9 some typical Nyquist plots for $L_q(j\omega)$ given by Eqn. (3.33) are shown and Fig. 3.10 shows the steady state reactive absorption limit curve against the regulator gain. Three distinct regions in Fig. 3.10 are labelled AB, BC and CD . On the same figure are also shown the stability limit curves for the proportionate regulator and first derivative regulator with broken lines with and without crosses. All these curves allow for the practical angle device. The region AB on these curves is common and corresponds to the zero frequency point A in Figs. 3.4 and 3.7. The zero frequency point A for all the Nyquist plots in Fig. 3.9 is off the scale.

In Fig. 3.9 the Nyquist plot for -1.4 p.u. vars is a typical representative of conditions in the region AB. The curve for vars = -0.4 p.u. is a representative of

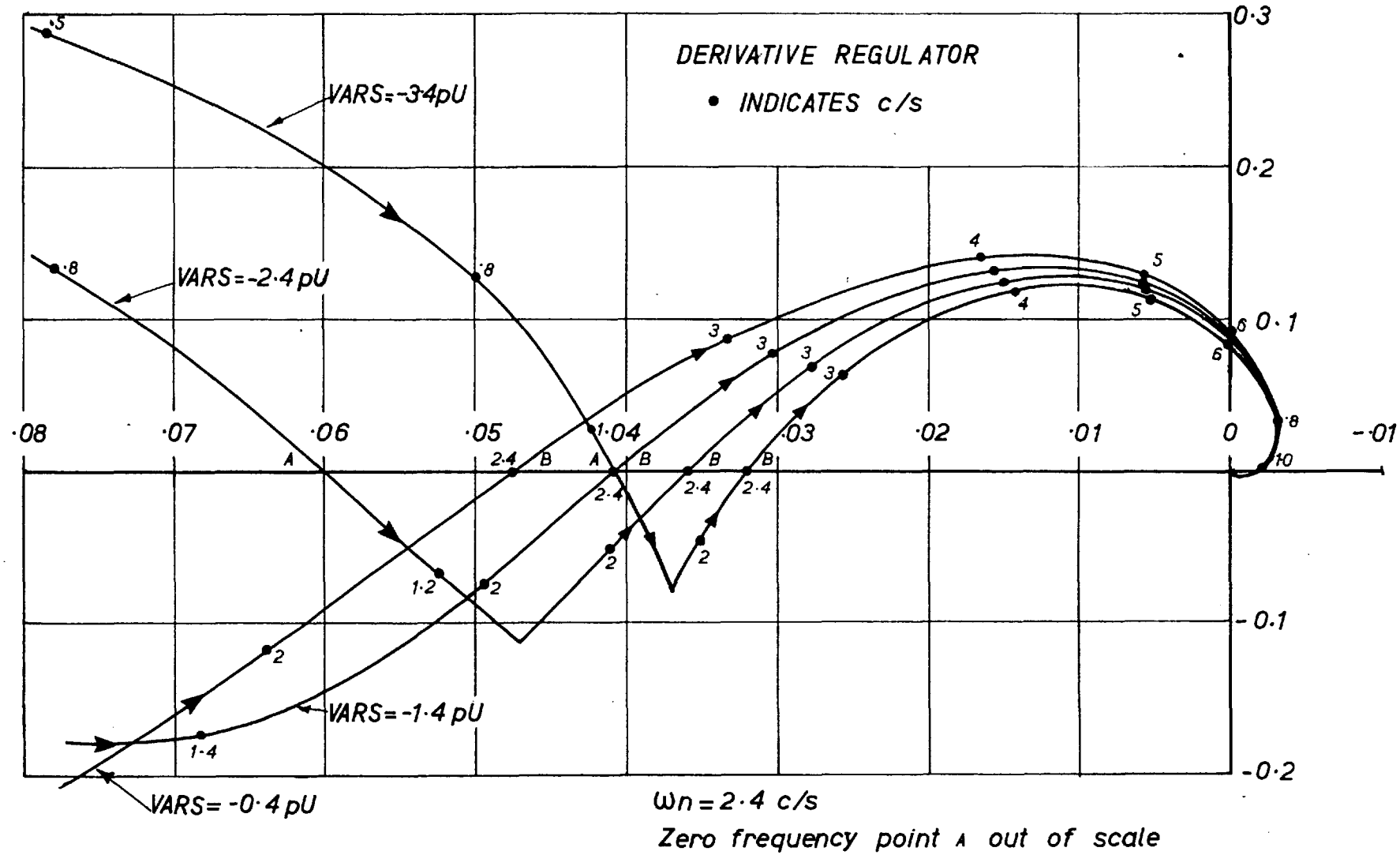

FIG. 3.9. $L_q(j\omega)$ PLOTS FOR EQN. (3.33)

FIG. 3.10. STEADY STATE LIMIT CURVES.

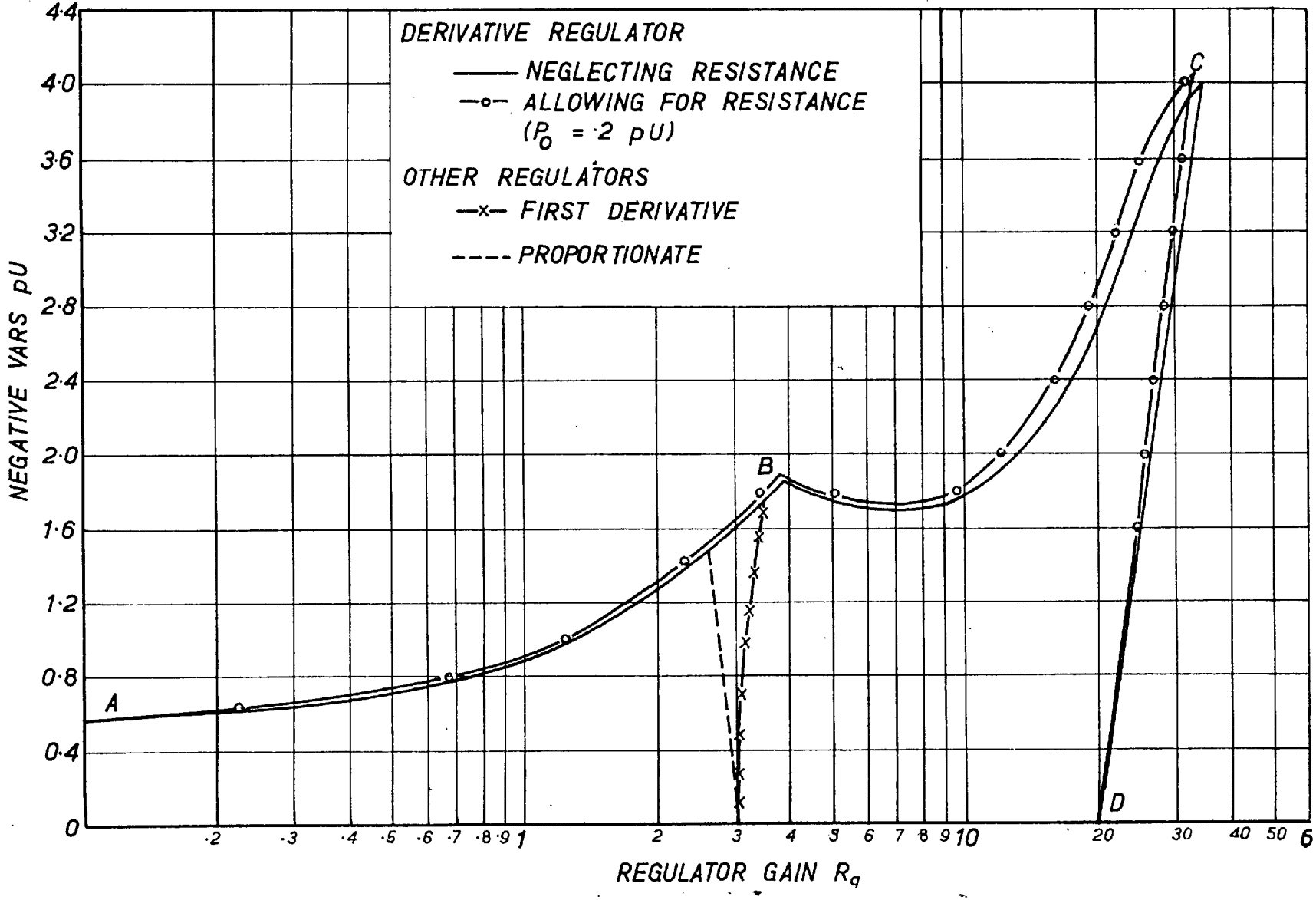

cases for which $R_q(\min) = 0$, but $R_q(\max)$ depends on the point B (see Sect. 3.5.1.1.1). In Fig. 3.10 the newly created region BC corresponds to $R_q(\min)$ and point A' in Fig. 3.9. The frequency of A' and its location depends on the vars. Two typical Nyquist plots for the region BC corresponding to -2.4 and -3.4 p.u. vars are shown. The curve from A to A' is partly shown (since A is off the scale), however, it represents the unstable part, because it could only encircle the (0,-1) point clockwise (see Sect.3.5.1.1.1). In Fig. 3.10 the region CD corresponds to $R_q(\max)$ and point B on the Nyquist plots in Fig. 3.9. In fact the broken lines with and without crosses also correspond to the point B on the respective Nyquist plots for simpler regulators, but with the derivative regulator the point B is so shifted that $R_q(\max)$ is considerably increased to give the region CD.

The following chart gives the comparative theoretical figures for the three regulators.

Type of Regulator	Maximum permissible steady state reactive absorption p.u.	Maximum permissible gain at any var level	Maximum Gain limit at vars = -1.0 p.u.
Proportionate (with practical angle device)	-1.52	3.0	2.78
First derivative only	-1.82	3.6	3.15
'Derivative'	-4.0	34.2	22.8

3.5.3 Effect of Alternator Damping

If the damping is included the alternnator transfer function $B_{q2}(p)$ becomes

$$B_{q2}(p) = \frac{\frac{1}{\sqrt{2}} V_{qo} Y_q}{T'_q J p^3 + J p^2 + (Q_o + V_{qo}{}^2 Y'_q) T'_q p + (Q_o + V_{qo}{}^2 Y_q)} \times \frac{1+T_{kq}p}{1+T''_q p} \qquad (3.34)$$

The term associated with damping in Eqn. (3.34) is $\left(\frac{1+T_{kq}p}{1+T''_q p}\right)$, its effect is equivalent to a lag term in the total transfer function $B_{q2}(p)$, because $T''_q > T_{kq}$.

How much the modified alternator transfer function affects the Nyquist plots of the open-loop transfer function $L_q(p)$ depends on the magnitude of T_{kq} and T''_q. Their order is usually so low that it does not affect the Nyquist plot to any appreciable extent around point B (see Figs. 3.4, 3.6, 3.7), where the frequency is .7 - 2.5c/s. The above argument supports the conclusions in Ref.1 that the damping has little effect on the steady state stability limits. However, it can be added that the little effect it has, is equivalent to a small lag term in the open-loop transfer function.

3.5.4 Effect of Resistance

With resistance and without damping the alternator transfer function $B_{q2}(p)$ is

$$B_{q2}(p) = \frac{\frac{1}{2}Y_q \left[V_{qo}-2r_a(I_{qo}+r_a I_{do}Y_d(p))\right]}{\left[Q_o+Jp^2+V^2Y_q(p)-2r_a I_{qo}Y_q(p)+r_a{}^2(Jp^2-I_{do})\right](1+T'_q p)} \qquad (3.35)$$

Using the above alternator transfer function in the expression for $L_q(p)$ given by Eqn. (3.33), the steady state limit points are plotted in Fig. 3.10. A comparison with the steady state limit curve for the derivative

regulator shows that the resistance has a stabilising effect, because it slightly increases the reactive absorption limit for the same regulator gain.

In the alternator transfer function given by Eqn. (3.35), I_{qo} terms are present which makes it a function of power. There should be a slight increase in the stability limit with increase in power. The effect of resistance is in any case quite small.

CHAPTER 4

4. EXPERIMENTAL EQUIPMENT

The experiments were conducted on the three phase micro-machine equipment arranged as shown Fig. 4.1 and Fig. 4.2 for the direct and quadrature axes regulation schemes respectively. In both cases the micro-alternator is connected to the fixed supply treated as an infinite bus through a series reactance X_c . The micro-machine is a small alternator specially designed to give a large range of parameters on a per unit (p.u.) basis. The equipment includes a time constant regulator which controls the constants of the excitation circuit and the feedback regulator simulated by an analogue computer using conventional circuitry.

In Fig. 4.1, the main voltage feedback circuit consists of a rectifier and filter followed by the regulator. There is also an auxiliary feedback circuit which consists of an air-gap transformer with its primary winding in series with the field circuit and the secondary winding feeding the regulator through a filter and an adjustable amplifier. The steady state excitation level of the alternator can be changed by

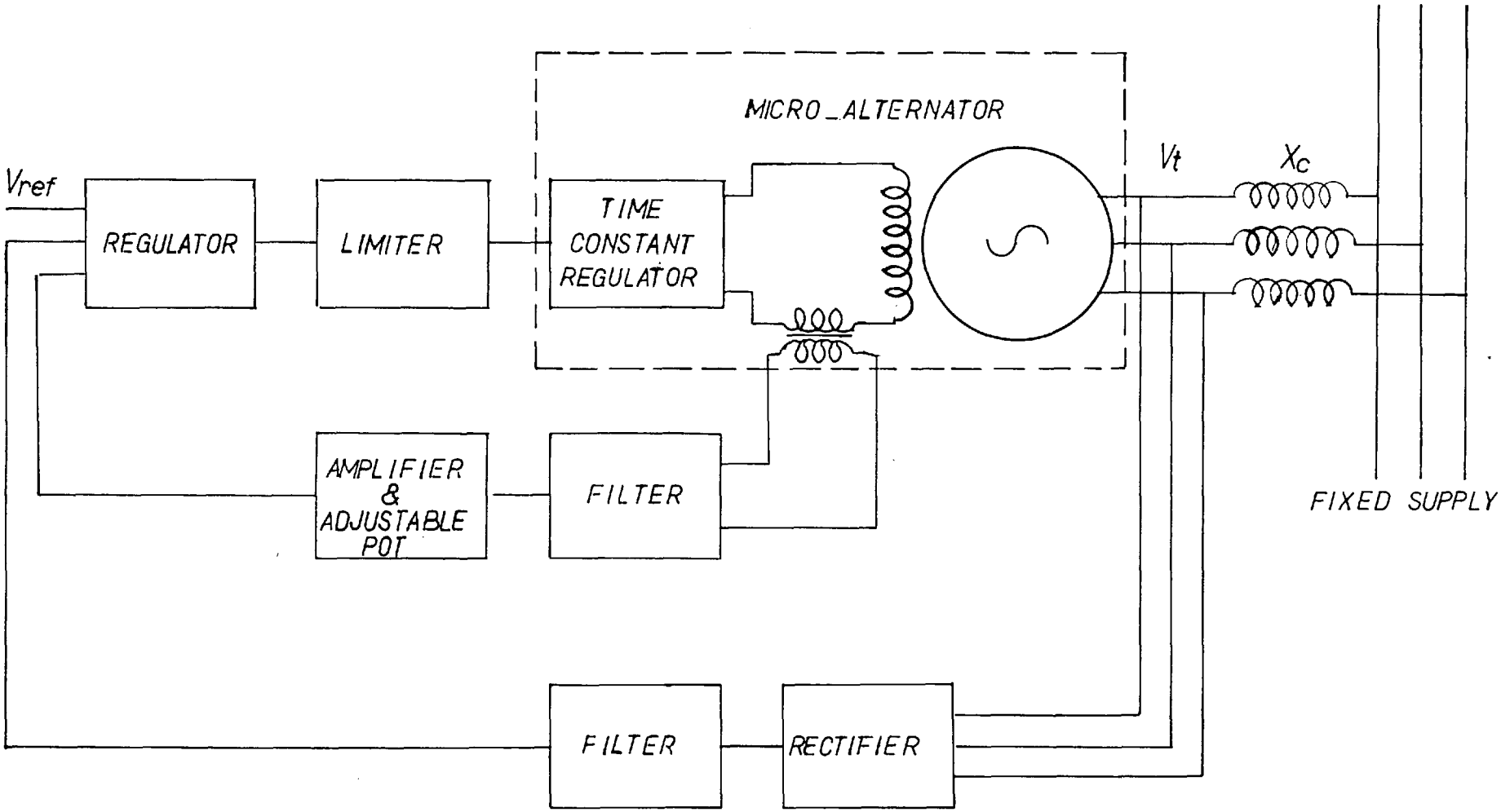

FIG. 4.1_ THE EXPERIMENTAL SYSTEM FOR DIRECT_AXIS FEEDBACK

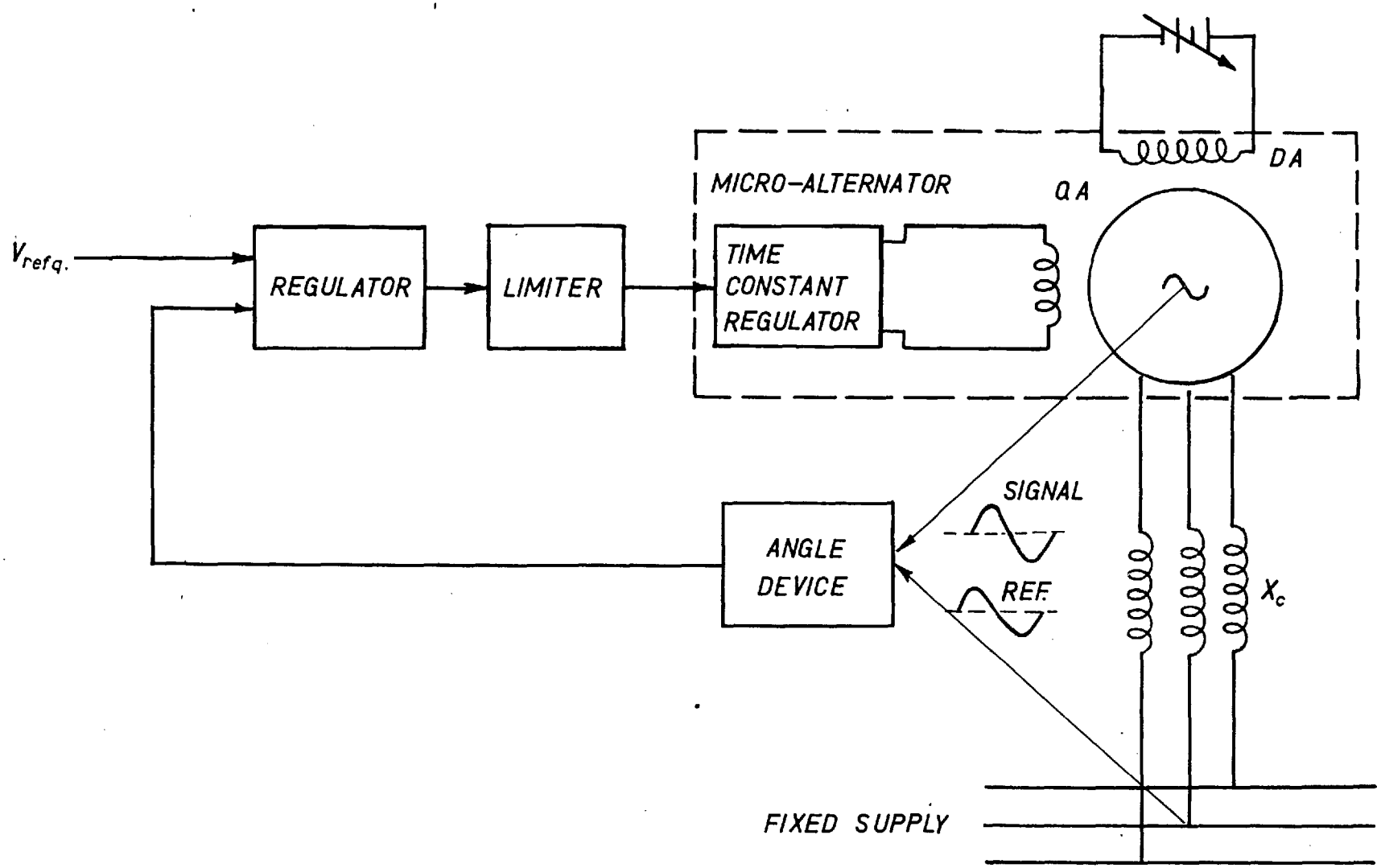

FIG. 4·2 THE EXPERIMENTAL SYSTEM FOR QUADRATURE FEEDBACK

adjusting V_{ref}.

In Fig. 4.2, the quadrature-axis angle feedback circuit consists of an angle measuring device followed by the regulator. The direct-axis field is supplied from an adjustable d.c. source. The quadrature-axis steady state excitation is automatically controlled by the angle feedback circuit.

4.1 The Micro-machine and its Parameters

The experimental micro-machine had different rotors for the direct and quadrature axes regulation schemes but the same stator was used. The rotor for the direct-axis regulation scheme had a conventional direct-axis field winding and a damper circuit. The stator-rotor combination and the parameters were the same as for the machine used in Ref. 1 (see table I). The rotor for the quadrature-axis regulation scheme had a direct-axis winding and a winding in quadrature but without damper circuits. The parameters are dealt with in the following sections.

4.1.1 The Quadrature-axis Regulation Machine Parameters

The parameters of the micro-machine were chosen to represent a large synchronous machine on a p.u. basis.

The p.u. voltage and the voltamperes are the same as for the direct-axis regulation scheme. A relatively low voltage was chosen in order to reduce the effect of saturation. The range of operation considered for this scheme is from no-load to full-load and it is difficult to find a set of parameters compatible with the full operating range because of saturation. The parameters also vary from positive to negative vars even at a particular power. However, the parameters used were determined at 0.2 p.u. power averaged over a range of vars.

For calculations the series reactance X_c was treated as part of the machine leakage reactance. The operational impedances $X_d(p)$ and $X_q(p)$ were determined by the variable frequency response static impedance test[21,22] and the conventional[23] short circuit and open-circuit test. The direct and quadrature axes synchronous reactances were determined from the steady state equilibrium diagrams (see Sect. 3.4).

4.1.1.1. Determination of X_d and X_q

In order to determine X_d and X_q from a steady state test, using the equilibrium diagram given in Fig. 3.2b , the alternator was synchronized with the

fixed supply. The power generated was adjusted to 0.2 p.u. The steady state m.m.f in the quadrature-axis was adjusted until the zero angle equilibrium was established. The supply voltage, vars at the fixed supply terminals, the line current were noted. From the open-circuit voltage characteristic for the direct and quadrature axes, and the steady state relations (Eqns. 3.17 to 3.20) for the equilibrium diagram, Fig. 3.2b , X_d and X_q were determined. The open-circuit characteristics for the direct and quadrature axes are approximated straight lines through the origin and the 1 p.u. voltage point. The values of X_d and X_q given in table II are the average values from a number of tests for .2 p.u. power averaged over a range of vars.

4.1.1.2 Variable Frquency Response Static Impedance Test

The transient reactances for the direct and quadrature axes are determined by fitting curves to the experimental points from the frequency response static impedance test as briefly described below. The curve fitting is done with the knowledge of the transient reactance from the standard short-circuit test which is similarly extended to the quadrature-axis here.

The test consisted of connecting the two phases of the machine in series with an external resistance while the rotor was locked in the direct-axis position. The external resistance was first used for measuring current in conjunction with a transfer function analyser (T.F.A) equipment and later to provide one voltmeter reading when the test was repeated with the three voltmeter method. The T.F.A equipment consists of three interconnected units, an ascillator, an angle resolver and an amplitude measuring unit. A variable frequency reference signal from the oscillator is given to a system or a circuit the frequency response of which is to be measured, the output is connected to the amplitude unit which in conjunction with the angle resolver gives the magnitude and angle of the output with respect to the reference signal.

The T.F.A. reference signal was fed to an amplifier and exciter arrangement of an auxiliary time constant regulator (see Fig. 4.5), to circulate a current signal at reference signal frequency of approximately 250 mA through the machine circuit described above. With respect to the T.F.A. reference signal, the voltage V_r across the resistance and V_c across the coil (i.e., two machine phases in series) were measured, giving the

impedance z of two machine phases at the operational frequency $f = \dfrac{\overline{V}_c}{(\overline{V}_r/R)}$; R being the external resistance (equal to 1 ohm). Thus, the operational impedance

$$\left.\begin{matrix} X_d(p) \\ X_q(p) \end{matrix}\right\} = \frac{z-2r_a}{2} \times \frac{50}{f} \quad .$$

For the quadrature-axis the rotor was locked in the quadrature-axis position and the test was repeated with the quadrature-axis time constant regulator in operation to control the effective quadrature field winding resistance (see Sect. 4.2.2.). A steady state field current of 750 mA was circulated to keep the operation of the quadrature-axis time constant regulator in the linear region (see Sect. 4.2.3). This experiment was repeated for both the axes, by using a motor generator set and the three voltmeter method for measurement (using an oscilloscope for low frequencies). The averaged experimental points were plotted for direct and quadrature axes operational admittances in Fig. 4.3 and Fig. 4.4 respectively. Though the experiment was done on the machine alone, the points on the above figures include the transmission line reactance X_c . The points Y_d (i.e. $Y_d(o)$) and Y_q ..... continued

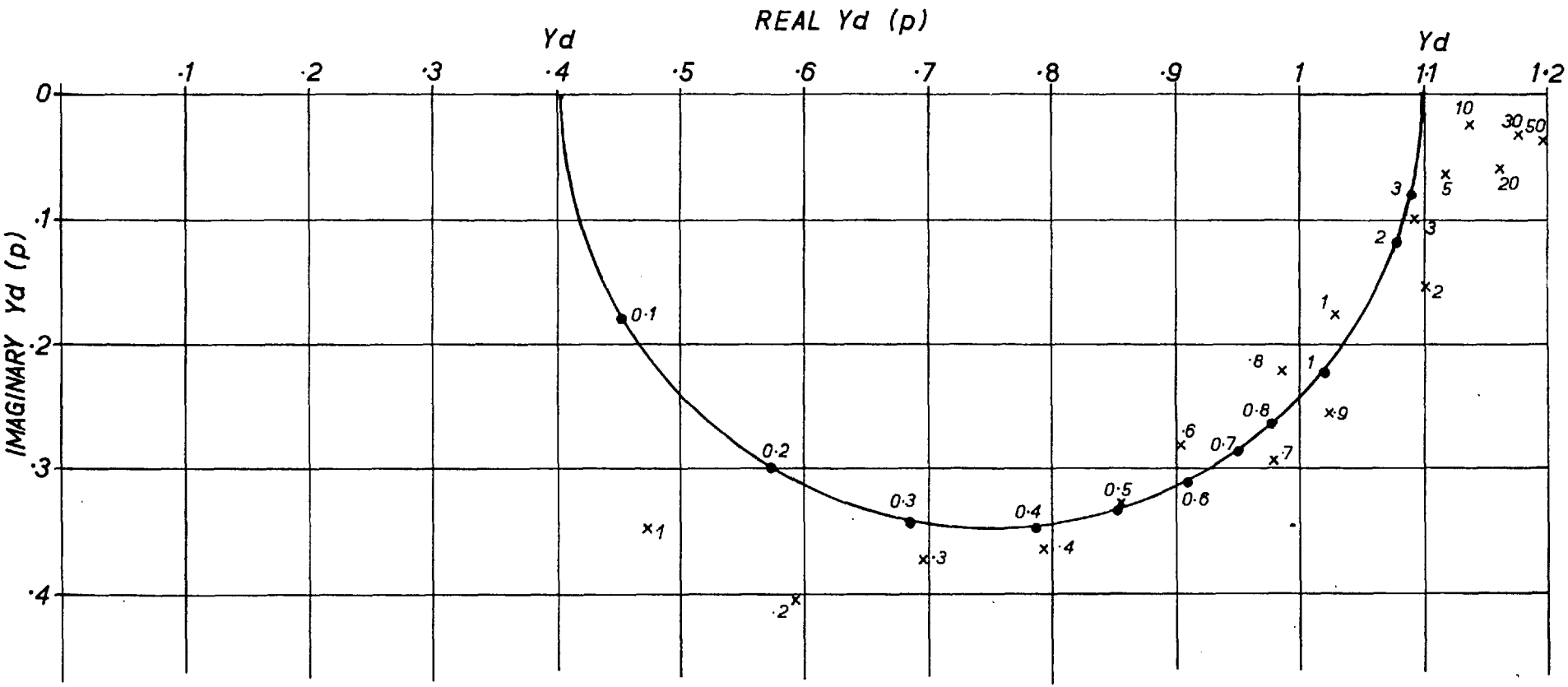

FIG. 4.3. OPERATIONAL ADMITTANCE Yd (p) CURVE

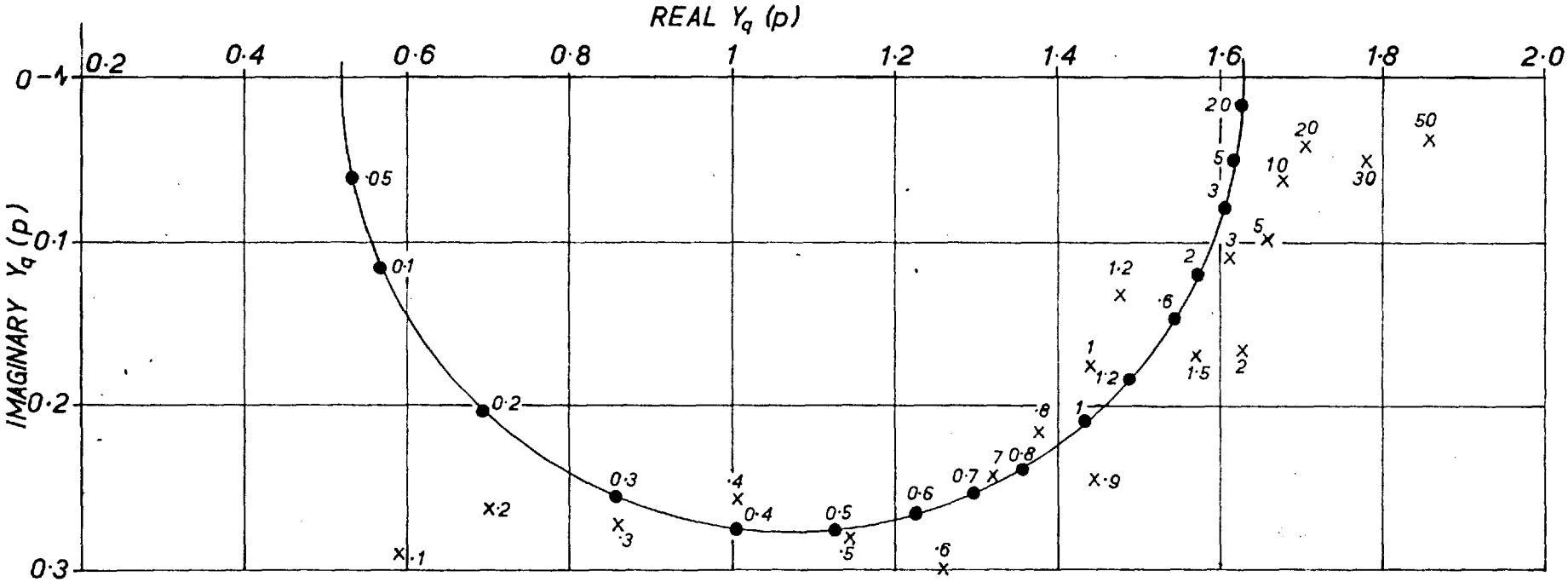

FIG. 4.4. OPERATIONAL ADMITTANCE Y_q (p) CURVE

(i.e. $Y_q(o)$) were established from the equilibrium diagram in Sect.4.1.1.1., the points $Y_d(\infty)$ and $Y_q(\infty)$ (i.e. Y'_d and Y'_q) established by the standard short-circuit test assisted in fitting a suitable curve through the experimental points. A close fit was attempted in the lower frequency region due to the importance of this region in the present investigation. The discrepancy at very low frequency points could be attributed to the resistance measurement error which is more pronounced at low frequencies. There are no damper windings on the rotor, however the experimental points indicate some damping effect which may be due to the iron (though laminated) in the rotor.

4.2 Time Constant Regulator - T.C.R.

The field resistance (r_{fd} or r_{fq}) of the small micro-machine is larger than it should be for a correct simulation of a large synchronous machine and the time constant regulator is used to reduce its value. The circuit employed uses a winding mutually coupled to the field winding, this convential scheme[24,25] is discussed briefly in Sect. 4.2.1. The quadrature field winding of the second rotor is however not provided with a mutually coupled winding on the rotor, and an alternative

circuit to achieve the desired time constants is developed in Sect. 4.2.2.

4.2.1 Conventional Time Constant Regulator

In Fig. 4.5 is shown the time constant regulator[24], which consist of a d.c. exciter supplying the alternator field, a high gain d.c. amplifier supplying the exciter field and a suitable feedback circuit. The feedback circuit controls the rate of rise or decay of the field winding flux linkages. To achieve this the feedback term should consist of the change of field flux linkages term and the resistive drop term. Since the gain of the d.c. amplifier is very large a 'Virtual Earth' is always established at the input of the amplifier.

Thus, $$e - e_{fb} = 0 \qquad (4.1)$$

where, e is the input voltage and e_{fb} is the feedback voltage.

$$e_{fb} = p\psi_f + R_{fb}i_f \qquad (4.2)$$

and

$$\psi_f = L_f i_f + Mi_{kd} + Mi_d \qquad (4.3)$$

ψ_f the flux-linkages for the field winding are also

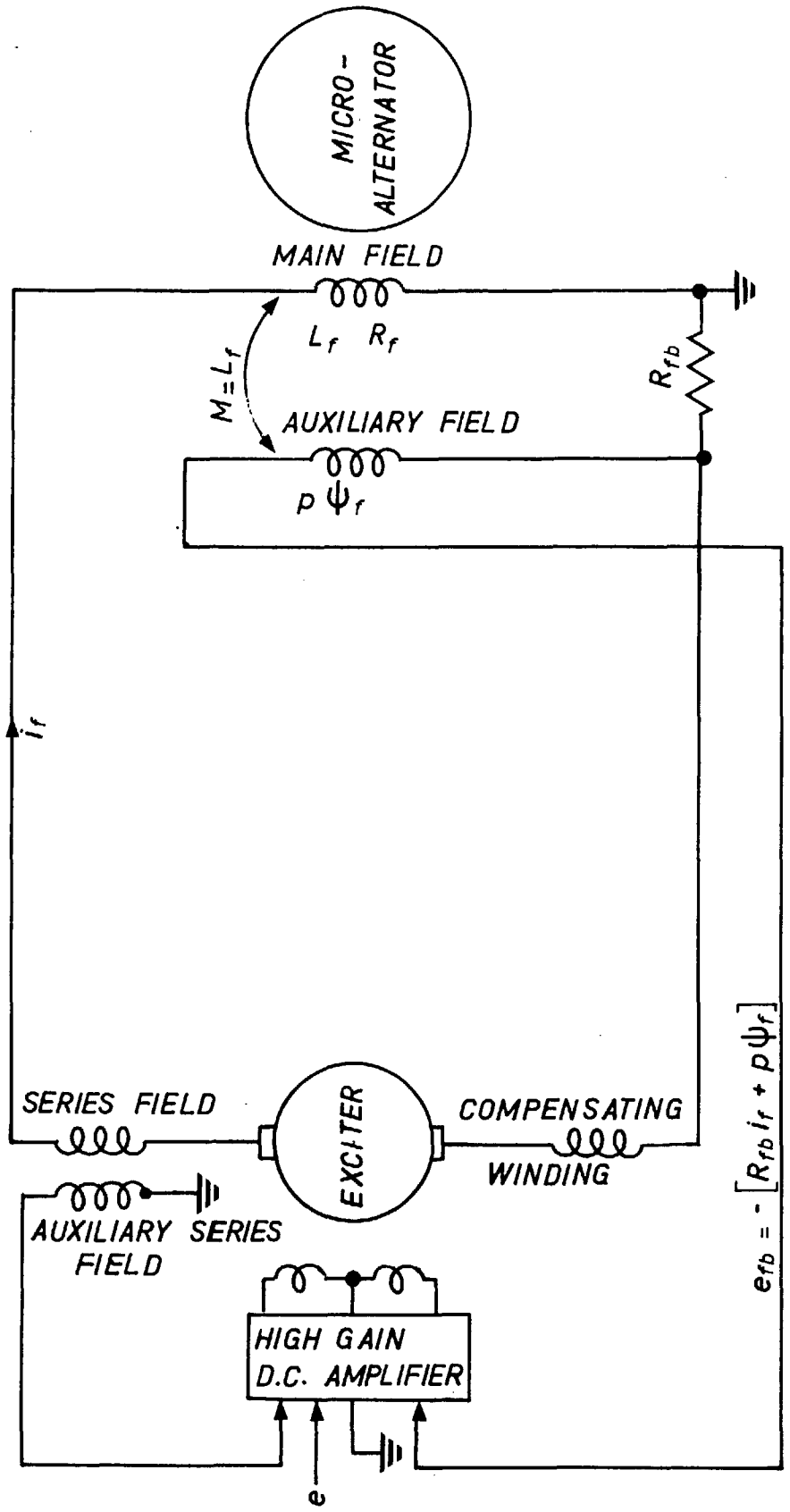

FIG. 4.5. CONVENTIONAL TIME CONSTANT REGULATOR.

the flux-linkages for the mutually coupled feedback winding, because the coupling is ideal and their windings are identical (i.e. their mutual inductance is also their self inductance). From Eqns. (4.1) and (4.2) we have

$$\frac{i_f}{e} = \frac{1}{(R_{fb} + p\psi_f)} \qquad (4.4)$$

For the open circuit transient behaviour of the alternator $p\psi_f = pL_f i_f$, for this condition Eqn .(4.4) becomes

$$\frac{i_f}{e} = \frac{1}{(R_{fb} + pL_f)} \qquad (4.5)$$

thus the resulting time constant T'_{do} of the system is $\frac{L_f}{R_{fb}}$. By changing R_{fb} , T'_{do} can be adjusted to a desired value. Under the steady state conditions $p\psi_f$ is zero and $i_f = \frac{e}{R_{fb}}$. Thus looking at the input of the high gain d.c. amplifier the field circuit behaves as if it has the adjustable resistance R_{fb} and not the actual field resistance R_f .

In the scheme shown in Fig. 4.5 the two parts of the feedback, namely $p\psi_f$ and $R_{fb}i_f$ are picked up independently. $p\psi_f$ is derived from the mutually coupled winding with the field circuit. In the absence of the mutually coupled winding as is the case with the quadrature-axis field

winding rotor the feedback circuit is modified to achieve the same feedback quantities, see Eqn. (4.2). The modified scheme is dealt with in Sect.4.2.2.

In this simplified analysis the exciter is treated as part of the high gain d.c. amplifier considered to be ideal without delay. The controlled excitation effect of the exciter is boosted by a series winding which is on the same magnetic axis as the control winding. To counter the interaction between the series winding and the control field winding a feedback from a winding mutually coupled to the series winding is used, the details for which are given in Ref. 24. In the following modified scheme the amplifier and exciter are left unchanged and treated as ideal high gain d.c. amplifier.

4.2.2 Modified Time Constant Regulator

The modified time constant regulator is shown in Fig. 4.6. The amplifier and the exciter is shown simplified, but in practice is the same as in Fig. 4.5, only the feedback circuit is altered. An adjustable resistance R_{fb} , which is small compared with the field resistance R_f, is inserted in series with the field winding and the end farther from the field winding is

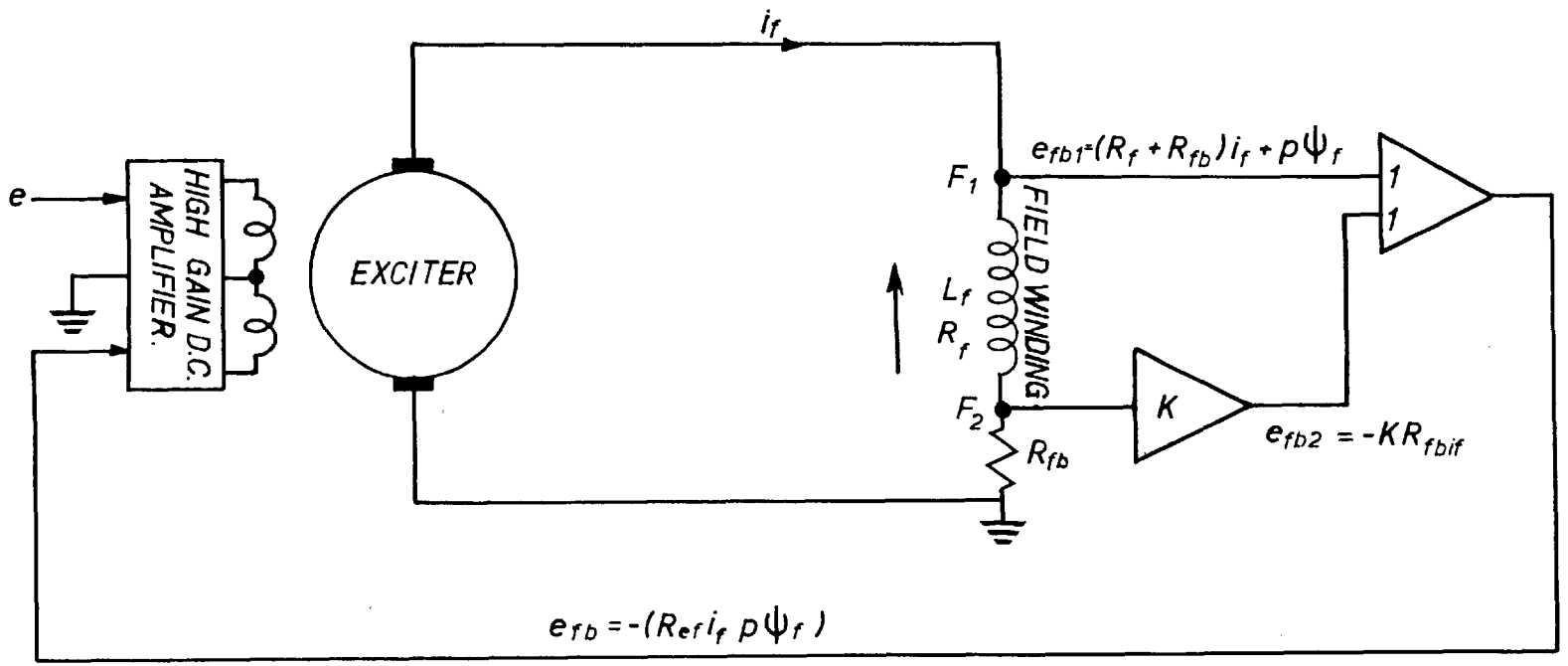

FIG. 4·6. MODIFIED TIME CONSTANT REGULATOR

earthed, instead of the field side end, see Fig. 4.5. This is done because of a change of polarities as will be clear later. The voltage picked up by the field coil end F_1 with respect to the earth constitutes a part e_{fb1} of the feedback e_{fb}. The expression for e_{fb1} is:

$$e_{fb1} = [(R_f + R_{fb})i_f + p(\psi_f] \qquad (4.6)$$

In Eqn. (4.6) $p\psi_f$ is the useful part but $(R_f + R_{fb})i_f$ is very large and must somehow be cancelled. This is achieved by countering it by the other part of the feedback e_{fb2}, which comes from R_{fb} amplified by K times and inverted in its polarity. The expression for e_{fb2} is

$$e_{fb2} = (R_{fb} \times i_f) \times -K = -KR_{fb}i_f \qquad (4.7)$$

The two feedback voltages given by Eqns. (4.6) and (4.7) are summed up in an operational amplifier thus the resultant feedback e_{fb} at the out put of the summer unit is:

$$e_{fb} = -[e_{fb1} + e_{fb2}] \qquad (4.8)$$

Substituting e_{fb1} and e_{fb2} in Eqn. (4.8) the final expression for the feedback quantity is

$$e_{fb} = - [\quad R_f - R_{fb}x(K-1) \quad + p(\psi_f]$$

or

$$= - [R_{ef} + p(\psi_f] \tag{4.9}$$

where $R_{ef} = R_f - (K-1)R_{fb}$

Thus an adjustable R_{ef} is achieved depending on the amplifier gain K, which can easily be adjusted from 1 to 40 with one operational amplifier.

The feedback expression given by Eqn. (4.9) is similar to the expression given by Eqn. (4.2). Assuming there is no phase shift introduced by the operational amplifiers of the modified scheme in Fig. 4.6 and R_{ef} is the same as R_{fb} of the conventional T.C.R., then the two circuits will behave identically. If e is the input voltage then from the 'Virtual Earth' concept established in Sec. 4.2.1, using Eqn. (4.1) and Eqn. (4.9) we have

$$\frac{i_f}{e} = \frac{1}{[R_{ef} + p(\psi_f]} \tag{4.10}$$

Under the open-circuit transient conditions $p(\psi_f = pL_f i_f$

and Eqn. (4.10) yields the open-circuit transient time constant $T'_{do} = \frac{L_f}{R_{ef}}$ (4.11)

Under the steady state condition $p\psi_f = 0$ and Eqn. (4.10) yields

$$i_f = \frac{e}{R_{ef}} \qquad (4.12)$$

Equations (4.11) and (4.12) establish the identity of the modified T.C.R. with the conventional T.C.R.

The modified T.C.R. is used in conjunction with the quadrature-axis field winding. Some important parameters measured (average measurement) with 1 amp current in the field circuit are mentioned here. The current range is mentioned because of certain nonlinearities in the circuit discussed in the next section. The quadrature-axis field winding resistance is 14.86 ohms and its inductance 2.22 Henrys , thus giving an open-circuit transient time constant T'_{qo} of about .15 sec., whereas, when R_{ef} is modified to 2.02 ohms, $T'_{qo} = 1.1$ sec. The measured (average) value of R_{fb} is 1.435 ohms and the operational amplifier gain K is 9.95. This circuit gave rise to certain difficulties which are dealt with in the following section.

4.2.3 Difficulties with the Modified T.C.R.

The parameters of the modified T.C.R. are not independent of the operating conditions and this is not a desirable feature. Change in the inductance of the field

coil at different flux levels makes both the conventional and modified T.C.R. vulnerable to saturation effects. Besides saturation this circuit is affected by changes in R_{ef}, which is dependent on R_{fb}, R_f and the operational amplifier gain K, see Eqn. (4.9). It is reasonable to assume that the operational amplifier gain remains constant for the range of frequencies of interest to us, leaving R_{ef} dependent on the variations in R_{fb} and R_f. The feedback resistance R_{fb} is made of very low temperature coefficient material and so does not appreciably change for the range of temperature variations encountered, thus leaving R_{ef} entirely dependent on the variations in R_f.

The field winding resistance R_f changes with temperature variation and also with the current level in the circuit because of the carbon brush contact resistance. In Fig. 4.7 is plotted the quadrature-axis field resistance against the current when the machine was warm. The field resistance is reasonably constant for currents greater than 500 mA, but at lower currents the carbon brush resistance increases sharply. For this reason the circuit is considered reliable only for current levels above 500 mA.

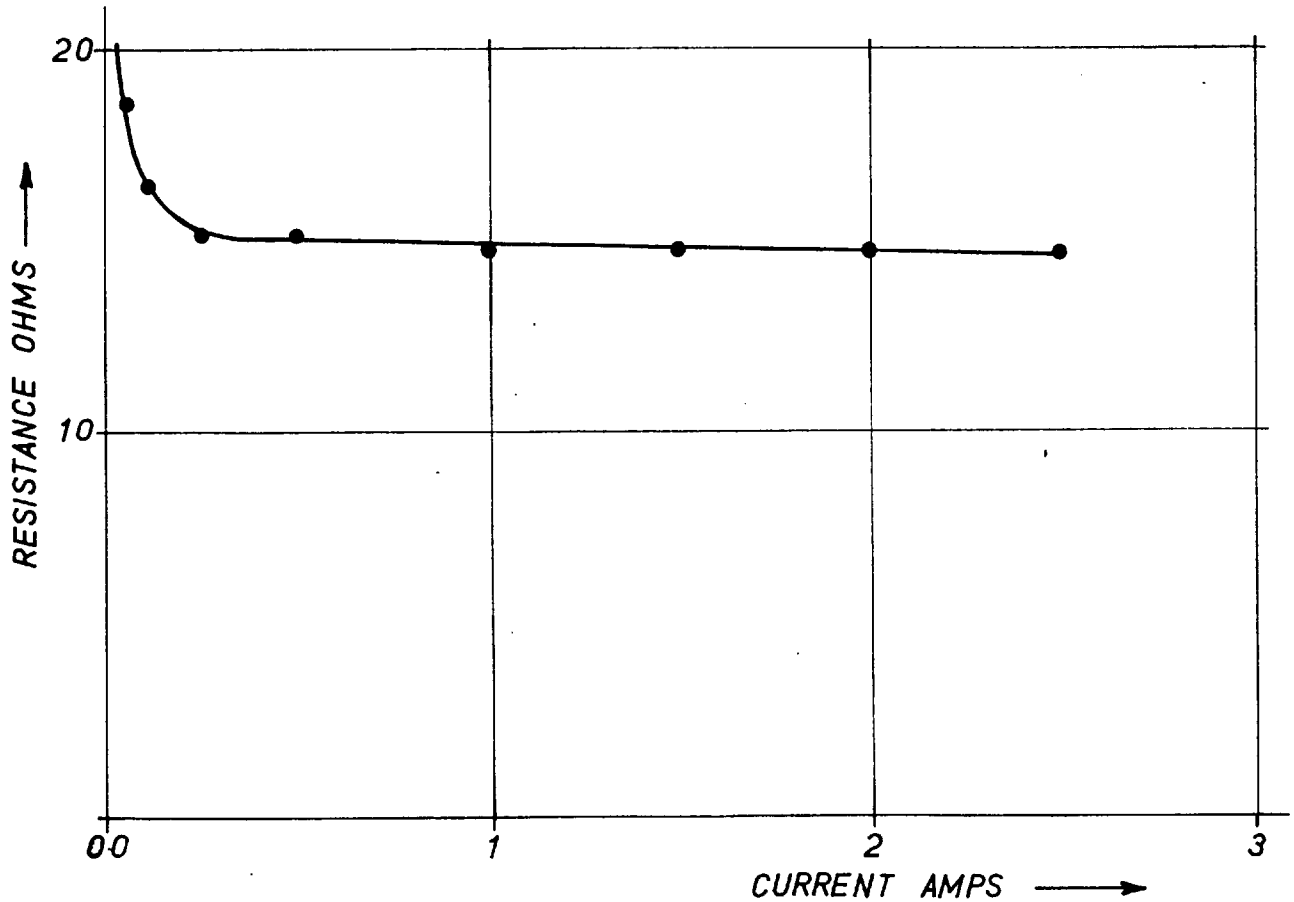

FIG. 4.7. RESISTANCE VARIATION OF THE QUADRATURE AXIS FIELD COIL WITH RESPECT TO CURRENT.

R_f also changes with temperature. This variation was kept under control by always running the set under full-load conditions for about ½ hr. to achieve a reasonably steady temperature before taking any measurement.

Other difficulties with the circuit stem from the fact that R_f contributes to the feedback voltage. The conventional T.C.R. circuit is not affected in this way because R_f does not contribute to the feedback voltage. In spite of these variations the scheme is workable within limits.

4.3 Feedback Circuits

For the direct-axis regulation the feedback circuits consisted of the main voltage feedback and the auxiliary derivative of field current feedback, see Fig. 4.1. The quadrature axis feedback consisted of the rotor angle feedback, see Fig. 4.2. These circuits are described in the following sections.

4.3.1 Direct-axis Feedback circuits

4.3.1.1 The Voltage Feedback Circuit

The voltage feedback circuit (Fig. 4.1) is the same as that used in Ref. 1. Six silicon diodes are used for the rectifier bridge circuit. In between the bridge

rectifier circuit and the mains are three single phase transformers, connected in delta on the mains side and star for six phase connection on the rectifier side. The most dominant harmonic frequency because of the rectifier bridge circuit is 300 c/s; it is attenuated by a tuned double - T filter section. Higher noise frequencies are attenuated by low-pass R-C filter sections in cascade with the double-T bridge filter. For low frequencies relevant to our purpose, it is fair to assume that the rectifier and the filter do not introduce any appreciable phase shift.

4.3.1.2 The Field Current Feedback Circuit

To obtain derivative of the field current an air-gap transformer is inserted in series with the field circuit. The transformer is specially designed with a large air-gap (12 mm) to give a straight line flux-MMF curve in the working range. The mutual inductance between the primary and the secondary winding of the transformer is .725 Henrys. For any a.c. variation in the field current the voltage induced in the secondary winding of the transformer is to a fair approximation 90^{o} out of phase with respect to the current in the field circuit. The induced voltage in the secondary winding of the

transformer is thus used as a derivative signal of the field current variations. The field current feedback circuit is shown in Fig. 4.8. The derivative signal of the field current contains a large noise at 50 c/s because of the stray pick-up in the field circuit. A R.L.C. T-bridge filter circuit tuned to 50c/s is used to cut out the 50c/s noise. The transfer function of the filter is as below.

$$\frac{1+\tau^2 p^2}{1+2\xi_1 \tau p+\tau^2 p^2}$$

where

$$\xi_1 = .25 \quad \text{and} \quad \tau = \frac{1}{314} \ .$$

The frequency response curve of the filter is given in Fig. 4.9. Under ideal conditions the total transfer function of the transformer and the filter and the subsequent amplification stage is:

$$Mp \left(\frac{1+\tau^2 p^2}{1+2\xi_1 \tau p+\tau^2 p^2} \right)$$

For low frequencies the signal transmission through the filter can be assumed to be without attenuation and delay since the input impedance to the filter is very low. For low frequencies the field current feedback transfer function then is approximated to Mp. In

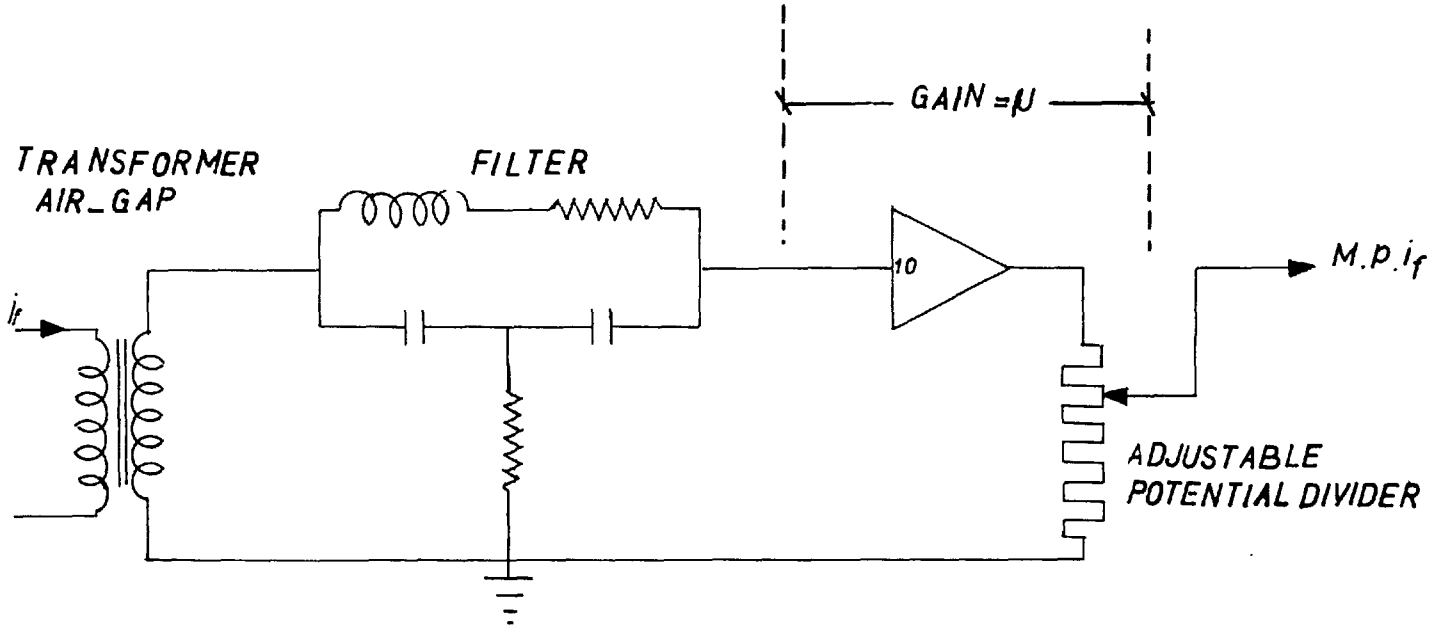

FIG. 4.8._THE FIELD CURRENT FEEDBACK CIRCUIT

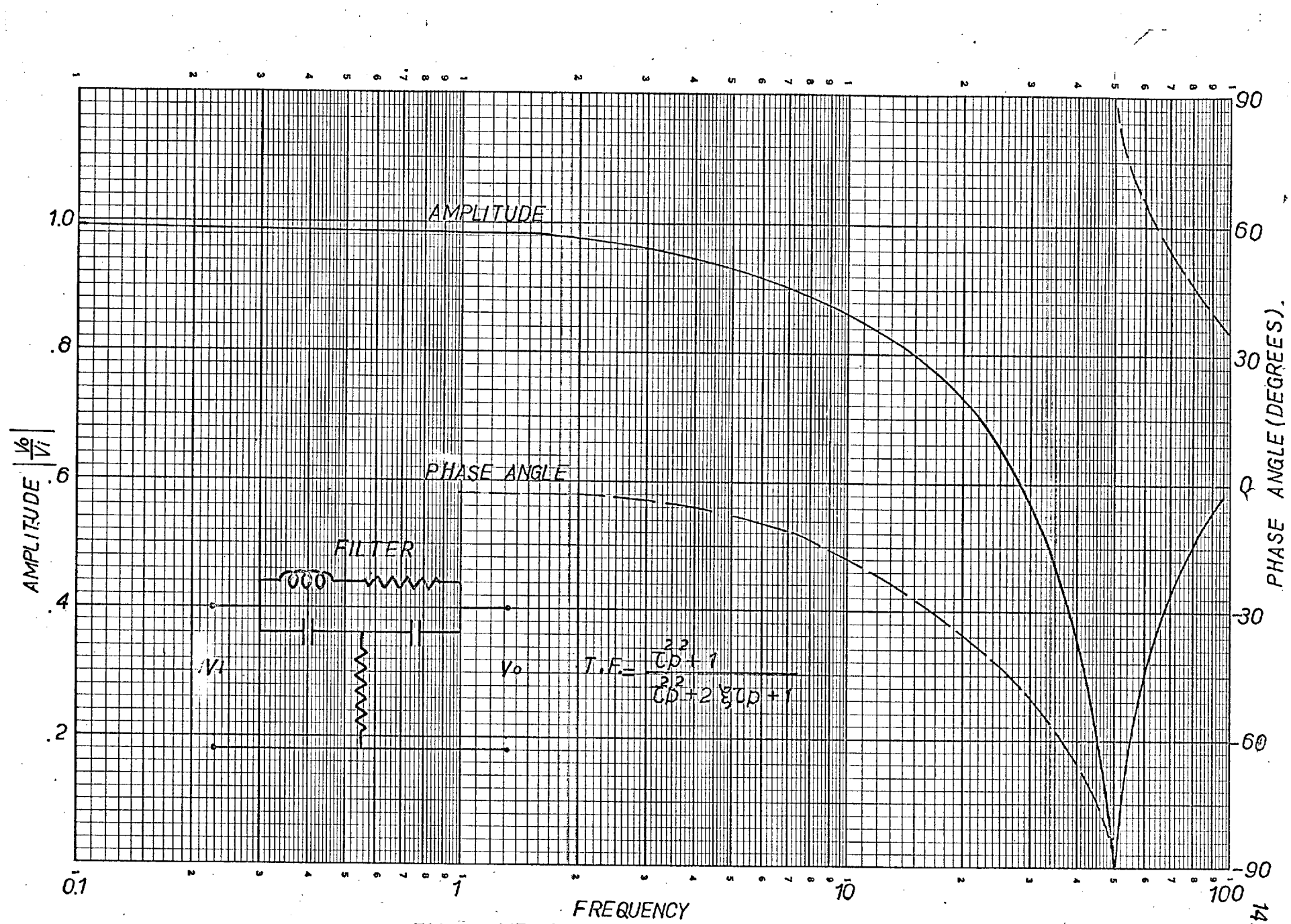

FIG. 4.9 MEASURED FILTER CHARACTERISTICS.

Fig. 4.8 the transformer is directly coupled to the filter section. The output impedance of the transformer causes mismatch at the filter input and so there is bound to be some delay introduced in the transmission of the signal even at low frequencies. However, in the theory it has not been taken into account.

4.3.2 Quadrature-axis Feedback Circuit

A signal proportional to the angle of the rotor with respect to the infinite bus (fixed supply) is developed. An a.c. tachogenerator which generates the frequency of the system when coupled to the rotor of the micro-alternator will give a waveform that will change in phase with respect to the infinite bus waveform in accordance with the rotor position. Thus the rotor angle signal problem is converted into the phase detection and generation of a signal proportionate to phase variation. In the following sections a conventional phase detection circuit is discussed briefly and based on it a modified circuit is developed.

4.3.2.1 A conventional Phase Detection Circuit

Out of various conventional phase detecting circuits[26,27] considered the one described below was

adopted in principle becuase it can indicate by sign inversion whether the incoming signal is lagging or leading with respect to the reference (all sine waves), a characteristic necessary for our purpose. The phase detection circuit[27] using phase splitting, rectification and filtering is shown in Fig. 4.10a. The various voltages labelled on the figure are as follows

$$e_1 = E \sin \omega t \tag{4.13}$$

$$e_2 = E \sin(\omega t + \phi) \tag{4.14}$$

$$e_{oA} = \text{Maximum of } (E \sin \omega t + E \sin \overline{\omega t + \phi}) \tag{4.15}$$

$$e_{oB} = \text{Maximum of } (E \sin \omega t - E \sin \overline{\omega t + \phi}) \tag{4.16}$$

In Eqns. (4.15) and (4.16) it is assumed that the condenser C holds the maximum value to which it is charged during the period the diode d_1/d_2 conducts. In other words the R.C time constant is very large compared to the time constant of the rectified waveform impressed upon the R.C. combination. Eqns. (4.15) and (4.16) give the output voltage

$$V_o = e_{BA} = 2E(\cos \frac{\phi}{2} - \sin \frac{\phi}{2}) \tag{4.17}$$

The output voltage V_o is a function of the phase angle ϕ between the two waveforms. The curve relating the output voltage V_o and the phase angle ϕ (Fig. 4.10b)

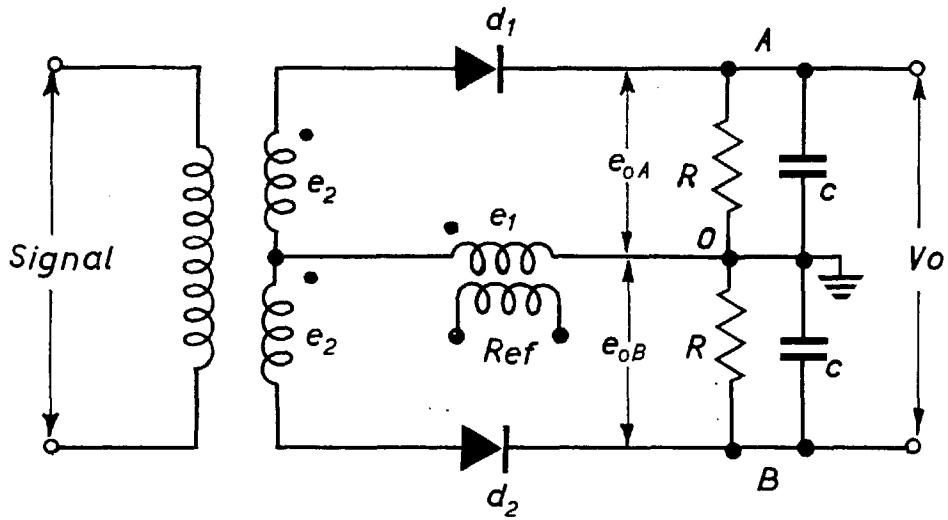

4·10a. CONVENTIONAL PHASE DETECTION CIRCUIT

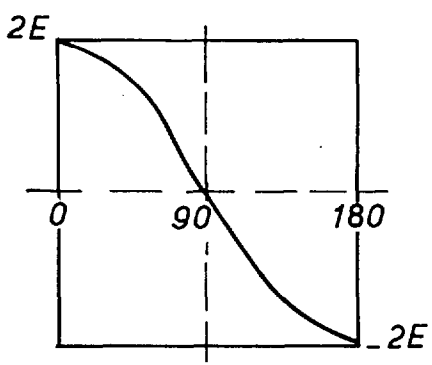

FIG. 4·10b. THE OUTPUT CHARACTERISTIC OF CIRCUIT IN FIG. 4.10a.

is a cosine curve giving zero output at 90° phase angle. The region of 90 ± 30 is practically a straight line and can be used as a proportionate signal with sign inversion at 90° phase angle. This circuit has its drawbacks. The output of the circuit is not earthed at either end and therefore, the circuit cannot be connected into the system with a common earth. The R.C combination is only a crude form of filtering. Transformers should be avoided if possible, because they are not ideal in their performance as is often assumed. With these points in view the modified circuit in the following section is developed.

4.3.2.2 The Angle Device

The circuit for the angle device (Fig. 4.11) is a modified circuit based on the phase detecting circuit in Sect. 4.3.2.1 and with improved filtering. It consists of a phase detecting unit and a filtering unit. In the phase detecting unit the diode action of transmitting the signal in a controlled way in Fig. 4.10a is replaced by a complementary pair[28] of switching transistors T_1 and T_2. The switching action of the complementary pair of transistors is in accordance with the reference signal given to the common junction of the base

R - 10K	R_2 -10KΩ	R_4 5·3KΩ
Ra (Ra_1/Ra_2) - 200KΩ	R_3 -250KΩ	c_3 ·3μF.
Rb (Rb_1/Rb_2) - 50KΩ	c_1 -·31μF.	
Rba - 47KΩ	c_2 -·1μF.	

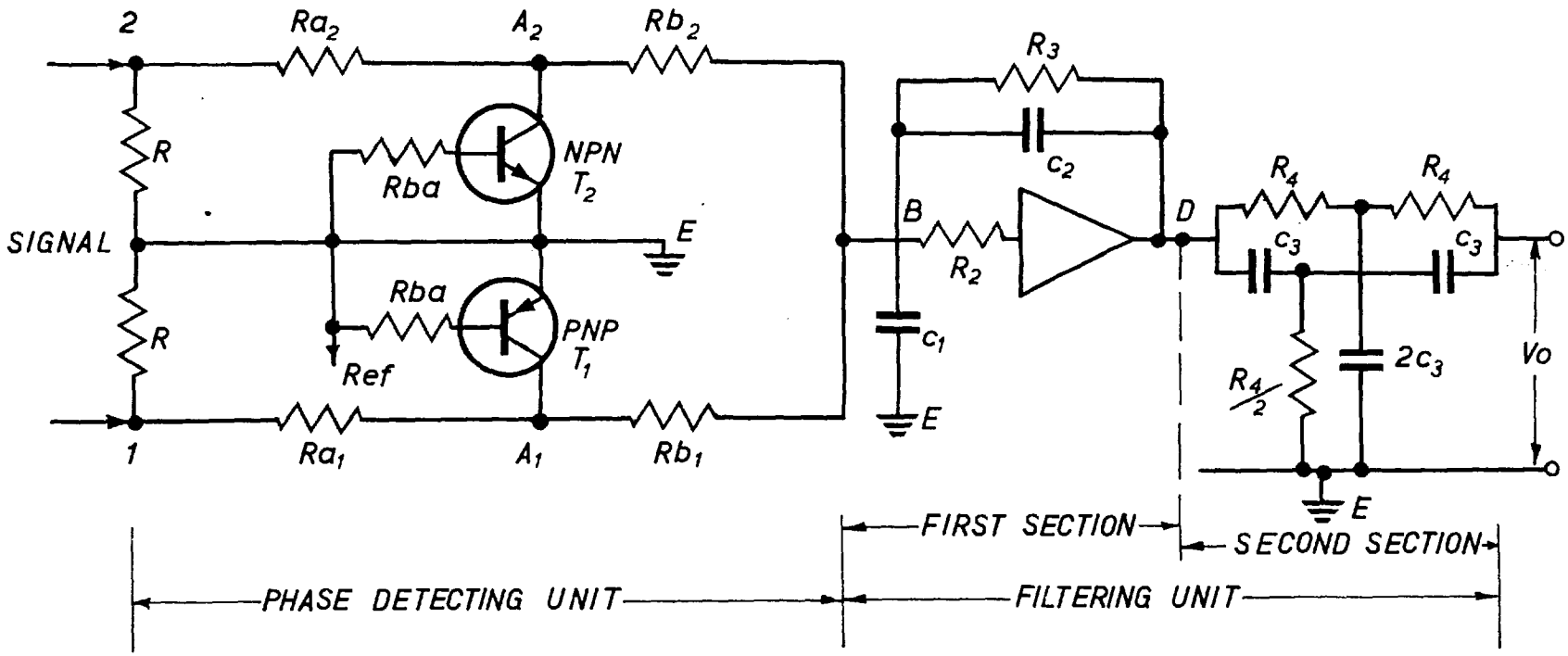

FIG. 4.11. THE ANGLE DEVICE.

resistances (R_{ba}) of T_1 and T_2. The phase splitting by the centre tapped transformer of Fig. 4.10a is replaced by two centre tapped equal resistors R. The resistances $R_a(R_{a1}/R_{a2})$ and $R_b(R_{b1}/R_{b2})$ provide a suitable potential divider arrangement so that the voltage at $A(A_1/A_2)$ does not exceed the permissible collector emitter value. The output of the circuit is with respect to the common earth E and the fundamental harmonic of the chopped output waveform has twice the signal frequency, that is because of the complementary switching action of transistors T_1 and T_2. This feature is of added advantage in filtering. The R.C filtering in Fig. 4.10a is replaced by a more sophisticated operational amplifier summation and filtering unit. The output characteristic curve is the same as that shown in Fig. 4.10b. The measured characteristic curve of the angle device is given in Sect. 6.2. The operation of the device is described in the following section.

4.3.2.3 The Angle Device Operation

The waveform of tachogenerator, of constant amplitude and variable phase is applied to the input terminals 1-2, see Fig. 4.11. The reference waveform from one phase of the infinite bus, reduced in amplitude by a

potential divider arrangement (not shown in Fig. 4.11), is applied to the junction of the base resistance R_{ba} of T_1 and T_2 in complementary connection. The transistor T_1 is a PNP transistor and T_2 a NPN transistor. A negative input signal forward biases T_1 and causes it to conduct, thus bringing point A_1 to practically earth potential. A positive input signal forward biases T_2 and causes it to conduct, thus bringing A_2 to earth potential. When one transistor conducts, the other is non conducting, because the signal that forward biases one transistor, reverse biases the other transistor. In Fig. 4.12 are shown the voltage waveforms at various stages of the circuit. The voltage waveforms at the various stages correspond to the reference and tachogenerator waveforms shown in Figs. 4.12a and b with a phase difference ϕ. In Fig. 4.12b the tachogenerator input waveform is marked 1-2 and the waveforms at terminals 1 and 2 with respect to the centre tapped point (which is at earth potential) are respectively marked 1 and 2. In Figs. 4.12c and d are shown the waveforms at A_1 and A_2. Fig. 4.12e shows A_1 and A_2 superimposed. In Fig. 4.11 the phase detecting unit is followed by the filter unit, the details of which are dealt with in Sect. 4.3.2.4. The filter unit receives

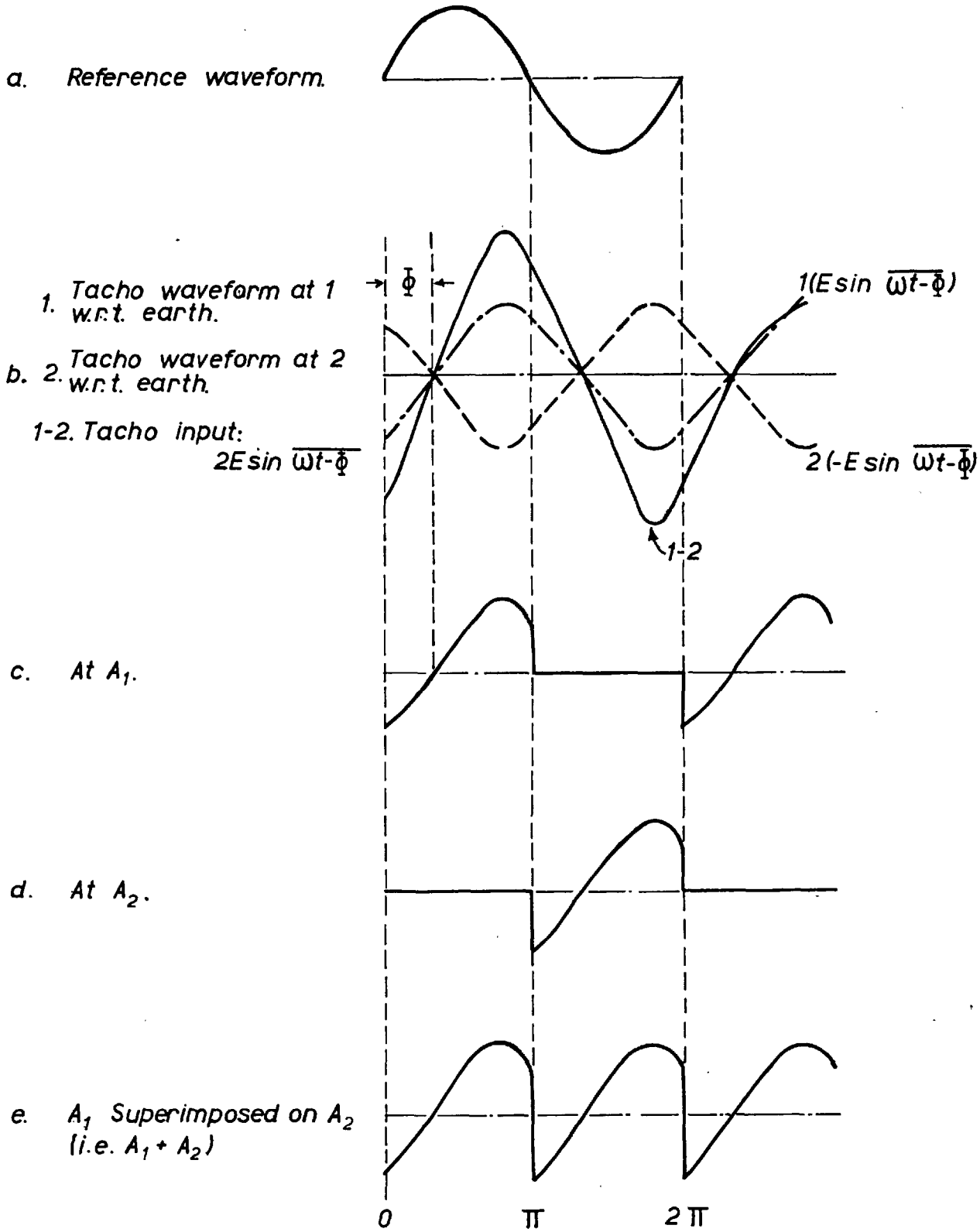

FIG. 4.12. ANGLE DEVICE VOLTAGE WAVEFORMS

the signal (see Fig. 4.11) from 1 or 2, depending on whether A_2 or A_1 is at earth potential. Thus the signal getting through the filter unit is, in shape the waveform A_1 and A_2 superimposed, see Fig. 4.12e, and in magnitude the waveforms 1 and 2 of Fig. 4.12b similarly chopped as A_1 and A_2 and superimposed. If the filter units are designed to absorb all the a.c. component of the chopped input wave, the output will be only a d.c. component. If the tachogenerator input is $2E \sin(\omega t - \phi)$ then by Fourier analysis the d.c. component of the filter output

$$= \frac{2}{\pi} \left[\int_0^{\pi} E \sin(\omega t - \phi) d\omega t + \int_{\pi}^{2\pi} - E \sin(\omega t - \phi) d\omega t \right]$$

$$= \frac{2}{\pi} E \cos \phi \qquad (4.18)$$

The output characteristic given by Eqn. (4.18) is a cosine curve as shown in Fig. 4.10b. The calibration of the circuit shown in Fig. 4.11 is done in Sect. 6.2.

During the switching operation the resistances R_{b1} and R_{b2} are earthed at A_1 and A_2 alternatively, depending on whether the transistor T_1 or T_2 is conducting. Consequently the filter unit always finds the resistance $R_b(R_{b1}/R_{b2})$ at B connected to earth, see Fig. 4.11. This assumes the switching in and

switching out operation of transistors T_1 and T_2 instantaneous. The earthing of the resistance R_b and B affects the following filter unit. Its effect has been incorporated in designing the filter unit in the following section.

4.3.2.4 The Filter Unit

The filter unit is an integral part of the angle device. It allows the superimposed chopped waves in and gives out the d.c. component of the chopped wave with very much suppressed a.c. component of the input wave. It is designed to allow the low frequency variations of the d.c. component to pass with minimum possible attenuation and delay. However, in the theoretical formulation for the quadrature axis regulation exact transfer function of the angle device is considered. As a consequence of chopping and superimposing, see Fig. 4.12e, 100c/s chopped waveforms are generated from 50c/s input waveforms. Thus the dominant frequency to be suppressed is 100 c/s. However, because of slight asymmetry in components 50c/s is also present in practice.

The filter unit is designed in two sections. The first is the active generation of a second order polynomial[29] in the denominator with a general transfer

function

$$\frac{K'}{Ap^2 + Bp + C} \qquad (4.19)$$

The second section is the passive generation of imaginary zeros[30] to suppress 100c/s in particular with the transfer function

$$\frac{1+ \tau^2 p^2}{\tau^2 p^2 + 4\tau\ p + 1} \qquad (4.20)$$

In Fig. 4.11 the two filter sections are shown. The various resistance and capacitance are labelled and their numerical values are given. For the first filter section if the resistance R_b is not taken in parallel with C_1 then the coefficients in Eqn. (4.19) are

$$K' = \frac{R_3}{R_1} \quad , \quad R_1 = R_a + R_b \quad ,$$

numerically $K' = 1$

$$A = R_2 R_3 C_1 C_2$$

$$B = \left(\frac{R_2 R_3}{R_1} + R_2 + R_3\right) C_2$$

$$C = 1$$

But when R_b is taken parallel with C_1 the coefficient B is modified and is:

$$B = \left(\frac{R_2 R_3}{R_b} + \frac{R_2 R_3}{R_1} + R_2 + R_3\right)C_2$$

The numerical values of these coefficients are chosen so to get an attenuation of 12db from 10c/s onwards.

For the second filter section $\tau(C_3R_4)$ in Eqn. (4.20) chosen is 1.59×10^{-3}, i.e. to give a notched attenuation characteristic at 100c/s. The second filter section is preceded by a cathode follower. The parameters of this stage are chosen that its impedance at 100c/s is greater than the minimum load impedance for minispace analogue computer which is 4KΩ, this is to avoid overload. Actual circuit impedance chosen at 100c/s is 5.3KΩ. The frequency response test of the angle device is given in Sect. 6.3.

4.4 The Regulator and Associated Circuitry

The simulation of the direct and quadrature axis regulators was done on a small analogue computer. In the following sections the regulators and the associated circuitry are described.

4.4.1 Direct-axis Regulator

The analogue simulation of the proportionate regulator used for the direct-axis regulation is shown in Fig. 4.13. An adder is used to sum up the two

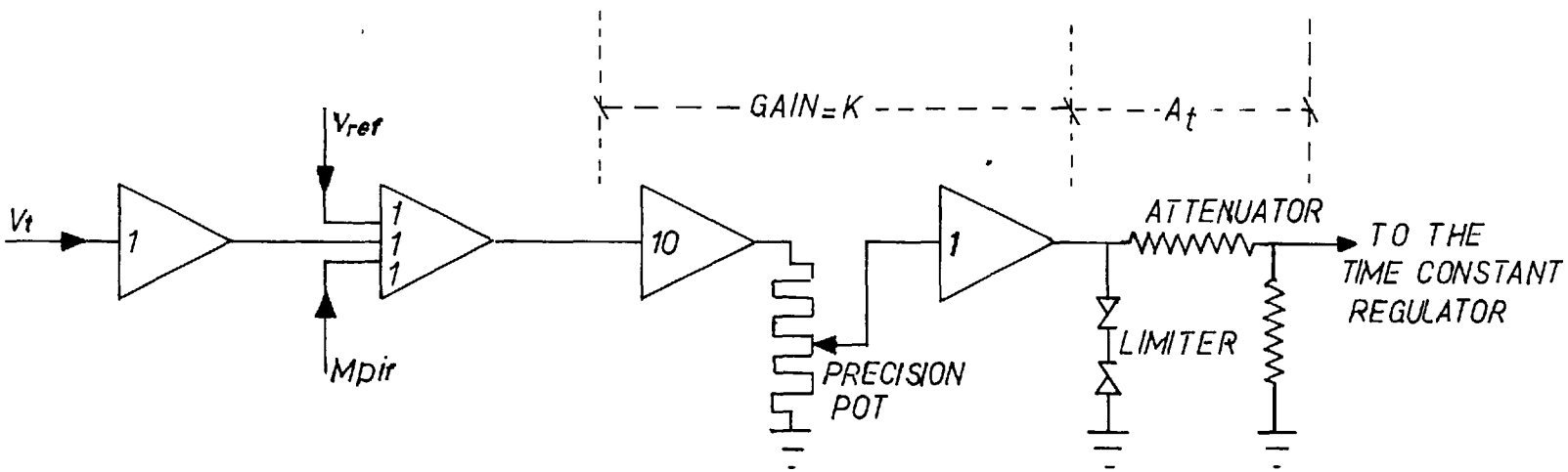

FIG. 4.13. THE REGULATOR AND ASSOCIATED CIRCUITRY.

feedback signals. V_{ref} is to adjust the steady state excitation of the system. A precision decade potentiometer is used before the last stage of amplification to adjust the gain R.

The limiter is simply two back to back Zener diodes to cut off if the output signal exceeds 16 volts level.

4.4.2 Quadrature-axis Regulator

Two types of quadrature-axis regulators were used, namely, the proportionate angle regulator and the regulator with proportionate and derivatives signals. The proportionate regulator can be treated as a special case when the derivatives of the signal are omitted. In Fig. 4.14 is shown the derivative regulator with the following transfer function

$$R_q\left(1 + \frac{.1p}{(1+.01p)(1+.01p)} + \frac{.02p^2}{(1+.01p)(1+.01p)(1+.02p)(1+.01p)}\right)$$

In the circuit diagram conventional differential circuits[31] are used. These circuits work as differentiators at low frequencies but cut off high frequencies or noise and are suitable for our purpose because we deal with frequencies 0—5 cycles. However, in theoretical computations the effect of delays is also considered. The numerical values of the parameters used for the differential circuits are

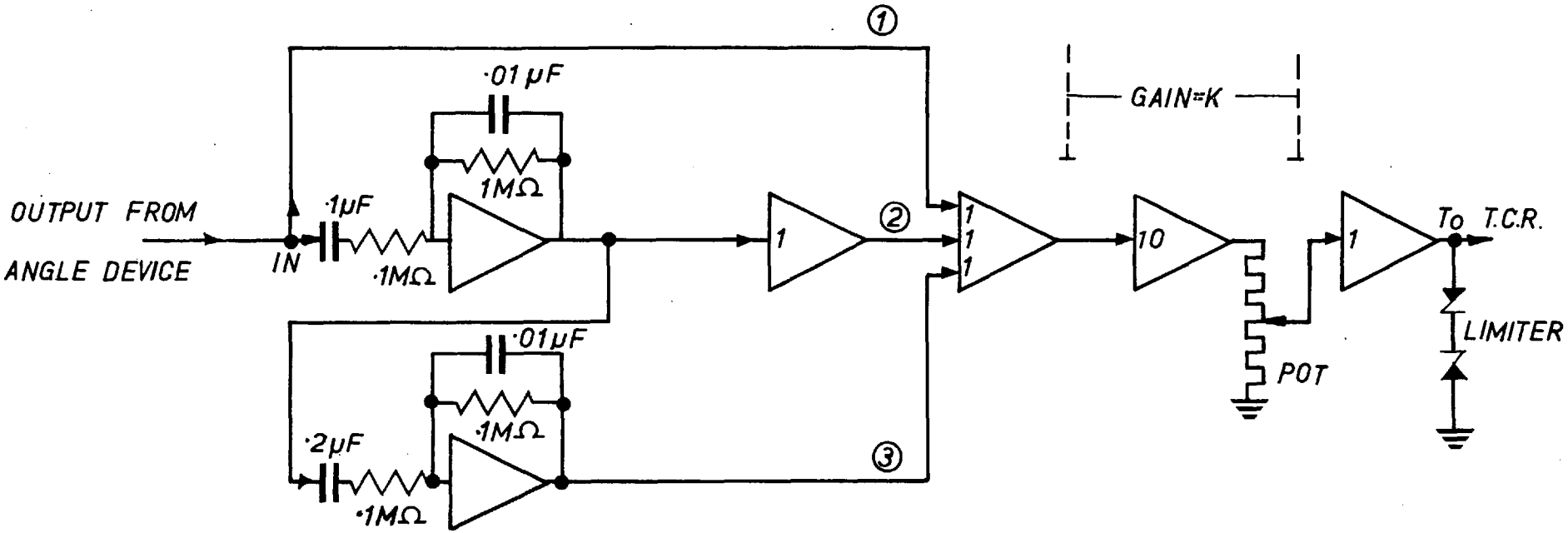

$$T.F. = R_q \left(1 + \frac{\cdot 1p}{(1+\cdot 01p)(1+\cdot 01p)} + \frac{\cdot 02p^2}{(1+\cdot 01p)(1+\cdot 01p)(1+\cdot 02p)(1+\cdot 01p)}\right)$$

FIG. 4.14. QUADRATURE-AXIS DERIVATIVE REGULATOR

given on the figure. For sign inverters and summing units the standard representation is used. The angle signal comes at a point marked 'IN'. The circuit marked '1' carries the signal straight to the summing amplifier, the circuit marked '2' brings the first derivative signal and the circuit marked '3' the second derivative signal. The total signal is amplified and its level adjusted by a precision decade potentiometer. The signal is carried through a buffer amplifier to the time constant regulator. The limiter circuit at the output of the buffer amplifier is for the protection as described in Sect. 4.4.1. The frequency response of the circuit is given in Sect. 6.10.2.

The circuit described above represents the proportionate regulator when the first and second derivative feedback circuits marked '2' and '3' are omitted.

CHAPTER 5

5. DIRECT-AXIS STEADY STATE STABILITY EXPERIMENTAL RESULTS AND COMPARISON

5.1 The Stability

For the experimental investigation of the steady state stability of the system shown in Fig. 4.1 the question was, which system quantities to observe for small variations and from those observations when to declare the system unstable? Out of the various quantities considered, namely, the field current, the vars, the line current, the rotor angle, the last quantity was chosen for observation and declaration of stability primarily because it:

1. is associated with the conventional concept of the stability with the rotor angle,
2. maintained continuity with an earlier investigation[1].

5.1.1 The Stability Code

To maintain reasonable uniformity for the experimental investigations the following code was observed for declaring a condition of equilibrium unstable.

If under any condition of equilibrium the rotor:

1. drifted by 2^{o} from its equilibrium position and subsequently did not settle back within two minutes but continued to drift,
2. drifted and got into a limit cycle of 2^{o} about the mean position,
3. got into an oscillation of 2^{o} which increased in magnitude after a time.

5.1.2 Precautions Against Erratic Judgement

The spurious small variations of the system quantities could lead to an erratic stability judgement while observing the above code. The major spurious variations originated in the system from small variations in the fixed supply and the field current.

To minimise the possibility of erratic judgement because of the small variations of the fixed supply, the stability experiments were conducted in the evenings under the steadier load conditions in the laboratory.

Some spurious small oscillations of about 1 c/s in the field circuit were traced to the oscillations about the mean speed of the induction motor driving the excitor (see Fig. 4.5). The drive motor was a two pole induction motor. No detailed investigations were

carried out into the origin of these small oscillations around the mean running speed of the drive motor, but it was felt that these oscillations could possibly be due to the stator-rotor asymmetry. To avoid these oscillations, which were particularly important when taking a feedback from the field circuit, the drive induction motor was replaced by a synchronous motor with reasonable satisfaction.

5.2 The Regulator Constants

5.2.1 The Regulator Gain R

The regulator gain depends on several factors, namely,

X_{md}/r_{fd}: a constant merged with R, (see Sect. 2.2), numerically equal to 1.89/.001425, (see Table I),

R_e : the rectifier constant; the rectified output is treated as the terminal voltage, (see Sect. 2.1), numerically

$$R_e = \frac{\text{Rectifier Conversion factor x P.U. System Voltage}}{\text{P.U. Field Voltage}}$$

$$= \frac{0.193 \times 186/\sqrt{3}}{965} = .02418 ,$$

K : the adjustable gain constant, (see Fig. 4.13),

A_t : the fixed attenuation, (see Fig. 4.13), numerically equal to .1925.

Thus $R = X_{md}/r_{fd} \times R_e \times A_t \times K$

$= \frac{1.89}{.001425} \times .02418 \times .1925 \times K$

$= 5.485\ K$

5.2.2 The Current Feedback Gain M

The constituents of the current feedback are the mutual inductance of the air-gap transformer in p.u. and the adjustable amplifier gain μ , (see Fig. 4.8).

Thus $M = \frac{.725}{1405} \times \mu = .000516\ \mu$

5.3 The Steady State Stability Curves with the Direct-axis Regulator

5.3.1 With the Voltage Feedback Regulator

The micro-alternator of the system shown in Fig. 4.1 was synchronised with the fixed supply through the series reactance X_c . The power at the fixed supply was adjusted to 0.8 p.u. The voltage feedback circuit was closed. The regulator gain R was adjusted to 1.097, i.e. corresponding to $K = .2$, (see Fig. 4.13). To get the steady state stability limit of the rotor angle for the given regulator gain already adjusted, the

excitation level was decreased in small steps by adjusting V_{ref} , see Fig. 4.2. The small steps were used to avoid large disturbances. For every small decrease in the excitation the rotor advanced to a new equilibrium position. The new rotor angle was watched on the stroboscope (see Sect. 6.2), and the system declared stable or unstable in accordance with the code of Sect. 5.1.1. If the system was stable V_{ref} was further adjusted by a small step and the process was repeated until the steady state stability limit was reached. The process was repeated for a wide range of regulator gains. The experimental curve for the steady state stability limit of the rotor angle against the regulator gain was plotted in Fig. 5.1, Curve 1. The stability in the region marked AB was of a drifting nature and the region marked BC was of an oscillatory nature. The drifting rotor was found to get into a limit cycle oscillation, because when it started drifting the electrical power increased and the mechanical power decreased, but the rotor continued slowly drifting because of the basic instability.

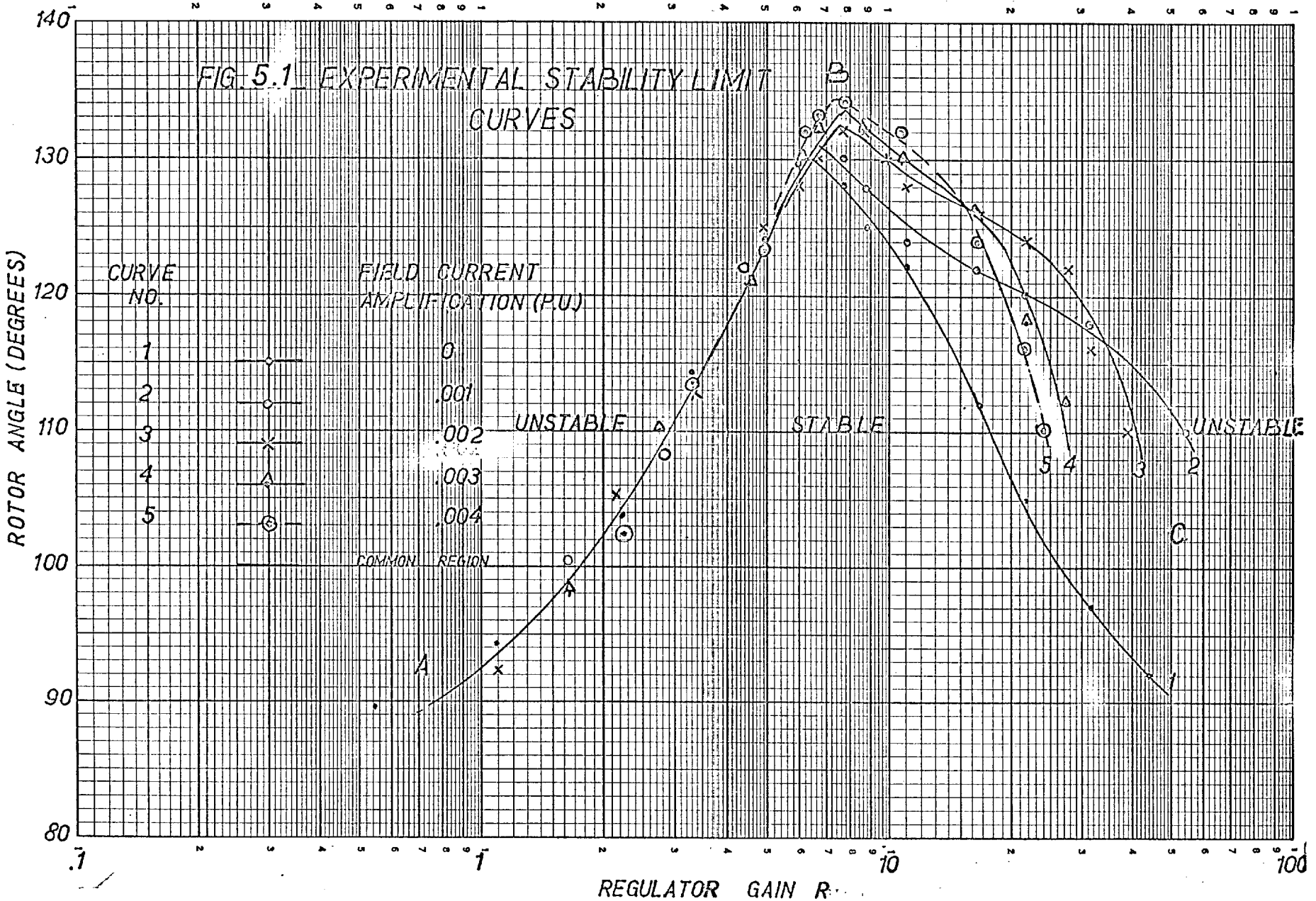
FIG. 5.1 EXPERIMENTAL STABILITY LIMIT CURVES
ROTOR ANGLE (DEGREES)
140
130
120
110
100
90
80
.1
1
10
100
REGULATOR GAIN R
CURVE NO.
FIELD CURRENT AMPLIFICATION (P.U.)
1 0
2 .001
3 .002
4 .003
5 .004
COMMON REGION
UNSTABLE
STABLE
UNSTABLE
A
B
C
1
2
3
4
5

5.3.2 With the Regulator having both Voltage and Field Current Feedback

The auxiliary field current feedback was used in combination with the voltage feedback in the following set of experiments. The gain of the field current feedback was adjusted to .001, .002, .003 and .004 p.u. by a precision decade potential divider as shown in Fig. 4.8, and the whole set of experiment in Sect. 5.2.1 was repeated for each field current gain level. The experimental steady state stability curves were plotted in Fig. 5.1 and marked 2,3,4,5 for the field current gains .001, .002, .003, .004 respectively.

5.4 A Comparison of the Theoretical and the Experimental Curves

The theoretical steady state limit curves for the various field current feedback gains labelled 2,3,4,5 are shown in Fig. 2.11 and corresponding experimental curves are shown in Fig. 5.1.

In the lower gain region AB the curves 2,3,4 and 5 coincide with curve 1. The current feedback seems to have no effect in the region AB. The agreement between the theoretical and the experimental curves in the region AB is good. In the optimum stability region

around the point B the experimental curves tend to give lower limits though only by about 5%. The discrepancy in this region may be attributed to the lag introduced by the field current feedback circuit because of the impedance mismatch at the input of the filter section, (see Fig. 4.8).

In the high gain region BC the experimental curves 1,2,3 are on the optimistic side, i.e. they give slightly higher limits than the theoretical ones. It is shown in Ref. 1 that with damping and resistance taken into account the drooping part BC is slightly lifted upwards for the voltage feedback only (curve 1). If we then extend the argument to the voltage and field current feedback case the experimental curves 2,3 show the right trend. It should be remembered that the filter lag effect in the field current would pull the stability curves slightly down, whereas the resistance and damping would lift it upwards. However, the latter effect seems to dominate the BC region. The theoretical curves show a sharp cut off region represented by CD in the theoretical curves Fig. 2.11. The experimental curves show a quick droop in later parts of the region BC , suggesting a trend similar to the region CD part of the theoretical curves. On the whole there is a

reasonable agreement between the experimental and the theoretical stability limit curves.

CHAPTER 6

6. QUADRATURE-AXIS REGULATION AND ASSOCIATED EXPERIMENTS, RESULTS AND COMPARISON

The experiments in this section relate to the quadrature-axis excitation regulation by signals derived from the terminal voltage and the rotor angle.

Two types of quadrature-axis voltage regulators were used, namely, the one with only a derivative term and the other with proportionate and derivative terms, but both did not give any improvement in the steady state stability limit of reactive absorption at zero power.

Some useful results were obtained for the scheme shown in Fig. 4.2 using a signal derived from the rotor angle. The following set of experiments were conducted. The system shown in Fig. 4.2 was synchronised with the fixed supply treated as the infinite bus. The angular position of the tachogenerator stator was adjusted to give the correct zero for the angle measuring device. The angle device output characteristic was determined to establish the feedback loop gain. With the quadrature-axis regulating loop in operation the steady state

stability limit tests were carried out for different gain levels of the proportionate regulator at 0.2, 0.5, 0.8 p.u. power. For the derivative regulator the same test was repeated at 0.2 p.u. power. The frequency response test of the feedback loop components, namely, the angle device and the regulator was carried out, followed by the closed-loop frequency response test of the system in Fig. 4.2 and from it was established the open-loop frequency response curve.

6.1 Voltage Feedback into the Quadrature-axis Excitation

The system shown in Fig. 4.2 was synchronized on the direct-axis excitation with the fixed supply. The voltage feedback arrangement as shown in Fig. 4.1 for the direct-axis was now used for the quadrature-axis excitation and the direct-axis excitation was left as shown in Fig. 4.2. The power at the fixed supply was adjusted to zero. For the voltage feedback circuit the regulator transfer function used was

$$\left[\frac{.2p}{(1+.02p)(1+.01p)}\right]R$$

The direct-axis excitation was decreased in small steps to avoid a large disturbance. The new equilibrium was

watched for instability in accordance with the stability code of Sect. 5.1. The above process was repeated till the steady state reactive absorption limit was established.

The experimental curve 1 in Fig. 6.1 shows the limiting negative vars for a range of regulator gain. The numerical figures mentioned in the figure for the regulator gain are only the loop constant terms including the rectifier conversion factor, the adjustable gain K and the fixed attenuation A_t . The numerical value is = .193 x 10.0 K x .192 = 3.72K . Thus it has no relation with the direct-axis regulator gain R or the quadrature-axis regulator gain R_q . However, curve 1 suggests that the limiting value of reactive absorption for a wide range of regulator gain is about -.51 which is very close to $-V_{qo}{}^2 Y_q$ limit, thus supporting the theoretical deduction in Sect. 3.3.2.

In the next experiment the regulator transfer function was altered as follows to include a proportionate term

$$\left[1 + \frac{.2p}{(1+.02p)(1+.01p)}\right] R$$

The experimental result is shown in curve 2 of Fig. 6.1. It is similar to curve 1 and suggests

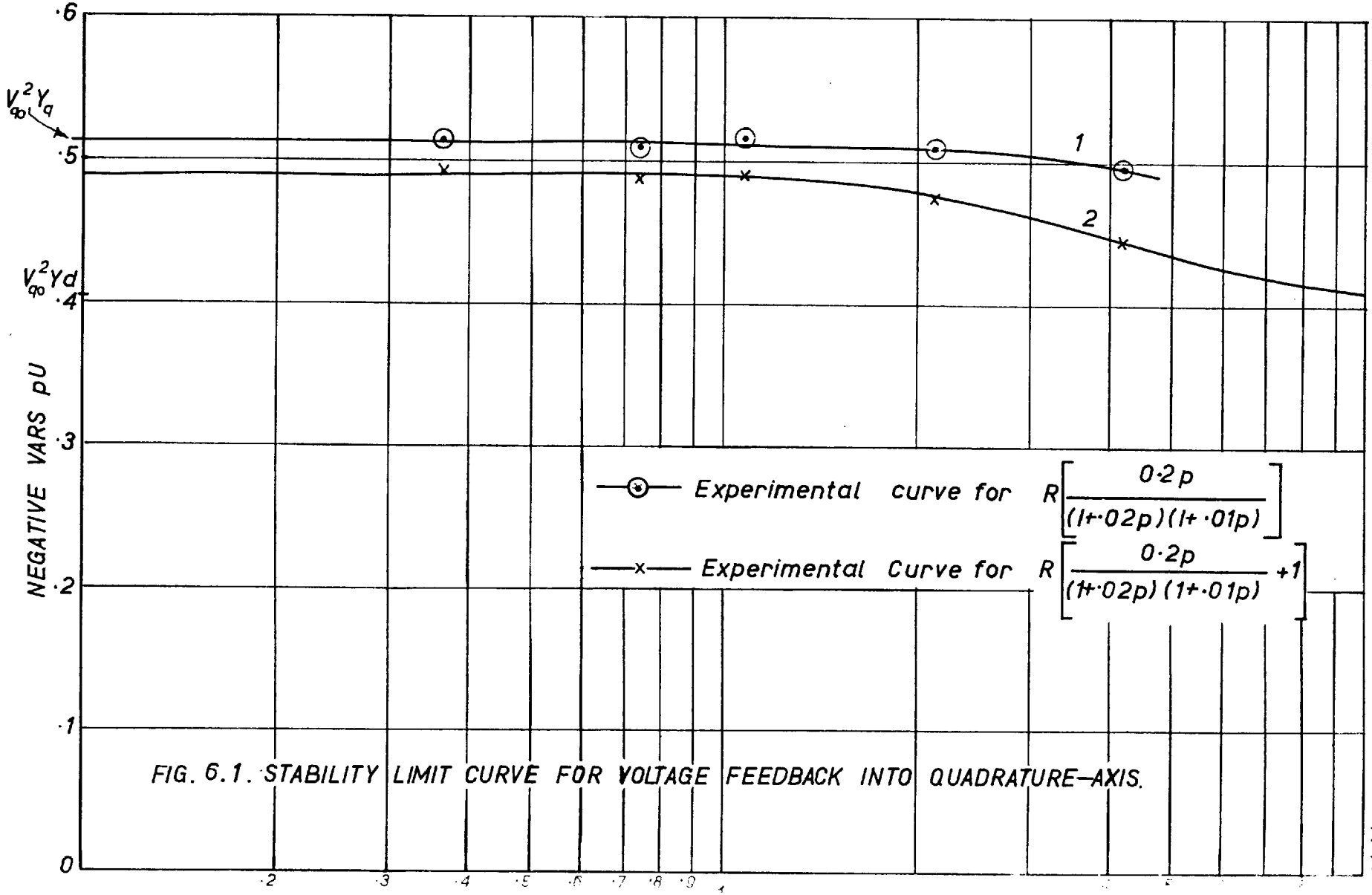

FIG. 6.1. STABILITY LIMIT CURVE FOR VOLTAGE FEEDBACK INTO QUADRATURE-AXIS.

1. the reactive absorption is nearly constant for a wide range of the regulator gain though its value tends to be slightly lower than $-V_{qo}{}^2Y_q$.
2. at higher gains the curve droops and the reactive absorption limit tends towards $-V_{qo}{}^2Y_d$.

It seems that the proportionate term in the transfer function is ineffective in increasing the reactive absorption. With the terminal voltage decreasing the flux is pushed into the quadrature-axis and the system appears to settle for a reactive absorption limit of $-V_{qo}{}^2Y$ where Y is an admittance in quadrature to the new m.m.f. axis created by the proportionate term.

The two experiments indicate that the reactive absorption limit of $-V_{qo}{}^2Y_q$ at zero power cannot be increased by a voltage feedback into the quadrature-axis.

6.2 The angle Device Output characteristic and Zero Setting

The device described in Sect. 4.3.2.2 provides a signal proportional to $\cos(\delta-\delta_o)$, where δ is the mechanical load angle and δ_o depends on the angular position of the tachogenerator stator. Since it is desired to obtain a signal proportional to δ the tachogenerator is set so that $\delta_o = 90^o$ and hence the signal varies as $\sin\delta$ or approximately as δ over

the range $\pm 30^{o}$.

For calibration of the angle device the system in Fig. 4.2 was synchronised and the aligned angle device was switched on. The output of the angle device through a buffer amplifier was connected to a centre-zero voltmeter. The buffer amplifier was provided to prevent the voltmeter from loading the second section of the filter unit (see Fig. 4.11). To calibrate the angle device for motoring and generating action of the machine the tachogenerator stator was manually rocked on both sides of the aligned position. The tachogenerator stator position was read on a graduated annular ring with respect to the reference arrow on a disc coupled to the rotor and moving inside the annular ring, but visually made standstill because of synchronism with a stroboflash. The angle device output for the corresponding tachogenerator position was noted from the centre-zero voltmeter.

Fig. 6.2 shows the calibrated output characteristic of the angel device, giving the output voltage as a function of the rotor angle (in the experiment the tachogenerator stator was rocked). As expected the calibrated curve is a straight line in the region $\pm 30^{o}$ of rotor angle and has a gradient of 570 mV per degree.

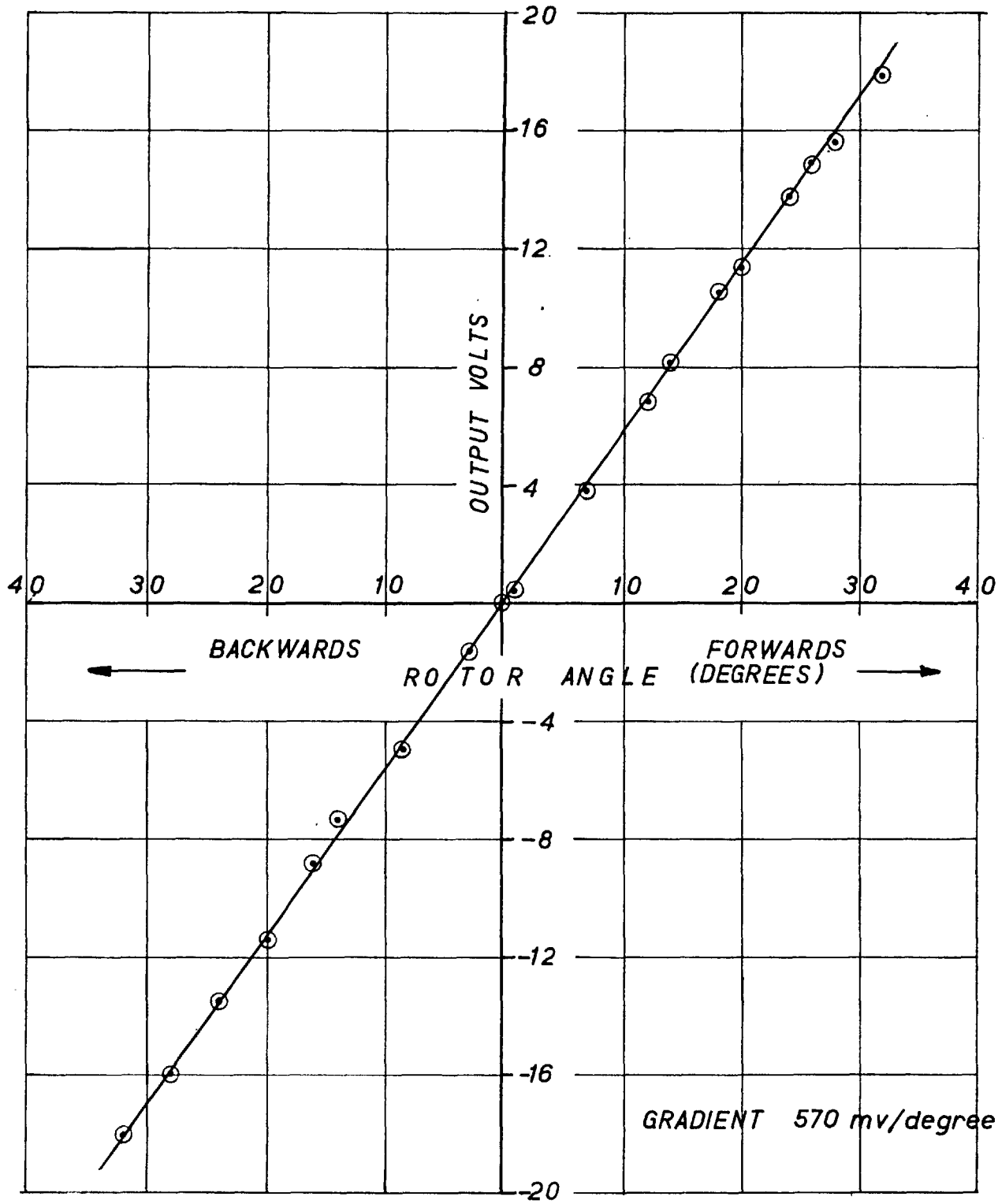

FIG. 6.2. ANGLE DEVICE OUTPUT CHARACTERISTIC.

6.3 Angle Device Frequency Response Test

Strictly the frequency response test of the angle device shown in Fig. 4.11 means applying the reference signal of 50 c/s at the junction of the base resistances (R_{ba}) of T_1 and T_2, and modulating the phase of the constant amplitude of the incoming signal at the required frequency. However, if we assume instantaneous switching and switching off of the complementary pair of transistors T_1 and T_2, the phase detecting unit of the angle device presents to the subsequent stages a chopped waveform with different harmonic contents and a d.c. content which would change with the modulating frequency, see Sect. 4.3.2.3. Our interest is centred on how the variation of the d.c. content is transmitted through the angle device, i.e. equivalent to studying the attenuation and transmission lag of a signal with the transistors T_1 and T_2 representing a set operational condition of one shorted and the other open. The switching operation of T_1 and T_2 does effect the configuration of the following circuitry but interchange of switching does not, that is why a set operational condition of T_1 and T_2 is mentioned above.

In Fig. 6.3 is shown the experimental set up. A variable frequency signal from the oscillator of the

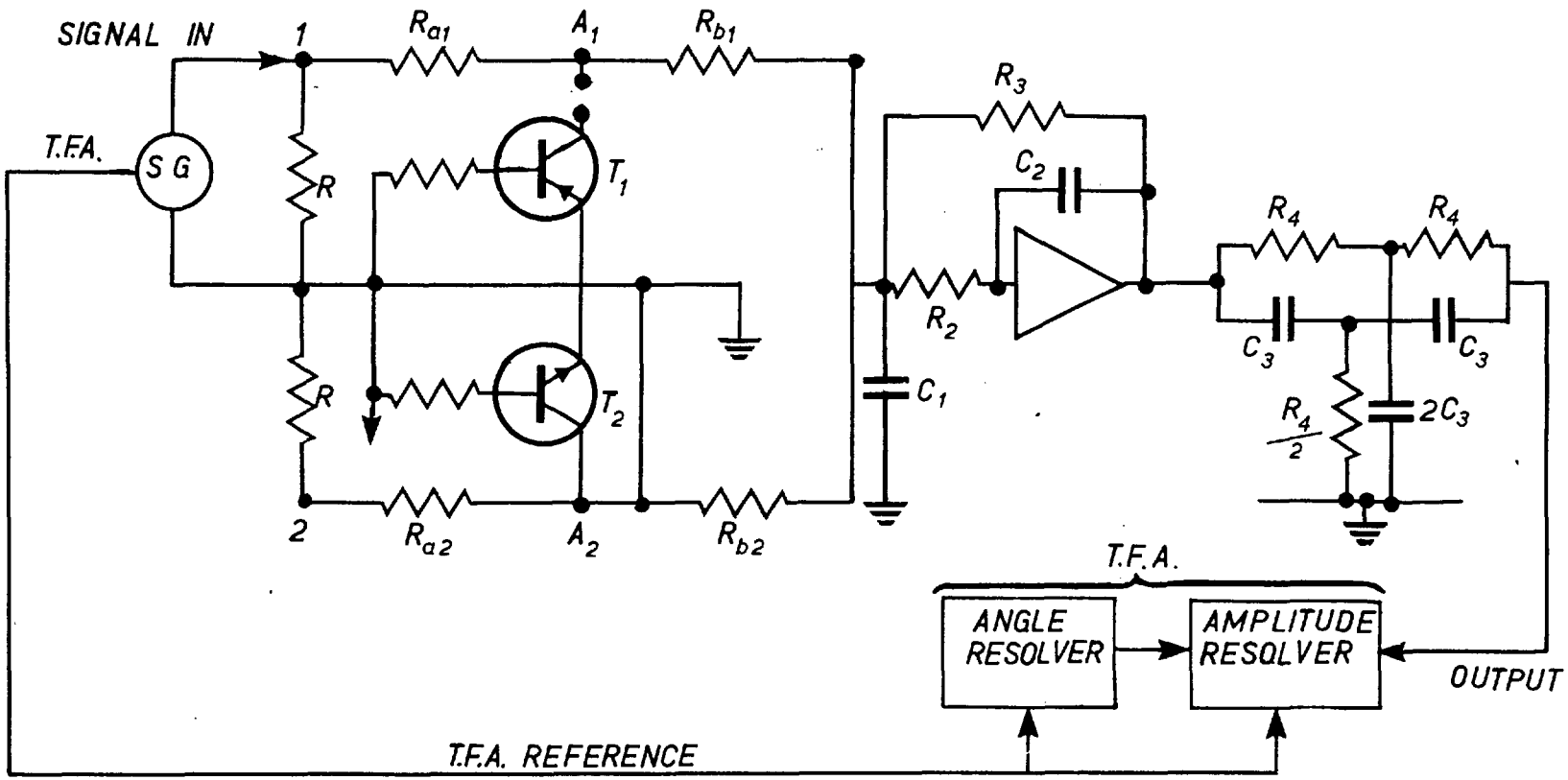

FIG. 6.3. ANGLE DEVICE FREQUENCY RESPONSE TEST

transfer function Analyser (T.F.A.) equipment was applied at terminal 1. To represent the operational states of transistors T_1 and T_2, transistor T_1 was opened at A_1 and T_2 was shorted by earthing A_2. The output of the angle device was connected to the T.F.A. (amplitude resolver). Using the T.F.A. the frequency response was determined up to 30 c/s.

Fig. 6.4 shows the experimental points for the phase shift and the amplitude output to input ratio for various frequencies. The full and broken lines in Fig. 6.3 are the computed curves respectively for the amplitude and phase angle for the circuit in Fig. 6.2. The experimental points show a good agreement with the computed curves.

6.4 The Regulator Gain

The regulator gain R_q depends on several factors, namely,

A_t : the fixed attenuation, numerically equal to .1927, (see also Sect. 5.2.1.),

K_1 : the angle decice constant, numerically = angle device output characteristic slope $(\frac{\text{volts}}{\text{degree}})$ x degrees per radian x $\frac{1}{\text{p.u. Field voltage}}$

$= .57 \times 57.3 \times \frac{1}{646} \frac{\text{p.u. voltage}}{\text{radian}}$, (see Sect. 6.2 and Table II),

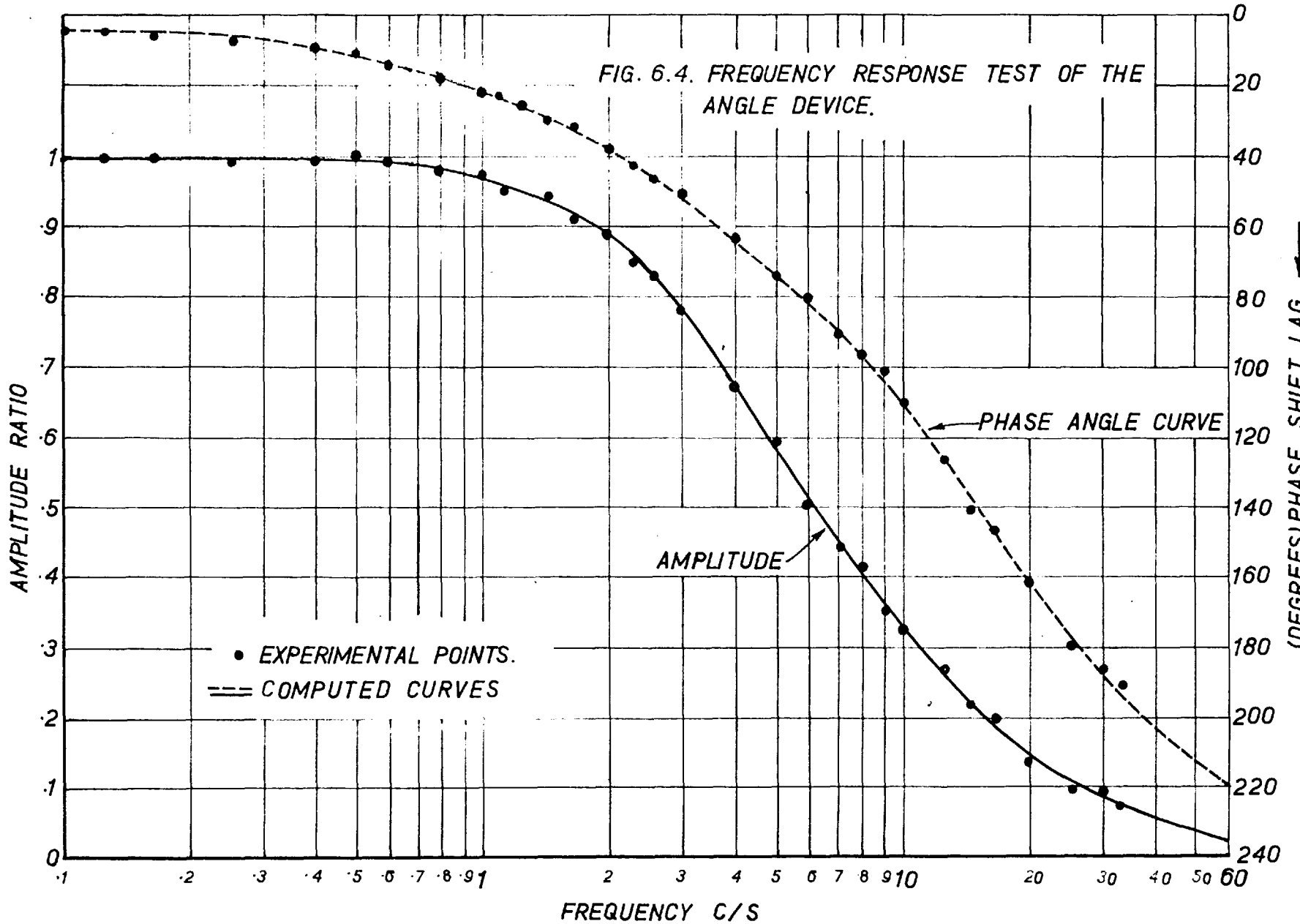
FIG. 6.4. FREQUENCY RESPONSE TEST OF THE ANGLE DEVICE.
PHASE ANGLE CURVE
AMPLITUDE
EXPERIMENTAL POINTS.
COMPUTED CURVES
AMPLITUDE RATIO
(DEGREES) PHASE SHIFT LAG
FREQUENCY C/S
0
·1
·2
·3
·4
·5
·6
·7
·8
·9
1
2
3
4
5
6
7
8
9
10
20
30
40
50
60
0
20
40
60
80
100
120
140
160
180
200
220
240

$\frac{X_{mq}}{r_{fq}}$: a constant merged with R_q, numerically equal to $\frac{1.5}{.00482}$, (see Table II),

K : the adjustable amplifier gain constant.

Thus,

$$R_q = A_t \times K_1 \times \frac{X_{mq}}{r_{fq}} \times K$$

$$= .1927 \times .57 \times 57.3 \times \frac{1}{646} \times K$$

$$= 3.04\ K$$

6.5 Starting of the System

In all the following stability experiments the system shown in Fig. 4.2 was synchronised with the fixed supply on the direct-axis excitation. The quadrature-axis time constant regulator was introduced but no steady state quadrature-axis excitation was established. The angle device was made operative by switching on its reference supply. The simulated regulator was brought into the circuit by closing the patch panel of the last adjustable gain stage, (see Sect. 4.4.2). Keeping the regulator gain below the limiting level the quadrature-axis feedback circuit was closed. Before any experiments were conducted the system was loaded to 0.8 p.u. power and was run for half an hour to establish a reasonably

steady temperature to ensure that the temperature of the quadrature-axis field winding resistance conformed to that of the measurement and was the same for every experiment, (see Sect. 4.2.3).

6.6 Zero Angle Equilibrium

In the theoretical study it is assumed that the angle regulator establishes the zero angle equilibrium conforming to the equilibrium diagram in Fig. 3.2b. In practice to establish an appropriate excitation in the quadrature-axis there has to be some deviation of the rotor from the reference. The magnitude of this rotor deviation from the reference depends on the load and the regulator gain. For experiments in the following sections a condition of equilibrium upto 1^{o} of rotor deviation from the reference was taken practically as the zero angle equilibrium. All the experiments to determine the steady state reactive absorption limit at any load and regulator gain setting were carried out at a condition of practically zero angle equilibrium, which if necessary was secured by adjusting V_{refq}, see Fig. 4.2. In practice, however, a small deviation from the zero angle equilibrium would not cause concern.

6.7 Steady State Stability Limit Curves for Proportionate Regulator

After the starting and warming of the set (see Sect. 6.5), the power at the fixed supply was adjusted to 0.2 p.u. The regulator gain was adjusted by a decade potentiometer, see Sect. 4.4.2. For low regulator gains for example $R_q = .304$ (see Sect. 6.4) the zero angle equilibrium was assisted by adjusting V_{refq}, see Sect. 6.6 and Fig. 4.2, but for the later stability experiment the system was left unadjusted. To make the system deliver negative vars the positive excitation of the direct-axis was decreased in small steps to zero and then increased in the negative direction.

After every small change in the excitation the system was left for about 5 minutes to settle down particularly in the critical stages near to the stability limit. During the disturbance the rotor was visually watched on the stroboscope in order to assess stability.

The system was considered to be stable, if after the disturbance the rotor settled down asymptotically to zero equilibrium otherwise it was unstable. It was difficult to ascertain the start of instability particularly the drifting type, however, a reasonable uniformity in assessment of stability limits was achieved by

observing the procedure for declaring the system stable or unstable as well as the precautions against erratic judgement as mentioned in Sect. 5.1.

The decision for the loss of stability for the drifting type of instability is demonstrated in the following example.

Power =-0.2 p.u.

Regulator gain R_q = 1.52

For positive direct-axis excitation the system showed no sign of drift or oscillations. In the negative direct-axis excitation region the final stages of the loss of stability is demonstrated by the following chart.

Direct-axis Excitation Step	Negative vars p.u.	Remarks on the System Behaviour
Negative excitation increased by a small amount from the previous level	.966	The rotor deviated by 2° but settled down to zero angle equilibrium. Every now and then the rotor wandered by 1°. After observing for 5 mins. the system was declared stable.
"	..97	The rotor deviated in the following manner

Direct-axis Excitation Step	Negative Vars p.u.	Remarks on the System Behaviour
		$0/2^{\circ}/1^{\circ}/0^{\circ}/1^{\circ}/0^{\circ}/1^{\circ}/0$. Over 5 minutes the rotor showed tendencies of deviation but settled down within 1°. The system was declared stable.
"	.985	The rotor deviated as follows $0^{\circ}/2^{\circ}/0^{\circ}/3^{\circ}/0/4^{\circ}/0^{\circ}/4^{\circ}/0/4^{\circ}$ and then went into the limit cycle with a very slow drift. The system was declared unstable. However, within 5 mins. it did not slip.
"	1.02 (mean value over the swing)	The rotor behaviour summarized over five minutes: $2^{\circ}/6^{\circ}/2^{\circ}/8^{\circ}/2^{\circ}/8^{\circ}$ and continued drifting slowly but did not slip.
"	1.04 (mean value over the swing)	The rotor behaviour summarized over five minutes $2^{\circ}/9^{\circ}/2^{\circ}/10^{\circ}/3^{\circ}/10^{\circ}/3^{\circ}$

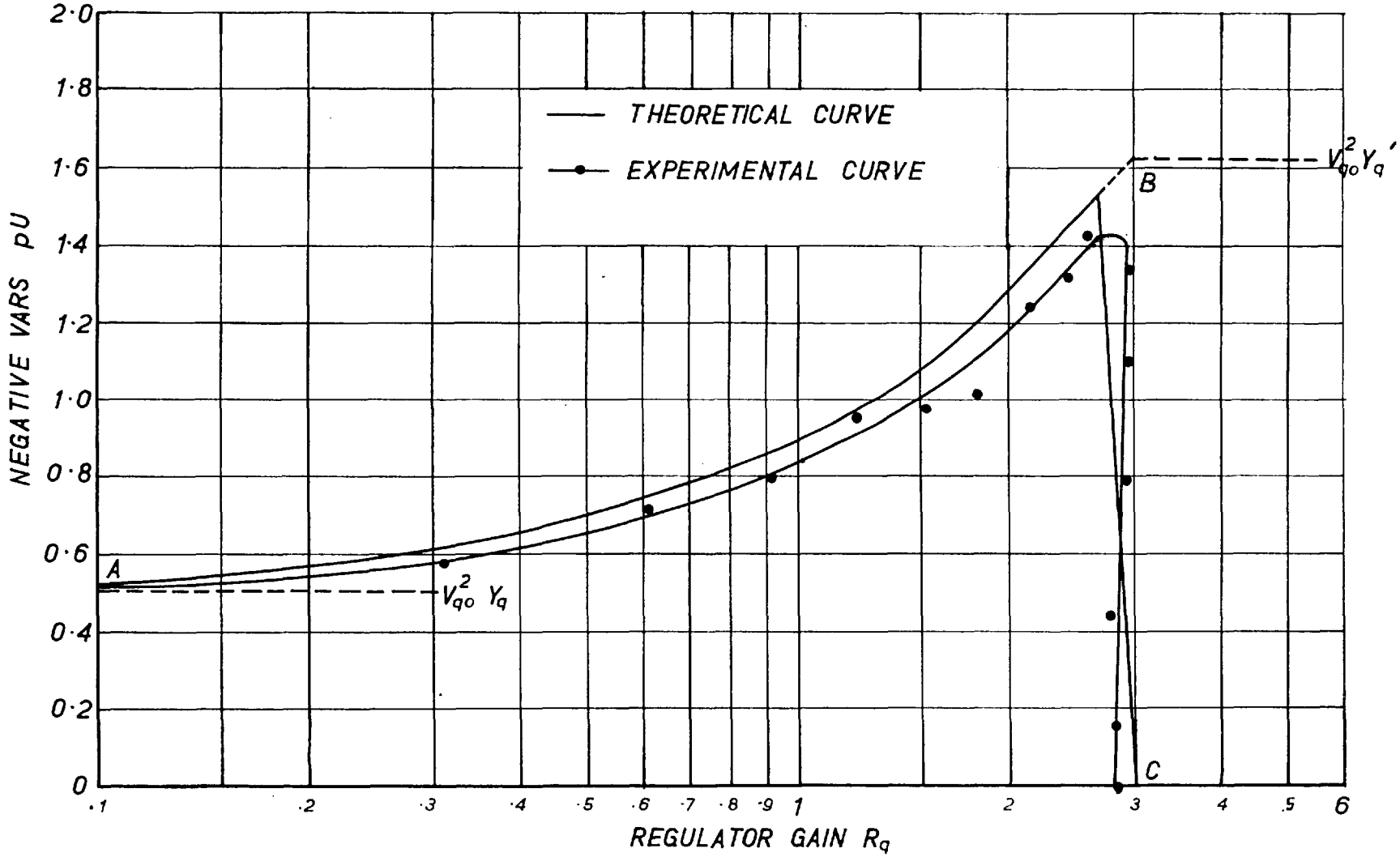

FIG.6.5. STEADY STATE STABILITY LIMIT CURVES FOR PROPORTIONATE REGULATOR AT POWER 0·2 pU.

After further steps the synchronism was lost at -1.1 vars (mean value over the swing), however, the system was declared unstable at vars =-.985 p.u., (see the above chart)

The regulator gain R_q was increased in steps and the above procedure was repeated to locate the steady state stability limit. In Fig. 6.5 the experimental points are marked as dots for the corresponding regulator gains. It can be seen that the steady state reactive absorption limit increases with the regulator gain upto about $R_q = 3$, and the system then becomes unstable at a sharply sloping stability limit curve.

After making some trials of the sloping region a more precise assessment was attempted. It was found easier to fix the reactive absorption and increase the regulator gain R_q in small steps. After every small step increase in the regulator gain R_q the system was observed for about 5 minutes for any instability as in the previous case. Since the instability in this region was an oscillatory nature, it was easier to judge. In the following example the final stages of the loss of stability are recorded.

Power = -0.2 p.u.

vars = -1.16 p.u.

Regulator Gain	Remarks on the System Behaviour
2.83	The rotor oscillated by 1° about zero angle equilibrium and settled down. The system was observed for 5 mins. and declared stable.
2.86	The system behaviour was the same as above and the system was declared stable.
2.89	The system oscillated more frequently by less than 2° but settled down. The system was declared stable.
2.92	The rotor oscillated freely as below $0^{\circ}/2^{\circ}/0/-2^{\circ}/0/3/0/-3^{\circ}/$ and the oscillations slowly kept increasing. The system was declared unstable.

After further steps the system grew violently unstable at $R_q = 3.04$.

The whole range of points on the sloping region of the steady state stability curve were found in a similar way and plotted in Fig. 6.5. The theoretical curve was

also plotted on the same figure.

Similar theoretical and experimental curves for 0.5 and 0.8 p.u. power are given in Figs. 6.6 and 6.7.

6.7.1 A Comparison of the Theoretical and Experimental Curves

For comparison the theoretical and experimental curves in Fig. 6.5, 6.6 and 6.7 are divided into regions marked AB and BC . The region AB corresponds to drifting instability and BC to oscillatory instability.

The determination of the experimental curves in Figs. 6.5, 6.6 and 6.7 depends on the procedure described in Sect. 5.1 for determining the system stability. The experimental curves in the region AB and BC would be shifted somewhat if the procedure was modified. For example if a variation of 4^{o} was adopted instead of 2^{o} the experimental curves in Figs. 6.5, 6.6 and 6.7 would shift slightly outwards and would agree better with the theoretical curves.

In the BC region the theoretical and experimental curves agree well for power 0.2 p.u. in Fig. 6.5, but the agreement is less good at higher power levels. This is probably because the parameters correspond better to the conditions in the first case. In particular saturation

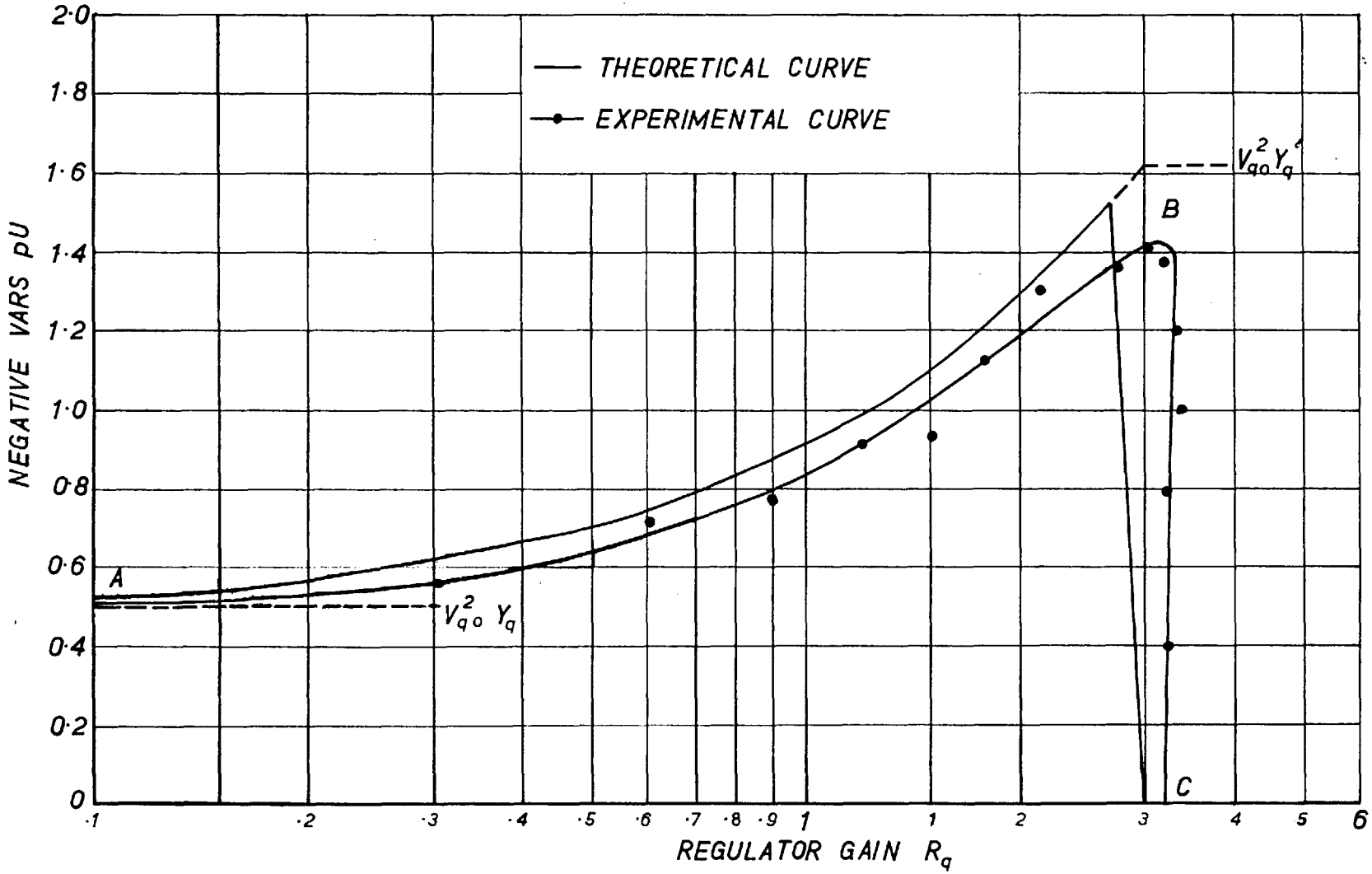

FIG. 6.6. STEADY STATE STABILITY LIMIT CURVES FOR PROPORTIONATE REGULATOR AT POWER 0·5 pU

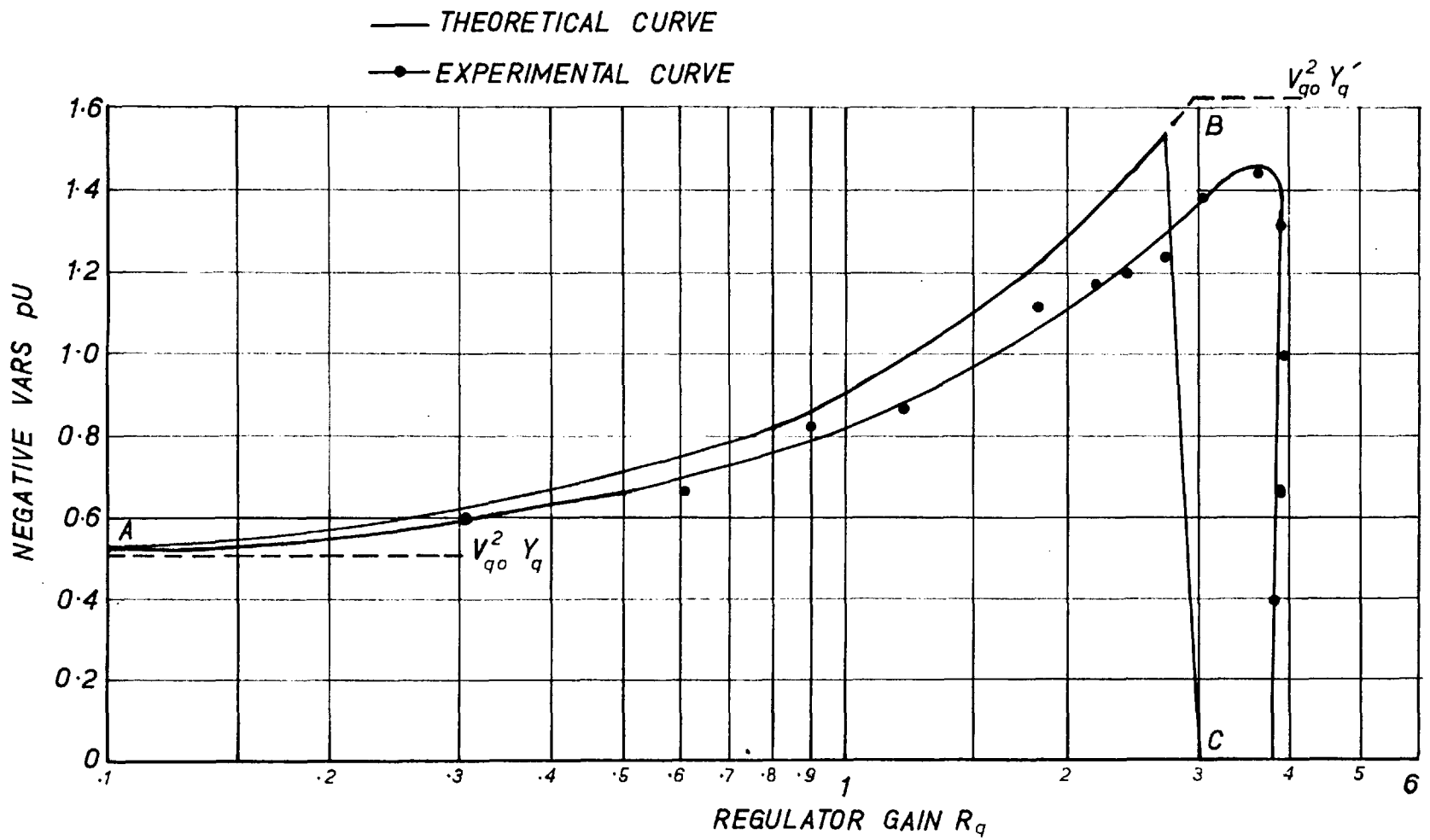

FIG. 6.7. STEADY STATE LIMIT CURVES FOR PROPORTIONATE REGULATOR AT POWER 0·8 pU.

in the quadrature-axis causes Y_q and Y'_q to increase. Hence the slight increase in reactive absorption and the gain, (see Eqns. 3.2b and 3.24) with increasing power. The experimental curves in Figs. 6.6 and 6.7 show slight increase in $Q_o(max)$ and $R_q(max)$ compared to Fig. 6.5. Fig. 6.7 shows a similar trend compared to Fig. 6.5. Thus, the discrepancies in the BC region at various power levels are probably due to parameter variation in Y_q and Y'_q .

6.8 The Steady State Stability Limit Curve for the Derivative Regulator

The following transfer function $R_q(p)$ for the regulator was simulated on the analogue computer, (see Sect. 4.4.2).

$$R_q(p) = R_q \left[1 + \frac{0.1p}{(1+.01p)(1+.01p)} + \frac{.02p^2}{(1+.01p)(1+.01p)(1+.02p)(1+.01p)}\right] \quad (3.32)$$

R_q was adjusted on the decade potentiometer as was done for the proportionate angle regulator. The power at the fixed supply was adjusted to 0.2 p.u.

Fig. 6.8 shows the curves obtained with the derivative

FIG. 6.8. STEADY STATE STABILITY LIMIT CURVES AT POWER 0·2 pU.

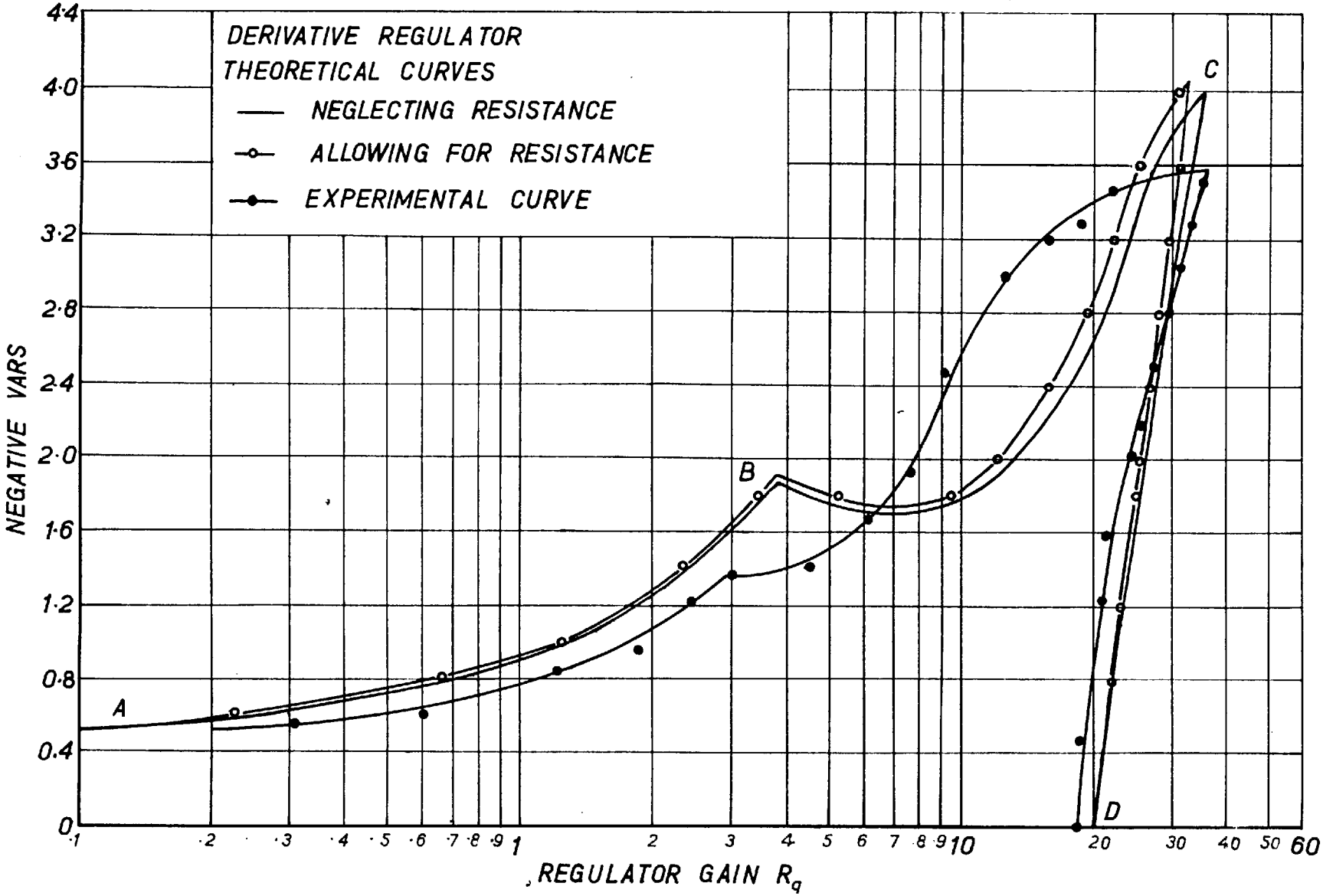

regulator. Compared with Fig. 6.5 the same limit curve is obtained at low regulator gain but the reactive absorption is greatly increased at higher gains. The very high current at $Q_o = -3.5$ p.u. causes difficulty with the measurements, and for this reason the curve was only measured at $P = 0.2$. Tests were however made to show that the system was stable at equally high values of Q at higher powers.

The procedure for determining the steady state reactive absorption limit in the region AB and BC (see Fig. 6.8) was the same as for the proportionate regulator.

Like the proportionate regulator the derivative regulator also eshibited the sudden loss of stability for regulator gains above the point C , (see Fig. 6.8). By trial it was observed that though the system was stable for higher reactive absorption but was unstable for decreased absorption. Thc instability in this region marked CD was of oscillatory nature. To locate the experimental steady state limit points in this region, the following procedure was adopted.

The system was brought to the maximum absorption limit. In very small steps the negative excitation was decreased. The disturbed system was observed for new

decreased reactive absorption. The system in this region had a very sharp definition of oscillations. If for 2-3 minutes no oscillations developed the negative excitation was further decreased by a small step. The above process was repeated till 2^{o} oscillations of the rotor were noticed. After noting the limiting - vars, the reactive absorption was again increased to stabilise the system. The regulator gain was slightly decreased and the above process was repeated. The experimental points in the region CD were plotted, see Fig. 6.8. From such points in the regions AB , BC and CD an experimental stability limit curve was plotted in Fig. 6.8.

6.8.1 A Comparison of the Experimental and Theoretical Curve

Fig. 6.8 shows the theoretical and experimental curves, the various regions are labelled as AB , BC , and CD.

For the experimental curve AB region is the same as in Fig. 6.5. A discussion provided in Sect. 6.7.1 is equally valid for the region AB here.

The theoretical and experimental curves show a great discrepancy in the region BC. Since the steady state reactive absorption increases in this region very much, consequently the current loading goes upto 4 p.u., therefore, it was expected that the resistance of the series reactance X_c and the machine could be having stabilising effect. For this reason a theoretical curve allowing for resistance was plotted as shown in Fig. 6.8. Allowing for resistance decreases the

discrepancy in the region BC to some extent. However, the overall effect of resistance is not very appreciable.

The region CD shows good agreement. This region gets affected by the transfer functions of various components and the parameter Y'_q. The reason for the good agreement may be because the parameters better correspond to this power level and the various feedback circuits give close agreement with the designed transfer functions in the frequency region associated with CD , i.e. about 2.5 c/s. The trend of the slopes of the experimental and theoretical curves is similar, though the experimental curve in the lower reactive absorption region tends to be less inward slanting than the theoretical. This trend shows that the system at high gains is unstable even in the region which is otherwise stable without the regulation.

Looking at the overall experimental and theoretical curve the agreement could be said to be reasonable.

6.9 A Comparison between the Proportionate and the Derivative Regulator

1. The maximum permissible regulator gain for the derivative regulator is about ten times that of the proportionate regulator.

2. The maximum permissible reactive absorption achieved for the derivative regulator is about -3.5 p.u.

compared to about -1.4 p.u. with the proportionate regulator.

3. The derivative regulator maintains zero angle equilibrium for a wide range of regulator gain, whereas, the proportionate regulator requires a separate adjustment of V_{refq} .

4. Though no quantitative results were obtained, it is worthy of record that the derivative regulator acted faster to establish the zero equilibrium than the proportionate regulator for any load variations under the same initial load conditions with any gain setting.

6.10 Frequency Response of the Quadrature-axis Regulator

6.10.1 The Proportionate Regulator

The proportionate regulator only involves d.c. amplifiers and a decade potentiometer, and the circuit arrangement is the same as for the direct-axis proportionate regulator shown in Fig. 4.13. A frequency response test using the Transfer Function Analyser (T.F.A.) showed preactically no phase shift and attenuation, as one would expect with analogue computer d.c. amplifiers. Thus, the transfer function of the proportionate quadrature regulator was taken simply as an adjustable constant.

6.10.2 The Derivative Regulator

The transfer function of the derivative regulator is given in Eqn. 3.32, (also see Sect. 6.8) and its simulation is shown in Fig. 4.14. A frequency response test was done on the simulated derivative regulator circuit of Fig. 4.14 using the T.F.A. equipment. In Fig. 6.9 is a polar diagram showing the computed and the experimental points. Fig. 6.9a shows the computed curve and the experimental points for the important range of frequencies (0 to 2.2 c/s). Fig. 6.9b shows the complete computed curve and the experimental points up to 100 c/s on a reduced scale. The experimental points are very close to the corresponding points on the computed curve upto 5 c/s and for higher frequencies also the agreement is reasonably good.

6.11 Open-loop Frequency Response Test of the System

In order to measure the open-loop frequency response of a servo system, the closed-loop is broken at a suitable point and the frequency response is measured. If however the loop cannot be broken for stability reasons as is the case here, the open-loop frequency response can be obtained from a closed-loop frequency response test. In Fig. 6.10 is shown a conventional servo-system. For

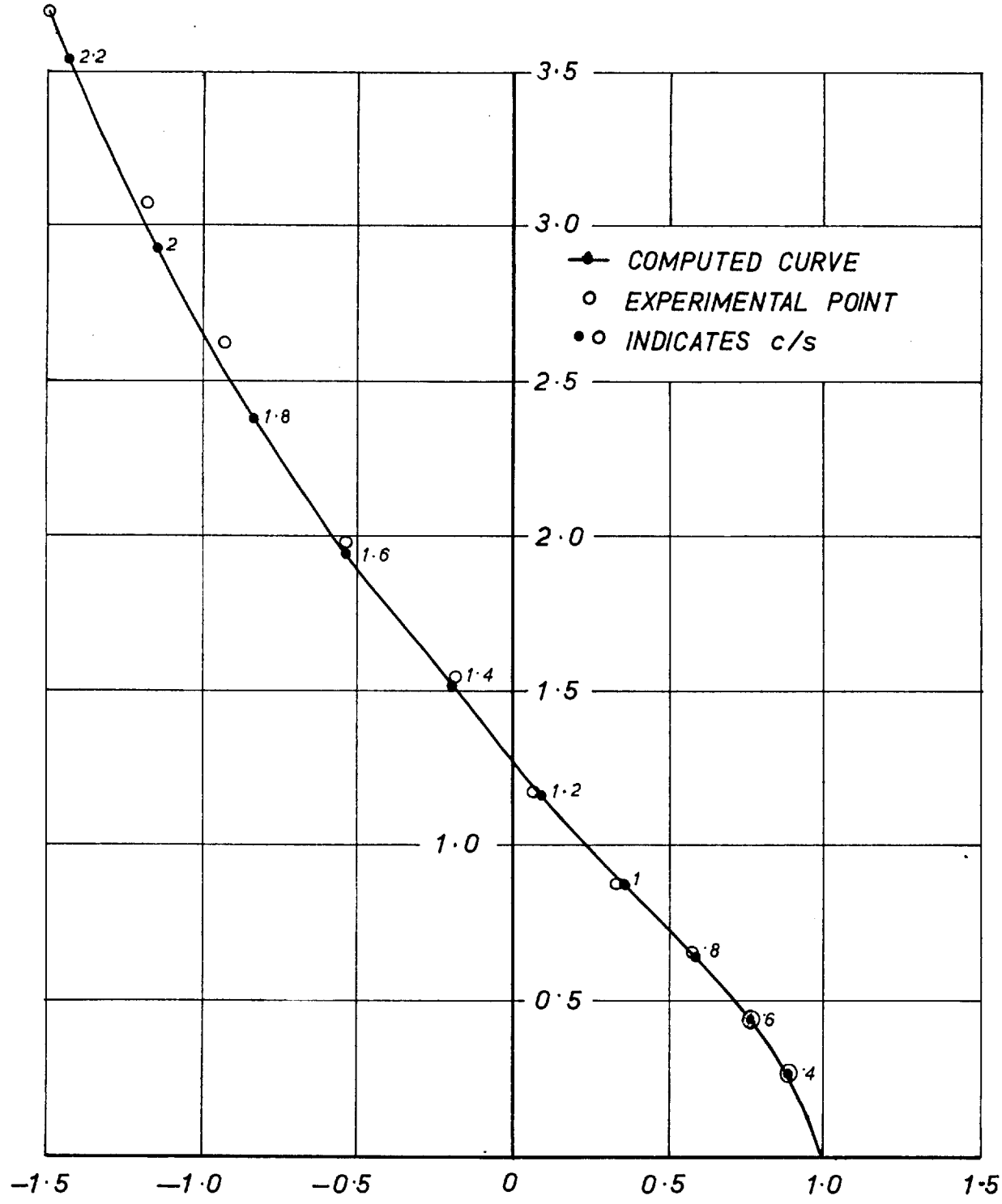

FIG. 6.9a. FREQUENCY RESPONSE TEST—DERIVATIVE REGULATOR.
FREQUENCIES 0 to 2·2 c/s.

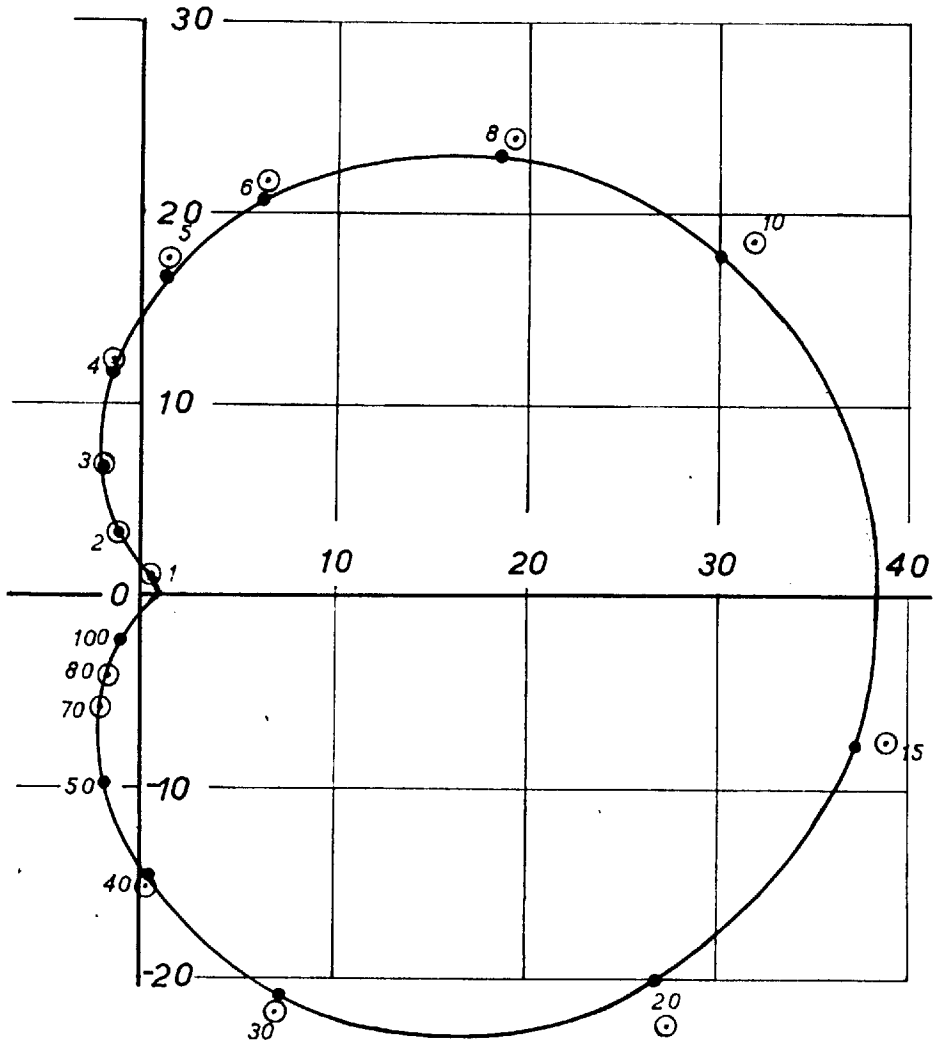

FIG. 6.9b. FREQUENCY RESPONSE CURVE FOR THE DERIVATIVE REGULATOR.
FREQUENCIES 0 to 100 c/s

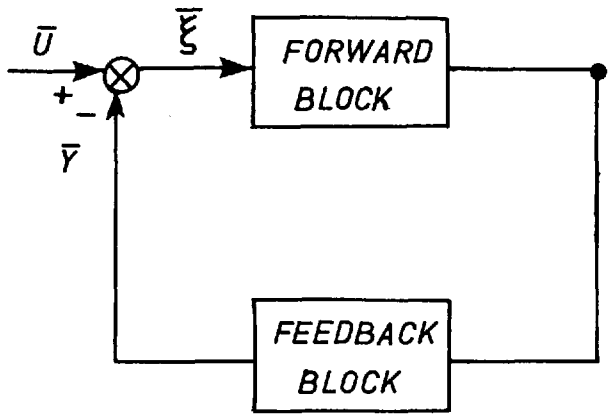

FIG. 6.10. CONVENTIONAL SERVO-SYSTEM

a disturbance $\bar{U}$ we have the error signal $\bar{\xi}_1$ and the loop output $\bar{Y}$ which are related as below

$$\bar{\xi}_1 = \bar{U} - \bar{Y} \tag{6.1}$$

The open-loop transfer function is

$$\frac{\bar{Y}}{\bar{\xi}_1} = \frac{\bar{U}}{\bar{\xi}_1} - 1 \tag{6.2}$$

Thus for any signal $\bar{U}$ injected into the system if $\bar{Y}$ and $\bar{\xi}_1$ are measured the openl-oop frequency response can be obtained.

The experimental arrangement using the above technique is shown in Fig. 6.11. The various items of equipment and quantities such as $\bar{U}$, $\bar{\xi}_1$, $\bar{Y}$ are labelled in the figure. The T.F.A. was used for injecting a signal $\bar{U}$ and for the measurement of $\bar{Y}$ and $\bar{\xi}_1$. Alternatively an oscilloscope arrangement described later was used for the measurement. Switches A and B were used in appropriate positions for connecting $\bar{Y}$ and $\bar{\xi}_1$ to the T.F.A. for measurements or to the oscilloscope arrangement.

After starting and warming the set as in Sect. 6.5, the power at the fixed supply was adjusted to 0.5 p.u.

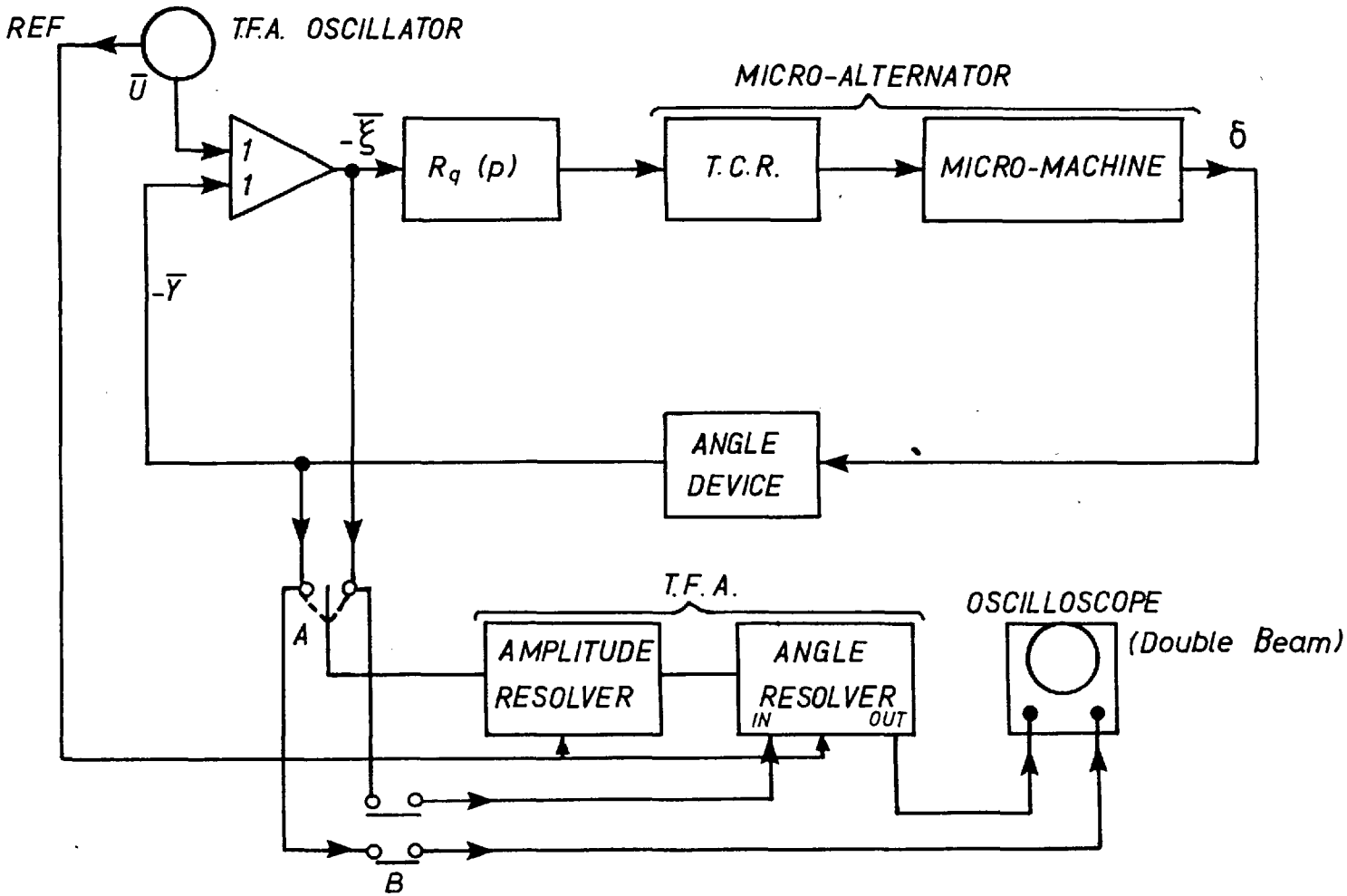

FIG.6.11. EXPERIMENTAL ARRANGEMENT FOR THE SYSTEM FREQUENCY RESPONSE TEST

The proportionate regulator gain R_q was adjusted to 1.52 (K = 0.5) and the reactive absorption to 0.8 p.u. A variable frequency signal from the T.F.A. of magnitude small enough to make the rotor oscillate by about 2^o was used. The angle and the magnitude of the error vector $\bar{\xi}_1$ and the output vector $\bar{Y}$ with respect to the input vector $\bar{U}$ were measured using the angle resolver and the magnitude measuring equipment of the T.F.A. This arrangement was used for frequencies of .5 c/s upwards. Below that the measurements with oscilloscope arrangement were preferred because for low frequencies the amplitude measuring unit of the T.F.A. oscillated about the mean value causing difficulty in reading, whereas, on the oscilloscope a trace was easily taken. The vector $\bar{Y}$ was taken to one beam of the oscilloscope with the time base cut off and the vector $\bar{\xi}_1$ through the angle resolver of the T.F.A. to the second beam of oscilloscope. The angle resolver was used to shift the phase of the vector $\bar{\xi}_1$ until the two beams were seen to be in phase. The angle resolver gave the angle of vector $\bar{Y}$ with respect to $\bar{\xi}_1$. Their magnitudes were measured on the oscilloscope using tracing paper. There was noise superimposed on the traces of vectors $\bar{Y}$ and $\bar{\xi}_1$ which made the observations

susceptible to errors, particularly the angle. The frequency response of a non-linear dynamic system running at a steady state condition cannot be measured accurately because for a good measurement the magnitude of the output quantities should be of measurable level, which means that the equilibrium must be disturbed sufficiently and so does not conform to the theory.

Fig. 6.12 shows the experimental and theoretical curves for the system frequency response. The experimental points indicate that the maximum gain in the oscillatory instability region is actually more than that given by the theoretical curve as was also observed in the stability limit experiment, (see Fig. 6.6). All low frequency points tend to be outside the theoretical curve which probably is due to the effect of resistance which has been ignored. At very low frequencies the error is greater and could be attributed to measurement error.

Fig. 6.13 shows the experimental and theoretical curves for the derivative regulator. The frequency response was only measured in the region where the noise did not affect the accuracy of measurement, this region for the derivative regulator happens to be the important one. The test was done at 0.2 p.u. power,-1.4 p.u. reactive absorption and with a regulator gain R_q of

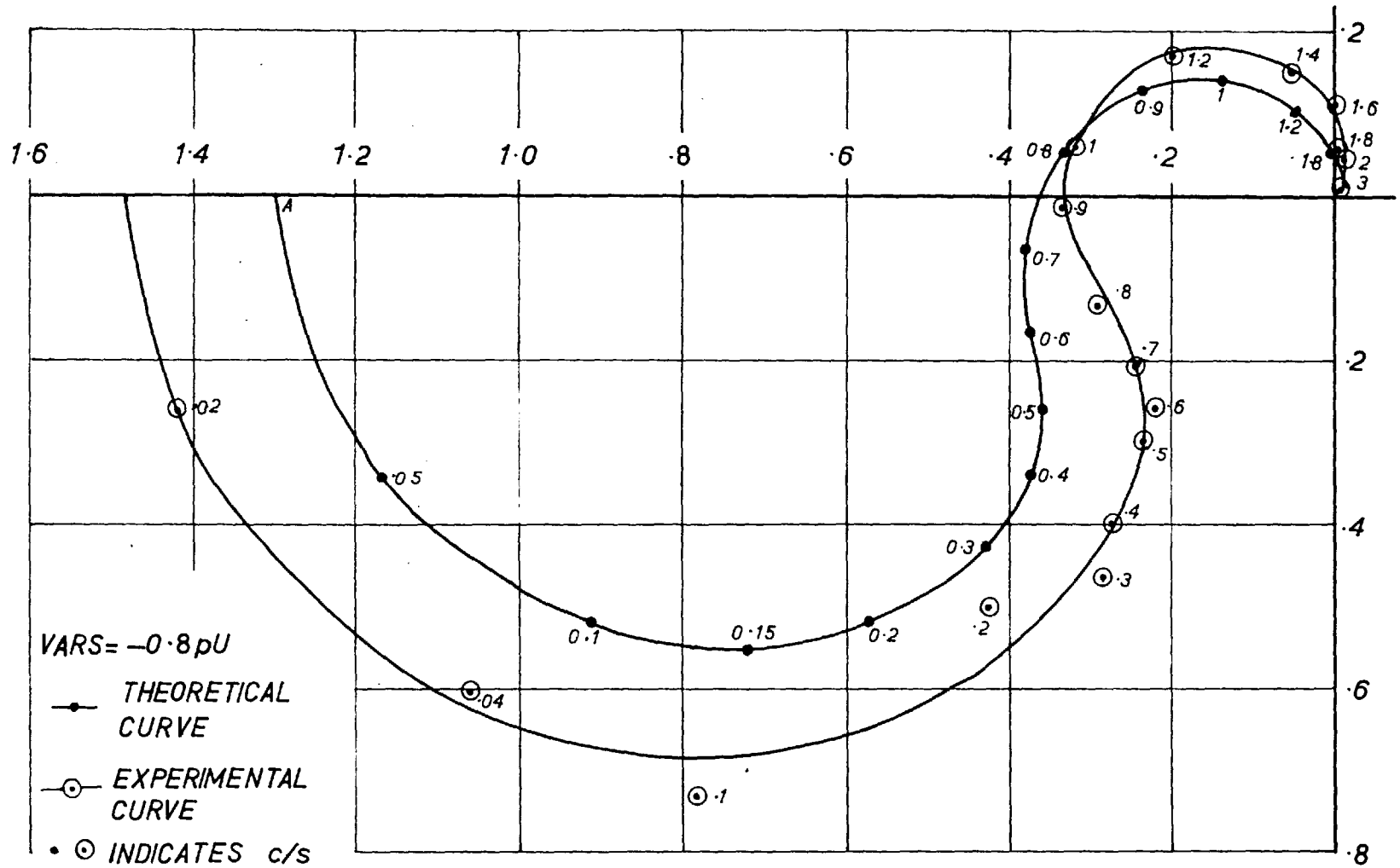

FIG. 6.12. THE SYSTEM FREQUENCY RESPONSE WITH THE PROPORTIONATE REGULATOR.

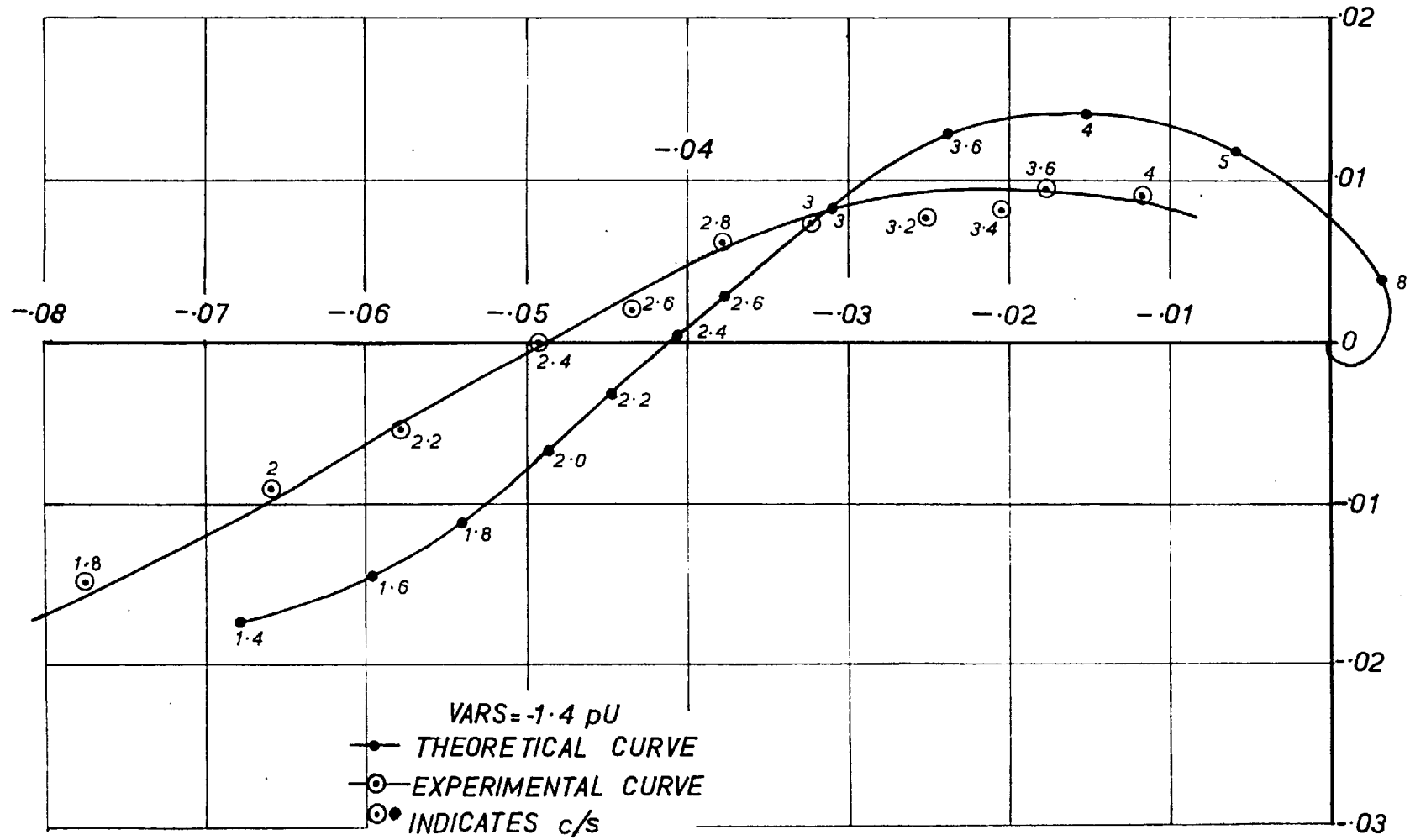

FIG. 6.13. THE SYSTEM FREQUENCY RESPONSE TEST WITH DERIVATIVE REGULATOR.

12.16 (K = 4) . The frequency of oscillations for $R_q(max)$ theoretically had the same value as determined by the frequency response test. Numerically as indicated on the figure it is 2.4 c/s. The frequency response curve also indicates that $R_q(max)$ experimentally obtained is less than the theoretical value and this was also confirmed by the stability test, (see Fig. 6.8). The test was only made upto 4 c/s because a large input signal was needed to make the rotor oscillate sufficiently for good measurements at higher frequencies.

The general conclusion is that for a dynamic non-linear system with the complex regulator the frequency response experimental points obtained in the high frequency region are reasonably correct and confirm the stability tests.

CHAPTER 7

7. EXTENSION OF THE LAPLACE APPROACH AND STATE VARIABLE METHODS

The systems considered in Sect. 2 and 3 were eventually reduced to a single loop configuration shown in Fig. 7.1, that of a plant and a controller. The plant consisted of the machine connected to an infinite bus through a transmission line, and the controller was the regulator. A good many problems in practice can be reduced to a single loop configuration because of the large time constant difference in the main and the auxiliary controller circuits. For example it would be reasonable to ignore the governor controller circuit compared with the excitation controller circuit (say a voltage regulator) when considering the stability of the system for small changes and thus, reducing the system configuration to that of Fig. 7.1. However, the most general configuration is of a plant with 'r' inputs and 'p' outputs ('r' and 'p' being arbitrary integers), where outputs and inputs are interconnected through a controller. Such a multivariable configuration is shown in Fig. 7.2.

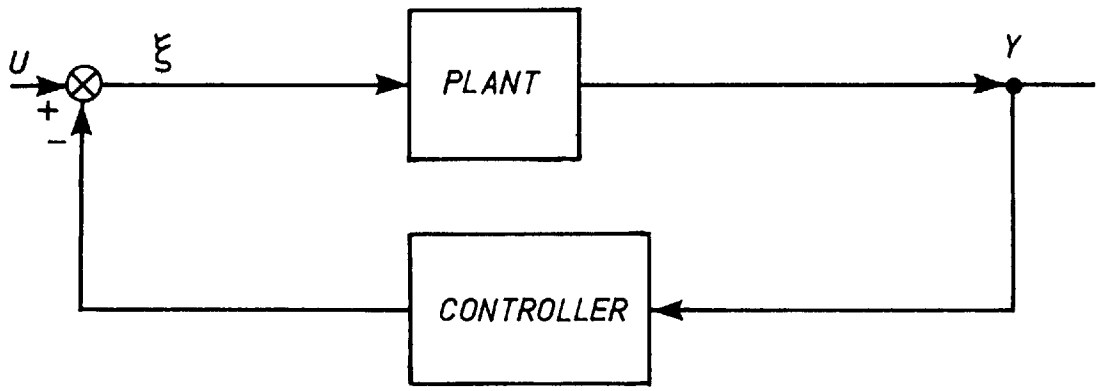

FIG. 7.1. SINGLE LOOP CONFIGURATION

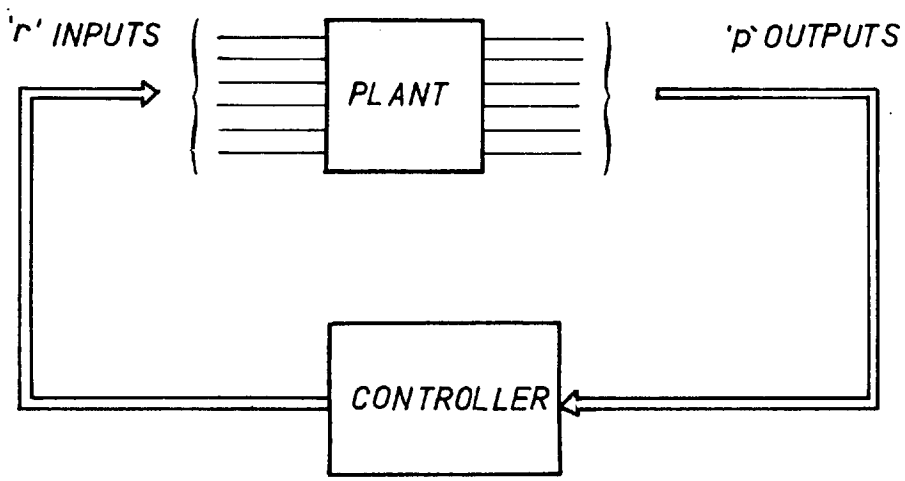

FIG. 7.2. MULTIVARIABLE CONFIGURATION

7.1 Extension of the Laplace Approach to Multivariable System

The Laplace approach for a very large multivariable system is cumbersome for application, because it is not possible to solve the operational matrices straight on a computer. However, for a limited multivariable case the extension of the Laplace transform approach is reasonable. The following extension is for a two input-output system, and may be applied to a two regulator system, one using the voltage signal and the other the angle signal, both acting through their respective controller circuits on the direct and quadrature axis field windings. However, Fig. 7.3 shows in general the two input-output schematic transfer function diagram, where

$$U(p) = \begin{bmatrix} U_1(p) \\ U_2(p) \end{bmatrix} \quad \text{input matrix}$$

$$Y(p) = \begin{bmatrix} Y_1(p) \\ Y_2(p) \end{bmatrix} \quad \text{output matrix}$$

$$G(p) = \begin{bmatrix} G_{11}(p) & G_{12}(p) \\ G_{21}(p) & G_{22}(p) \end{bmatrix} \quad \text{the transfer function matrix of the system}$$

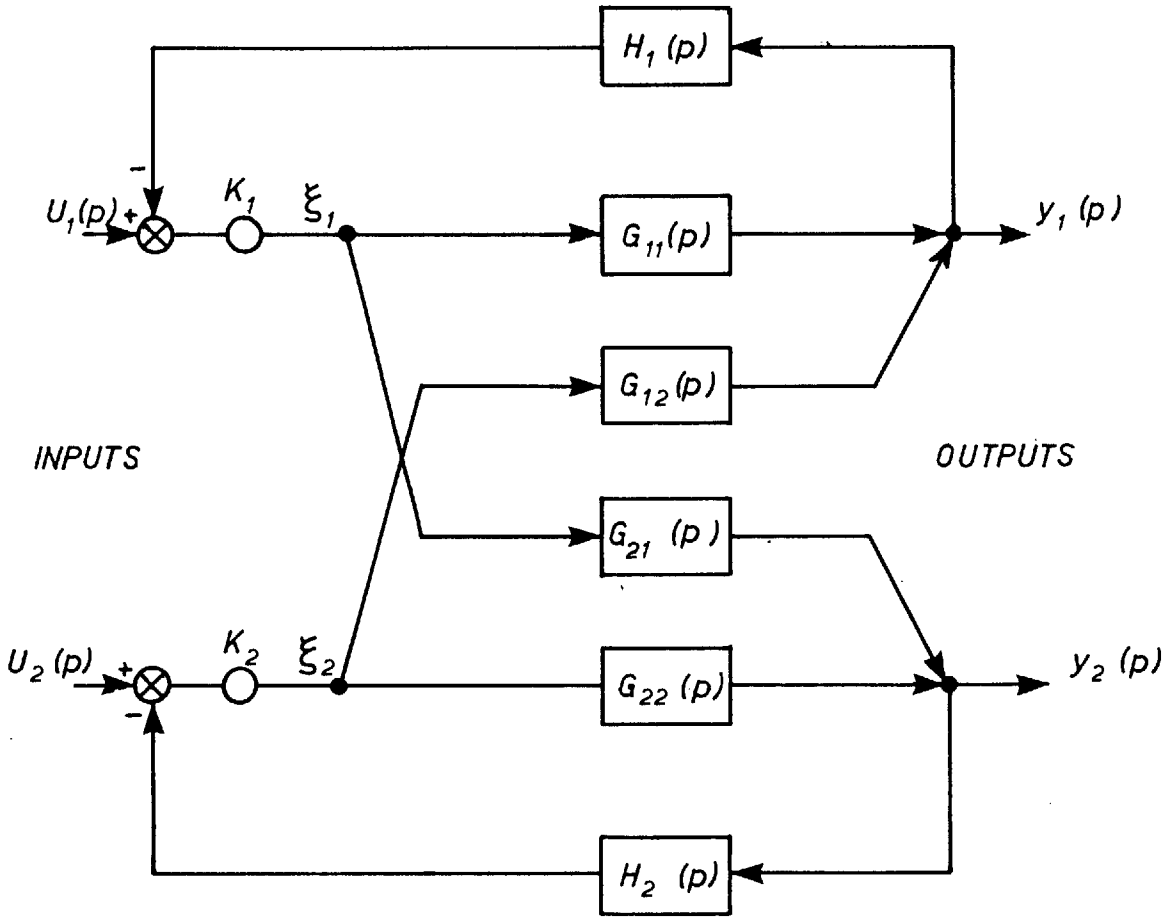

FIG. 7.3. SCHEMATIC TRANSFER FUNCTION DIAGRAM FOR TWO INPUTS AND TWO OUTPUTS

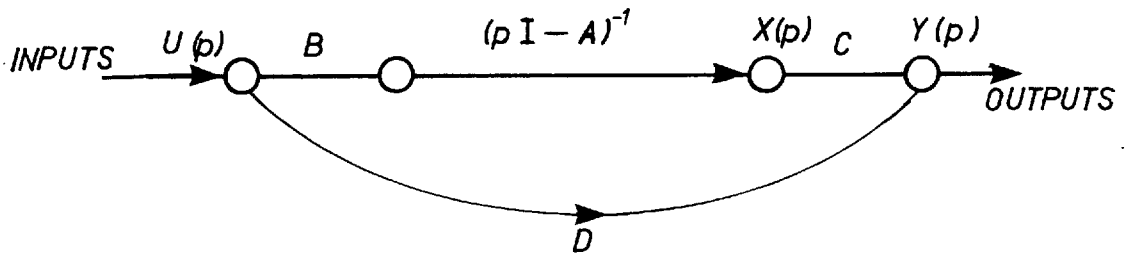

FIG. 7.4. FLOW DIAGRAM FOR EQNS. 7·5 & 7·6. [B, $(pI-A)^{-1}$, C, D ARE MATRICES]

$$K = \begin{bmatrix} K_1 & o \\ o & K_2 \end{bmatrix}$$

the gain constants shown on Fig. 7.3 as potentiometers

$$H_{(p)} = \begin{bmatrix} H_1(p) & o \\ o & H_2(p) \end{bmatrix}$$

the controller transfer function matrix

From Fig. 7.3

$$Y_{(p)} = G(p)\, \xi_{(p)}$$

where $$\xi_{(p)} = \begin{bmatrix} \xi_1(p) \\ \xi_2(p) \end{bmatrix}$$

Also

$$\xi_{(p)} = K(U(p) - H(p).Y(p))$$

Let $C(p)$ be the input-output transfer matrix then

$$Y(p) = C(p)\, U(p)$$

Solving $C(p)$ we have

$$C(p) = [I + KG(p).H(p)]^{-1}\ KG(p) \qquad (7.1)$$

Thus, the stability of the above system can be studied by applying the Routh criteria to the polynomial characteristic equation derived from the following determinant

$$\left| I + K \quad G(p) \quad H(p) \right| \quad = 0 \qquad (7.2)$$

The root-locus technique can also be applied to Eqn. (7.2) by keeping K_1 or K_2 fixed and varying the other from zero to infinity. In Ref. 15 the two inputs, namely, the governor and the voltage regulator are considered but only one output, namely, the rotor angle is taken. The system equations are linearized by a statistical technique for large oscillations the root-locus technique is used for analysis. Although the linearization is doubtful, the analysis is a particular case of the above generalisation.

7.2 State Variable Methods[32-34]

Alternative to the conventional Laplace Transform approach to stability problems are the state variable methods, where the system equations are expressed as the first order differential equations like

$$\begin{aligned} x_1 &= y \\ \dot{x}_1 &= x_2 \\ \dot{x}_2 &= x_3 \\ &\vdots \\ &\text{etc.} \end{aligned}$$

x_1, x_2, ... are referred to as the states of the system which define a state vector X, for example with n

states.

$$X = \begin{bmatrix} x_1 \\ x_2 \\ \vdots \\ x_n \end{bmatrix}$$

The short hand techniques of matrix theory are used in writing the whole set of system equations in a concise form. For an nth order system shown in Fig. 7.2 with r inputs and p outputs, the equations in general are:

$$\dot{X} = AX + BU \tag{7.3}$$

$$Y = CX + DU \tag{7.4}$$

where:

X is a state vector as defined above.
A is a nxn matrix defined as the system matrix.
B is the input matrix with n rows and r columns.
U is the input vector with r elements.
Y is the output vector with p elements.
C is the output matrix with p rows and n columns.
D is the transmission matrix with p rows and r columns.

Taking the Laplace transforms of Eqns. (7.3) and (7.4) we have

$$X(p) = (pI - A)^{-1} B\, U(p) \tag{7.5}$$

I is the nxn unit matrix

$$Y(p) = C\,X(p) + D\,U(p) \qquad (7.6)$$

Fig. 7.4 shows the flow diagram for Eqns. (7.5) and (7.6) relating input and output matrix through operational matrices.

The stability of the system can be studied by either an Eigen value approach or a Lyapunov Function V(x)

7.2.1 Eigen Value Approach

7.2.1.1 Eigen Values

For stability assessment the input vector U is taken as zero. Eqns. (7.3) and (7.4) reduce to

$$\dot{X} = AX$$

and $Y = CX$

For the system matrix A the characterisitc matrix is $(A-\lambda I)$, where λ is a parameter and I the nxn unit matrix. The characteristic equation of the system matrix A is

$$A - \lambda I = 0 \qquad (7.7)$$

The roots of the polynomial Eqn. (7.7) are the values of λ, namely, $\lambda_1, \lambda_2, \lambda_3$ .... called the eigen values

of the characteristic matric A.

The system is considered asymptotically stable, if all the eigen values of the system matrix A have -ve real parts. These eigen values are the poles of the system transfer function. This point is illustrated by taking an example of the simple voltage regulator system of Sect. 2.3.3.

7.2.1.2 Eigen Values for the Voltage regulator of Sect. 2.3.3.

To formulate the system equations (7.3) and (7.4), there is no definite procedure for choosing the various state (x_1, x_2 , ...) as state variables. If one has to start from scratch one could write these equations from the system dynamics, choosing the states by trial and error to get the most desirable form. However, if the systems transfer functions are known then by the direct analogue programming technique[33] Eqns. (7.3) and (7.4) can also be formulated. For the voltage feedback ease with all the simplifications as in Sect. 2.3.3 the forward loop transfer function

$$F_1(p) = \frac{a_2p^2 + a_o}{d_3p^3 + d_2p^2 + d_1p + d_o} \quad , \quad \text{where} \quad a_2, a_o$$

are given by Eqn. (IV.3) and d_3, d_2, d_1, d_o by

Eqn.(IV.5). The regulator transfer function is simply an adjustable constant R. Using the direct analogue computer technique the system is represented in Fig. 7.5. The three states chosen, labelled as x_1, x_2, x_3, are related by

$$\left.\begin{aligned} \dot{x}_1 &= x_2 \\ \dot{x}_2 &= x_3 \\ \dot{x}_3 &= -\left(\frac{d_o}{d_3} + \frac{a_o R}{d_3}\right)x_1 - \frac{d_1}{d_3}x_2 - \left(\frac{d_2 + a_2 R}{d_3}\right)x_3 + u \end{aligned}\right\} \quad (7.8)$$

$$y = a_o x_1 + a_2 x_3 \quad (7.9)$$

In the matrix form Eqn. (7.8) and Eqn. (7.9) become

$$\dot{X} = \begin{bmatrix} 0 & 1 & 0 \\ 0 & 0 & 1 \\ -\left(\frac{d_o+a_o R}{d_3}\right) & -\frac{d_1}{d_3} & -\left(\frac{d_2+a_2 R}{d_3}\right) \end{bmatrix} X + \begin{bmatrix} 0 \\ 0 \\ 1 \end{bmatrix} u \quad (7.10)$$

and

$$y = [a_o \quad 0 \quad a_2]X \quad (7.11)$$

From Eqn. (7.10) the characteristic matrix is

$$A-\lambda I = \begin{bmatrix} 0-\lambda & 1 & 0 \\ 0 & 0-\lambda & 1 \\ -\left(\frac{d+a_o R}{d_3}\right) & -\left(\frac{d_1}{d_3}\right) & -\left(\frac{d_2+a_2 R}{d_3} + \lambda\right) \end{bmatrix}. \quad (7.12)$$

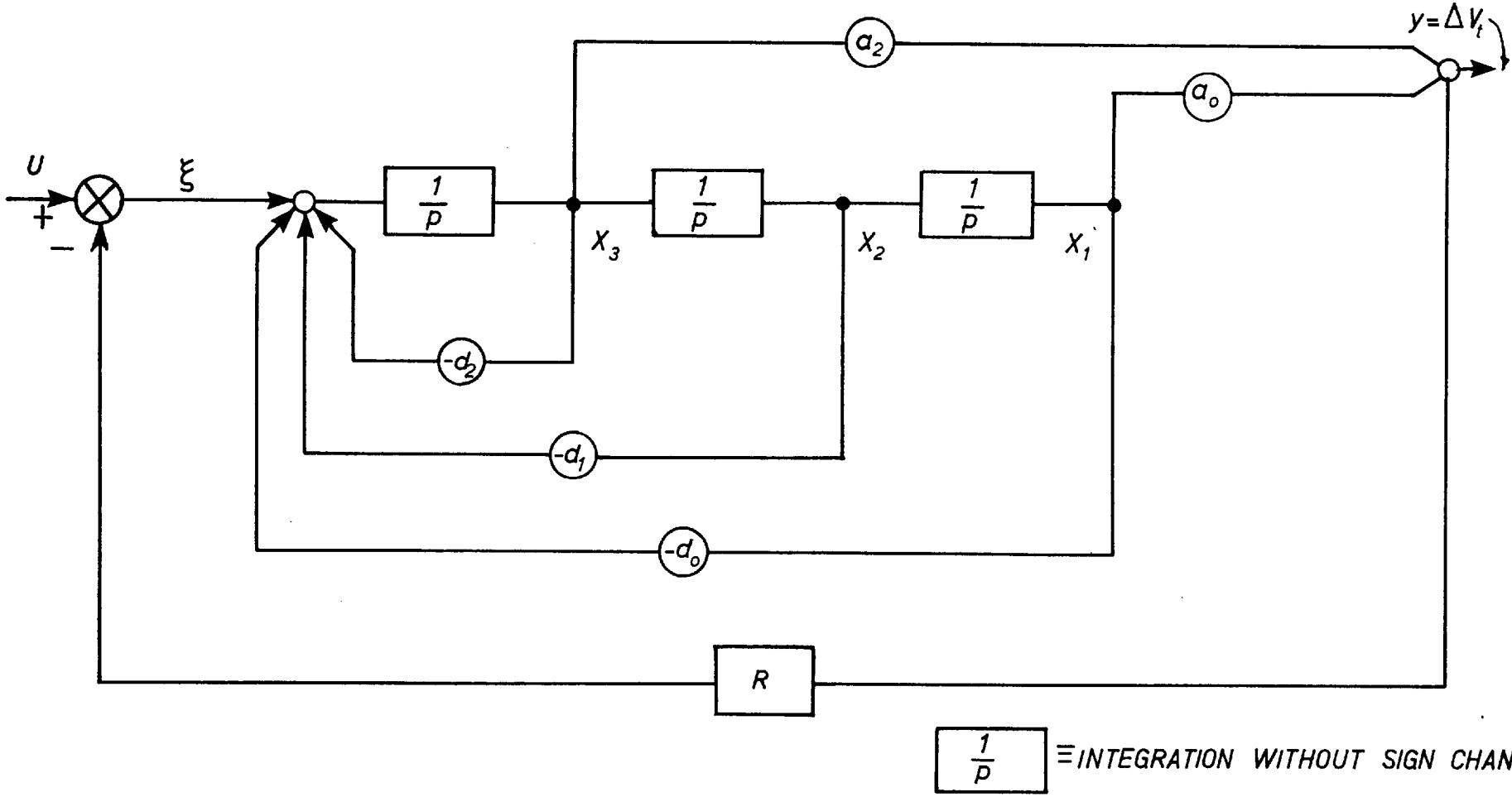

FIG. 7.5. DIRECT ANALOGUE PROGRAMME REPRESENTATION.

Using Eqn.(7.7)the characteristic equation of matrix A giving the eigen values λ is

$$d_3\lambda^3 + (d_2+a_2R)\lambda^2 + d_1\lambda + d_0 + a_0R = 0 \qquad (7.13)$$

Eqn. (7.13) is the same as Eqn.(2.24), if the values of coefficients 'd' and 'a' are substituted in Eqn. (7.13) and λ is replaced by 'p' . This shows that the eigen values are the same as the roots of the equation for the closed-loop system (given by Eqn. 2.24), i.e. also the poles of the closed-loop system.

7.2.2 Lyapunov Technique

7.2.2.1 Lyapunov Stability Criterion

The Lyapunov stability criterion stems from the concept of energy associated with the system in a given state. When a system is in equilibrium, its energy is a minimum and is a positive quantity. If the system is disturbed from its equilibrium and if the rate of change of energy is negative, then the system will settle down to its equilibrium. The concept of minimum energy associated with an equilibrium state of the system was developed by Lyapunov in his famous stability criterion:

If a system can be represented by $\dot{X} = \mathbf{f}(x,t)$, where X is a state vector and if there exists a function

$V(x)$ such that

i) $V(0) = 0$, ii) $V(x) > 0$ when $x \neq 0$, i.e. $V(x)$ is always positive definite, iii) $V(x)$ is continuous in x , iv) $V(x) \rightarrow \infty$ when $x \rightarrow \infty$ v) $\dot{V}(x) < 0$ when $x \neq 0$ then the system is said to be asymptotically stable. Everything hinges on the choice of the Lyapunov function $V(x)$. Usually the stability is tested around the origin. There is no loss of generality in actually doing so, because the origin itself can be shifted.

7.2.2.2 Lyapunov Function

No general way has been found to determine whether a suitable $V(x)$ exists for a system or if any given choice of $V(x)$ is the best. $V(x)$ = constant, represents closed surfaces around the origin and if $\dot{V}(x)$ is -ve then all the trajectories move inwards, closing in on the origin. Thus, we seek functions $V(x)$ which are +ve definite and which have a -ve definite derivative.

For a linear system it is usual to choose $V(x)$ to be a quadratic in x , since there are simple methods to check +ve definiteness of these functions. This point is dealt with later. There is an important theorem by Lyapunov which states:

A necessary and sufficient condition for $x_i = 0$

$(i=1, \ldots n)$ to be an asymptotically stable solution of the matrix equation $\dot{X} = AX$ (A being a real constant matrix) is that $X'PX$ be a +ve definite quadratic form where P is a symmetric matrix satisfying the equation

$$PA + A'P = -Q \tag{7.14}$$

$X'QX$ being any positive definite quadratic form and Q being a real symmetric matrix.

This shows that we may choose any Q + ve definite (usually a unit matrix is chosen) which will surely give $\dot{V}(x) = -X'QX$ as -ve definite. By solving Eqn. (7.14) P can be found. P being another symmetric matrix, Eqn. (7.14) yields $\frac{1}{2}n(n+1)$ linearly independent relations for $\frac{n}{2}(n+1)$ unknown elements of P matrix. Consequently the Lyapunov function:

$$V(x) = X'PX \tag{7.15}$$

Note: P is +ve definite if, and only if, all the principal minors

$$P_{11}\ ,\quad \begin{vmatrix} P_{11} & P_{12} \\ P_{12} & P_{22} \end{vmatrix}\ ,\quad \begin{vmatrix} P_{11} & P_{12} & P_{13} \\ P_{12} & P_{22} & P_{23} \\ P_{13} & P_{23} & P_{33} \end{vmatrix}, \ldots \det(P) \tag{7.16}$$

are positive.

The solution of Eqn. (7.14) is quite cumbersome. For P to be +ve definite the principal minors given by relation (7.16) must be positive. This eventually leads to the Routh-Hurwitz stability conditions, a result which is rigorously proved in Ref. 35. Thus, we see that Lyapunov technique is cumbersom and does not give any more than the Routh - Hurwitz stability criteria for linear systems. However, its main use lies in solving nonlinear problems where other techniques become useless.

Finding a suitable Lyapunov function is difficult. In Ref. 36 a variable gradient method is used to generate a Lyapunov function for the transient study of synchronous machines. For a similar study in Ref. 37 and 38 Lyapunov functions related to the total energy of the system are generated. However, there seems to be no paper dealing with the transient stability with regulators of synchronous machines using the Lyapunov function method.

CHAPTER 8

8. CONCLUSIONS

The conclusions derived in this section are based on the theoretical and experimental investigations into some aspects of the direct and quadrature axes excitation regulation. The system equations are derived so that any feedback from within or outside the alternator is formulated from the alternator output quantities; subsequently they are arranged on a model diagram shown in Figs. 2.1 and 3.1 which is of great assistance in

1. developing the open-loop transfer functions with any number of feedbacks.
2. understanding the effect of individual alternator output quantities.
3. programming the problem in the sequence as indicated on a digital computer, and or alternatively an analogue computer.

For stability analysis the conventional criteria of the Routh, the Nyquist, the root-locus method are used. Some useful deductions are made for the direct-axis regulation using the root-locus method and the Routh criteria. The root-locus method gives a graphical picture

of the system's modes i.e., the roots of the characteristic equation, but if all the details are included it becomes cumbersome because of the increased order. The same is true for the Routh criteria, but the algebraic relations can yield some useful information in regard to the principal effects for simplified cases.

For the quadrature-axis regulation the Nyquist criterion is mainly used because the details can be considered with relative ease. For the Nyquist criterion the increase is the order is just like another arithmetical operation on a digital computer. The effect of an individual detail can be studied by comparing the Nyquist plots with and without the detail. It also provides a direct comparison of the theoretical and experimental frequency response plots of the whole system or part of it. Each method has its own advantage and their application is a matter of convenience to obtain the best results.

For the analysis of a large system the use of techniques readily adaptable on digital computers is inevitable. In this respect state variable methods have an edge over the conventional Laplace approach because of the direct application of matrix algebra in conjunction with digital computers. For linear systems the eigenvalue approach which is the equivalent of the root-locus

method is being increasingly applied. For non-linear systems Lyapunov is a powerful method, although establishing a suitable Lyapunov function is not easy.

For the direct-axis regulation it has been established that a proportionate voltage regulator extends the steady state stability from the peak of the steady state load angle δ_s to the peak of the transient load angle δ'_s, but the gain range of such a regulator is poor. When derivative of the field current is incorporated, the stability limit pattern changes depending on the gain of the field current feedback. The ultimate stability limit is reached when the short circuit transient time constant T'_d is swamped by the field current feedback effect, see Eqn. (2.32), which indicates that the product of R and M is constant. For the lower values of M R(max) is increased but is comparable with the proportionate regulator, see Fig. 2.11. For M =.001; increase beyond δ'_s is very little, however, in the upper gain region BC the ultimate stable angle δ is slightly increased for the same gain R compared with the proportionate regulator. For higher gains of M though the steady state stability is extended beyond δ'_s but the gain range is decreased, see Fig. 2.11 for M =.004. This is a limitation from practical point of view, where increase

in the gain range with the increase in the steady state stability is a desired feature. It may be possible to improve the condition by using a derivative voltage regulator. However, if it is not required of the regulator to extend the stability range beyond $\delta = \delta'_s$ for practical reasons, a small amount of field current feedback (of the range $M = .001$) would prove useful (see Fig. 2.11 curves 1 and 2).

The experimental and theoretical curves show good agreement in the lower gain region and some departure in the higher gain region but the trend is the same, and the general agreement can be described as reasonable. Particularly considering that the theoretical curves are computed neglecting resistance and damping.

In the literature for the direc-axis regulation various schemes have been investigated for the full-load conditions and its limitations at the zero power are in most cases ignored. Some papers mention the steady state limit $Q_o = -V^2 Y_q$ for a simple regulator transfer function. However, the rigorous proof provided in Sect. 2.8 confirms this limit for any direct-axis regulation scheme.

The limitation of the direct-axis regulation scheme at zero power appears reasonable in the physical sense, because it cannot affect the parameters in the quadrature-axis

on which the limit depends. Thus the quadrature regulation scheme is a logical development.

The theoretical investigation for the quadrature-axis regulation at zero power shows that

1. the voltage-feedback modified by the regulator transfer function $R_q(p)$ cannot affect the steady state reactive absorption limit.

2. the signal derived from I_d is not effective.

3. the signal derived from I_q is not of the right polarity for stabilisation at negative vars. Moreover it changes sign from positive to negative vars, and therefore by itself is not a desirable feedback.

4. the signal derived from the rotor angle is the most effective because it is always a positive quantity and in conjunction with $R_q(p)$ can modify the characteristic equation suitably to extend the reactive absorption limit beyond $-V^2Y_q$.

The experimental investigation with the voltage feedback confirms the theoretical deduction. The rotor angle signal experimentally proves useful as theoretically expected and affects the steady state limits depending on the regulator transfer function.

The system with the angle controller on the quadrature-axis behaves like a position control servo-system

on the quadrature-axis. When the system is delivering power at the fixed supply the rotor can remain in the zero angle equilibrium with its stability taken care of by the angle controller, because the quadrature field winding can supply the necessary mmf for the equilibrium. The system behaves in the same way over the whole range of power. Under ideal condition at any power the rotor angle is zero, therefore, the conventional meaning of the load angle is not applicable, consequently the steady state stability limits are defined in terms of reactive power.

The proportionate angle regulator with an ideal angle device increases the steady state reactive absorption from $-V_{qo}{}^2 Y_q$ to $-V_{qo}{}^2 Y'_q$, a result which has its parallel with the direct-axis proportionate voltage regulator scheme. However, with a practical angle device this limit is reduced because of the delays associated with the practical angle device. The regulator gain range R_q is poor, because of the sharp slope of the stability limit curve (see Fig. 3.5).

The inclusion of the first derivative only improves the situation marginally (see Fig. 3.8) over the proportionate regulator and cannot be considered of practical advantage.

The derivative regulator (see Sect. 3.5.2.2) increases the reactive absorption limit and the gain range R_q many times compared to the above two quadrature-axis regulators, therefore, it can be considered of practical value. The following comparison based on the experimental investigations (see Figs. 6.5 and 6.8) proves the merit of the derivate regulator over the proportionate regulator.

1. The maximum permissible reactive absorption obtained with the derivative regulator is about -3.5 p.u. compared to about -1.4 p.u. for the proportionate regulator.

2. The maximum regulator gain R_q depends on the vars. At vars = -1.0 p.u. $R_q(max)$ is increased from about 2.8 for the proportionate regulator to about 21 for the derivative regulator, an increase of about 7.5 times.

3. The proportionate regulator for reasons of poor gain needs adjustment of the quadrature-axis field current for zero equilibrium when power is changed from one level to another, whereas, the derivative regulator in the high gain region maintains practically the zero equilibrium by itself under changing conditions.

The damping is equivalent to a small lag term in the open-loop transfer function and has little effect on the steady state stability limit curves. The

resistance has little stabilising effect but tends to improve the stability with increasing power.

The increase in the permissible reactive absorption limit with the derivative regulator is very much more than required for steady state operation; however, it is expected that it would contribute in extending the transient stability.

From experimental evidence it can be recorded that under any transient disturbance if the quadrature-axis regulation system slips it tries to restablise at the next equilibrium point after slipping one pole pitch ($=180^{\circ}$). With the excitation then reversed the system moves over into lagging region if it was in the leading region to start with, and vice versa.

The derivative regulator constructed for the practical investigations is by no means an optimum design. From consideration of the steady state performance alone it could be redesigned to give still further increase in the gain range R_q with or without increasing the reactive absorption any further. The optimum design must be related to the required performance, and in this field there is a great scope for further research.

APPENDIX I

Following is a summary[1,16] of equations which lead to matrix 2.1. and matrix 3.1.

$$v_d = V_m \sin\delta = p\psi_d + \omega\psi_q + r_a i_d - \psi_q p\delta \qquad \text{(I-1)}$$

$$v_q = V_m \cos\delta = -\omega\psi_d + p\psi_q + r_a i_q + \psi_d p\delta \qquad \text{(I-2)}$$

$$T_e = \frac{\omega}{2}(\psi_d\, i_q - \psi_q id) \qquad \text{(I-3)}$$

$$T_i = T_m - T_e = J\, p^2(\omega t-\delta) \qquad \text{(I-4)}$$

$$\psi_d = \frac{x_d(p)}{\omega} id + \frac{G(p)}{\omega} v_{fd} \qquad \text{(I-5)}$$

$$\psi_q = \frac{x_q(p)}{\omega} iq + \frac{G_q(p)}{\omega} v_{fq} \qquad \text{(I-6)}$$

APPENDIX II

II.1 Expressions For Transfer Functions $A_r(p)$

The terminal voltage v_t is given by the following the equation

$$v_t = [(v_d - i_q x_c)^2 + (v_q + x_c i_d)^2]^{1/2}$$

Therefore,

$$\Delta v_t = A_1(p)\,\Delta i_d + A_2(p)\,\Delta\delta + A_3(p)\,\Delta i_q \qquad \text{(II.1)}$$

The expressions for $A_r(p)$ are given in Eqn. (2.5)

II.2 Expressions for Transfer Functions $A'_r(p)$

The transfer functions $A'_r(p)$ are associated with the field current feedback. The basic equations[16] are:

$$\psi_d = L_{md} i_f + L_{md}\, i_{kd} + (L_{md} + \ell_a) i_d$$

$$0 = L_{md}\, p i_f + [r_{kd} + (L_{md} + \ell_{kd})p]\, i_{kd} + L_{md}\, p i_d \qquad \text{(II.2)}$$

Eliminating i_{kd} from the above set of Eqn. (II.2) we have:

$$\psi_d = \frac{G_1(p)}{\omega} \cdot i_f + \frac{X_{d1}(p)}{\omega} \cdot i_d \qquad \text{(II.3)}$$

where

$$G_1(p) = \frac{1+T_{kd}p}{1+T_2p} X_{md}$$

$$X_{d1}(p) = \frac{1+T_5p}{1+T_2p} X_d \qquad \text{(II.4)}$$

In Eqn. (II.4)

$$T_2 = \frac{1}{\omega r_{kd}} (X_{md}+X_{kd})$$

$$T_5 = \frac{1}{\omega r_{kd}} \left(X_d + \frac{X_{md}X_a}{X_{md}+X_a}\right) \qquad \text{(II.5)}$$

$$T_{kd} = \frac{X_{kd}}{\omega r_{kd}}$$

$\omega\psi_d$ from Eqn. (I-2) after neglecting $p\psi_q$ and $p\delta$ terms is

$$\omega\psi_d = - v_q + r_a i_q \qquad \text{(II.6)}$$

Eliminating $\omega\psi_d$ from Eqn. (II.3) and Eqn. (II.6) we have

$$-v_q = G_1(p)i_f + X_{d1}(p)i_d - r_a i_q \qquad \text{(II.7)}$$

From Eqn. (II.7) the small oscillation equation for i_f is

$$\Delta i_f = \alpha_1(p)\ \Delta i_d + \alpha_2(p)\Delta\delta + \alpha_3(p)\ \Delta i_q \qquad \text{(II.8)}$$

The expressions for $\alpha_r(p)$ $r = 1,2,3$ are given in Eqn. (2.6) and the relation between $A'_r(p)$ and $\alpha_r(p)$, $(r = 1,2,3)$ in Eqn. 2.8.

APPENDIX III

Expressions for $F_1(p)$ and $F_2(p)$

$F_1(p)$ and $F_2(p)$ are the transfer functions between the feedback signals (Δv_t and $M(p)\,\Delta i_f$) and the input voltage to the field winding (Δv_{fd}) . The expressions $F_1(p)$ and $F_2(p)$ are the sums of product terms derived from $A_r(p)/A'_r(p)$ and $B_r(p)$, (r=1,2,3). The expressions for $B_r(p)$ and $A_r(p)/A'_r(p)$ are given in Eqn. (2.3) and Eqn. (2.5)/(2.8a). Using these expressions $F_1(p)$ and $F_2(p)$ are obtained below

$$F_1(p) = \sum_{r=1}^{3} B_r(p).A_r(p) = B_1(p).A_1(p) + B_2(p)A_2(p)+B_3(p).A_3(p)$$

$$= \frac{(1+T_{kd}p)Y_d}{D(p)} \quad [(Q_o+Jp^2+V_{qo}{}^2Y_q(p)-2r_aV_{qo}I_{qo}Y_q(p)) \quad x$$

$$(X_cI_{do}+V_{qo}) \; x \; \frac{X_c}{V_{to}} + \tfrac{1}{2} \; (-V_{do}+r_a(2I_{do}+V_{qo}Y_q(p)-2I_{qo}Y_q(p)r_q)) \; x$$

$$\left(-\tfrac{1}{2}.\frac{P_o.X_c}{V_{to}} \right) - \quad (V_{qo}Y_q(p)V_{do}+r_a(Q_o+Jp^2-2V_{qo}I_{do})Y_q(p)) \quad x$$

$$-(V_{do}-I_{qo}X_c)\frac{X_c}{V_{to}} \quad]$$

(III.1) contd.

$$= \frac{(1+T_{kd}p).Y_d}{D(p)} \left[(V_{qo}Y_q(p)+I_{do}-r_aY_q(p).I_{qo}) \times (V^2-2r_ap_o+x_cQ_o)\right.$$

$$\left.+Jp^2 \left((V_{qo}+X_cI_{do})+r_a(V_{do}-X_cI_{qo})Y_q(p)\right)\right] \frac{X_c}{V_{to}} \qquad \text{(III.1)}$$

And

$$F_2(p) = \sum_{r=1}^{3} Br(p)A'_r(p) = B_1(p)A'_1(p) + B_2(p).A'_2(p) + B_3(p).A'_3(p)$$

$$= \frac{(1+T_{kd}p).Y_d}{D(p)} \left[(Q_o+Jp^2+V_{qo}{}^2Y_q(p)-2r_aV_{qo}I_{qo}Y_q(p)) \times \right.$$

$$\left(-\frac{x_{d1}(p)}{G_1(p)} \cdot \frac{M(p)}{R_e}\right) + \frac{1}{\sqrt{2}} \left(-V_{do}+r_a(2I_{do}+V_{qo}Y_q(p)-2I_{qo}Y_q(p)r_a)\right) \times$$

$$\left(\frac{\sqrt{2}}{G_1(p)} \cdot \frac{V_{do}.M(p)}{R_e}\right) - \left(V_{qo}V_{do}Y_q(p) + r_a(Q_o+Jp^2-2V_{qo}I_{do})Y_q(p)\right) \times$$

$$\left.\left(\frac{r_a}{G_1(p)} \frac{M(p)}{R_e}\right)\right]$$

(III.2) contd.

$$= \frac{(1+T_{kd}\ p).Y_d}{D(p)} \times \left[-(Q_o+V_{qo}{}^2Y_q(p)+V_{do}{}^2Y_{d1}(p)+Jp^2)\ X_{d1}(p) + \right.$$

$$r_a\ (2V_{qo}I_{qo}x_{d1}(p)+2V_{do}I_{qo}x_q(p)-V_{qo}V_{do})\ Y_q(p) -$$

$$\left. r_a{}^2\ (I_{qo}V_{do}-V_{do}I_{do}+Jp^2)\right]\frac{M(p)}{R_eG_1(p)} \qquad \text{(III.2)}$$

Note that the rectified constant term R_e is omitted in Eqn. (III.1) but appears in Eqn. (III.2), modifying the field current gain M to M/R_e, (see Sect. 2.2.4).

APPENDIX IV

To obtain the characteristic equation (2.18) from Eqn. (2.16), first we develop the expression for $L(p)$ $\left(= R\,\frac{N(p)}{D(p)} \right)$ as a ratio of polynomials in 'p' . Using Eqn. (2.12) we have

$$L(p) = R\,\frac{N(p)}{D(p)} = R\,F_1(p) + R\,F_2(p) \qquad \text{(IV.1)}$$

The expressions for $R\,F_1(p)$ and $R\,F_2(p)$ are obtained as ratio of polynomials separately and later combined to give $L(p)$.

Using the relation for $F_1(p)$ in Eqn. (III.1) and expanding in the form of polynomial we have

$$R\,F_1(p) = \frac{a_3p^3 + a_2p^2 + a_1p + a_o}{D(p)}$$

where

$$a_3 = \frac{J.T_{kd}.Y_d.X_c}{V_{to}}\ \left[(V_{qo}+X_cI_{do}) + r_a(V_{do}-X_cI_{qo})Y_q\right] R$$

$$a_2 = \frac{J.Y_dX_c}{V_{to}}\ \left[(V_{qo}+X_cI_{do}) + r_a(V_{do}-X_cI_{qo})Y_q\ \right].\ R \qquad \text{(IV.3) contd.}$$

$$a_1 = \frac{T_{kd} \cdot Y_d \cdot X_c}{V_{to}} \left[(V_{qo}Y_q + I_{do} - r_a Y_q I_{qo})(V^2 - 2rP_o + X_c Q_o)\right] . R$$

$$a_o = \frac{Y_d X_c}{V_{to}} \quad (V_{qo}Y_q + I_{do} - r_a Y_q I_{qo}) \times (V^2 - 2rP_o + X_c Q_o) \quad . R$$

(IV.3)

and

$$D(p) = D'(p)(1+T'_d p)(1+T''_d p) = d_4 p^4 + d_3 p^3 + d_2 p^2 + d_1 p + d_o$$

(IV.4)

In Eqn. (IV.4) the coefficients are as given below:

$$d_4 = J(T''_d T'_d + r_a{}^2 Y_d Y_q T'_{do})$$

$$d_3 = J(T'_d + T''_d + r_a{}^2 (T'_{do} + T''_{do}) Y_d Y_q)$$

$$d_2 = J + (Q_o + V_{qo}{}^2 Y_q) T'_d T''_d + V_{do}{}^2 Y'_d T'_d T''_{do} - 2r_a (V_{qo} I_{qo} Y_q T'_d T''_d + V_{do} I_{do} Y_d T'_{do} T''_{do}) + r_a{}^2 Y_d Y_q \left[(V_{do} I_{qo} - V_{qo} I_{qo}) T'_{do} T''_{do} + J\right]$$

$$d_1 = T'_d \cdot S'_o + (Q_o + V_{qo}{}^2 Y_q T''_d + V_{do}{}^2 Y_d T''_{do}) - 2r_a (V_{qo} I_{qo} Y_q T''_d + V_{qo} I_{qo} Y_q T'_d + V_{do} I_{do} Y_d T''_{do} + V_{do} I_{do} Y_d T'_{do}) + r_a{}^2 Y_d Y_q \left[(V_{do} I_{qo} - V_{qo} I_{do}) T''_{do} + (V_{do} I_{qo} - V_{qo} I_{do}) T'_{do}\right]$$

$$d_o = S_o - 2r_a (V_{qo} I_{qo} Y_q + V_{do} I_{do} Y_d) + r_a{}^2 Y_d Y_q (V_{do} I_{qo} - V_{qo} I_{do})$$

(IV.5)

The expressions for S_o and S'_o, i.e., the slopes of the power and transient power angle curves respectively are given in Eqn. (2.20).

To obtain $R\,F_2(p)$ in the polynomial form substituting $X_{d1}(p)$ and $G_1(p)$ from Eqn. (II.4) in Eqn. (III.2) we have

$$R\,F_2(p) = \frac{b_4p^4+b_3p^3+b_2p+b_1+b_o}{D(p)} \qquad \text{(IV.6)}$$

where

$$b_4 = -J(T_5+T_2r_a{}^2Y_q.Y_d)\,\frac{R\;M}{R_eX_{md}}$$

$$b_3 = -J(X_d+r_a{}^2Y_q).\,\frac{Y_d.R\;M}{R_e.X_{md}}$$

$$b_2 = Y_d\,[-((Q_o+V_{qo}{}^2Y_q)T_5+V_{do}{}^2Y_dT_2)\,X_d+2r_aY_q(V_{qo}I_{qo}X_dT_5 +V_{do}I_{do}X_qT_2)-r_aY_qV_{do}V_{qo}T_2-r_a{}^2T_2Y_q(I_qV_{do}-V_{qo}I_{do})]\,\frac{M\,R}{R_eX_{md}}$$

$$b_1 = [-S_oX_d+2r_aY_q(V_{qo}I_{qo}X_d+V_{do}I_{do}X_q)-r_aY_qV_{qo}V_{do} - r_a{}^2Y_q(I_{qo}V_{qo}-V_{qo}I_{do})]\,\frac{M.Y_d}{R_e.X_{md}}$$

$$b_o = 0 \qquad \text{(IV.7)}$$

$D(p)$ is given by Eqn. (IV.4).

Adding Eqn. (IV.2) and Eqn. (IV.6) gives

$$R\,N(p) = b_4p^4+(a_3+b_3)p^3+(a_2+b_2)p^2+(a_1+b_1)p+(a_o+b_o) \qquad \text{(IV.8)}$$

Substituting for $D(p)$ and $R\,N(p)$ from Eqn. (IV.4) and Eqn. (IV.8) respectively in Eqn.(2.17) we have the characteristic Eqn. as below

$$(d_4+b_4)p^4+(d_3+a_3+b_3)p^3+(d_2+a_2+b_2)p^2 + (d_1+a_1+b_1)p + (d_o+a_o+b_o)p = 0$$

or in more compact form as

$$c_4p^4 + c_3p^3 + c_2p^2 + c_1p + c_o = 0$$

The expressions for c_4, c_3, c_2, c_1 and c_o are given in Eqn. (2.19).

APPENDIX V

V. STABILITY CRITERIA[18-20]

V.1 Root-Locus Method

V.1.1 General

The Root-Locus technique is used for the explanations and stability determination for the direct-axis excitation control analysis. The technique is explained briefly in this appendix. The idea underlying the technique is to find the roots of the characteristic equation of the system from the open-loop transfer function pole zero configuration, with the loop gain varied from zero to infinity. Beside giving the loci of the roots, this method indicates what modifications are needed in order to stabilise an unstable system.

V.1.2 The Principle

Consider a simple linear control system shown in Fig. V.1. The closed-loop transfer function C(p) of the system is given by

$$C(p) = \frac{G_1(p)}{1 + R\,L(p)} \qquad (V.1)$$

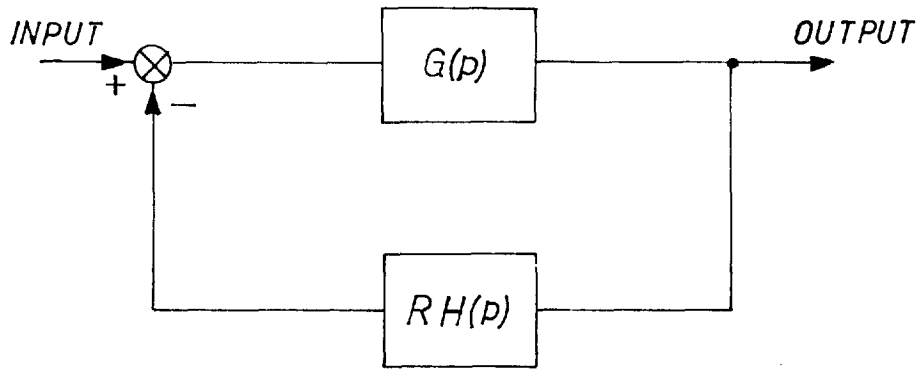

FIG. V.1. – CLOSED_LOOP SYSTEM BLOCK DIAGRAM.

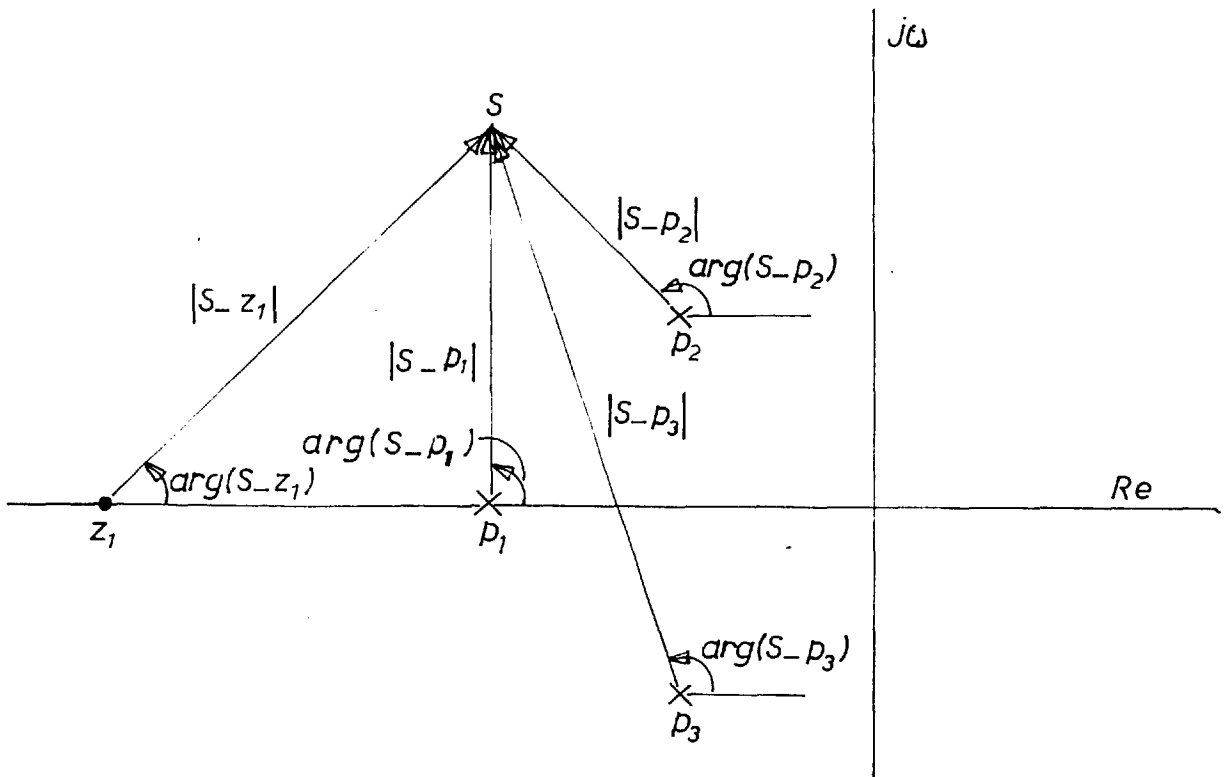

FIG. V.2. – VECTOR DIAGRAM FOR GRAPHICAL MEASUREMENT OF 'ANGLE' AND 'MAGNITUDE'.

where:

G(p) is the forward loop transfer function

H(p) is the backward loop transfer function

R is the variable loop gain

$$L(p) = G(p) \cdot H(p) \qquad (V.2)$$

H(p) is the open-loop transfer function.

L(p) in general is a ratio of polynomials in 'p' and can be expressed as $\frac{N(p)}{D(p)}$. Thus the roots of

$$N(p) = 0 \qquad (V.3)$$

are the zeros of the open-loop transfer function and the roots of

$$D(p) = 0 \qquad (V.4)$$

are the poles of the open-loop transfer function. The characteristic equation of the system is a polynomial equation in p given by

$$D(p) + R\,N(p) = 0 \qquad (V.5)$$

Let there be n zeros, namely, $z_1, z_2, \ldots, z_n$ and m poles, namely, $p_1, p_2, \ldots, p_m$ of the open-loop transfer

function. L(p) . The open-loop transfer function in factorised form is given by

$$L(p) = \frac{N(p)}{D(p)} = \frac{(p-z_1)(p-z_2).....(p-z_n)}{(p-p_1)(p-p_2).....(p-p_m)} \qquad (V.6)$$

In Eqn. (V.6) N(p) and D(p) are polynomials in p of the nth. and mth. order. In these polynomials the highest power coefficient is taken positive and unity, however, the constants can be merged with the loop gain R as desired. The case where the highest power coefficient in N(p) or D(p) has the negative sign is dealt with in Sect. V.1.3.5. In Fig. V.2 the poles and zeros of the open-loop transfer function are marked on the complex p-plane. For simplicity three poles and one zero, all in the left half p-plane are shown. This by implication means that all the coefficients of the polynomials N(p) and D(p) are taken positive for illustration, this however is not necessary. If a point 'S' in the complex p-plane is a root of the characteristic equation (V.5) then:

$$D(S) + R\,N(S) = 0$$

which leads to the following conditions in general

$$\frac{|N(S)|}{|D(S)|} = \frac{1}{R}$$

or

$$\frac{|S-z_1| \cdot |S-z_2| \ldots\ldots |S-z_n|}{|S-p_1| \cdot |S-p_2| \ldots\ldots |S-p_m|} = \frac{1}{R} \qquad (V.7)$$

And

$$\text{Arg } N(S) - \text{Arg } D(S) = \pi + 2\pi\lambda$$

(where λ is an integer) or

$$\text{Arg}(S-z_1) + \text{Arg}(S-z_2) \ldots\ldots + \text{Arg}(S-z_n) - \text{Arg}(S-p_1)$$

$$- \text{Arg}(S-p_2) \ldots\ldots - \text{Arg}(S-p_m) = \pi + 2\pi\lambda \qquad (V.8)$$

The conditions represented by Eqns. (V.7) and (V.8) are called the 'Magnitude' and 'Angle' conditions respectively. In Fig. V.2 the vectors $(S-z_1)$, $(S-p_1)$, $(S-p_2)$ and $(S-p_m)$ are shown. The magnitude of each is represented by the length and the angle by the inclination to the real axis.

The root-locus is defined from the angle condition as the locus of points S that satisfy Eqn. (V.8). The

magnitude condition given by Eqn. (V.7) enables one to obtain R at each point S of the locus. The root-loci can be constructed using the above mentioned conditions graphically, but much labour can in practice be saved by using a digital computer to find the roots of the characteristic equation for gains from zero to a reasonably large gain. However, the following rules are of great assistance in general when using the root-locus technique.

V.1.3 Rules

V.1.3.1 General

If the characteristic equation is of the mth order, it has m roots, which may be real or complex. The order of the characteristic equation is determined by the polynomial D(p) because its order is higher than or equal to that of the polynomial N(p). Since the characteristic equation has m roots, the root-locus has m branches, each of which corresponds to one root of the characteristic equation. The real roots are represented by points lying on the real axis, so that the branches which correspond to real roots consist of portions of the real axis. The branches which correspond to complex roots may be more or less complicated. Since the coefficients of the characteristic equation (V.5)

are real, the complex roots are complex conjugates and hence the branches of the root-loci which correspond to the complex roots are symmetrical in pairs with respect to the real-axis.

V.1.3.2 Starting point

The root-loci of the characteristic equation are plotted from zero gain to infinity. At zero gain the characteristic equation (V.5) reduces to:

$$D(p) = 0$$

which gives the starting point of the root-loci. $D(p) = 0$ gives the open-loop transfer function poles of the system. Therefore, each branch of the root-locus starts from the open-loop transfer function pole position.

V.1.3.3 Termination of Roots

Each root-locus terminates when the gain R is infinity. The characteristic Eqn. (V.5) of the system can be divided by R and written as

$$\frac{D(p)}{R} + N(p) = 0 \qquad (V.9)$$

When R tends to infinity Eqn. (V.9) reduces to:

$$N(p) = 0$$

$N(p) = 0$ gives the open-loop transfer function zeros of the system, which are n in number, whereas, the system has m roots. From Eqn. (V.9) it is clear that with the increase in the gain R the highest power coefficients, for m greater than n , approach to zero. As a result m-n roots of the characteristic equation approach to infinity. The other n roots of the characteristic equation terminate at the open-loop transfer function zero positions.

V.1.3.4 Branches on the Real Axis

The complex conjugate poles and zeros do not affect the existence of any branches of root loci on the real axis. The real branch of the root loci exists wherever the angle condition given by Eqn. (V.8) is satisfied by the real open-loop transfer function poles and zeros. In Fig. V.3a the branches of a typical root locus on the real axis are shown in accordance with the above rule. The pole-zero configuration is arbitrarily chosen.

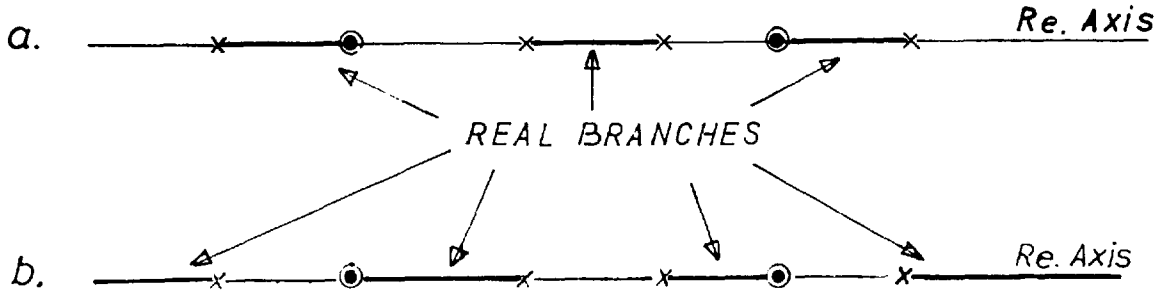

FIG. V.3._ REAL BRANCHES OF ROOT_LOCUS
a. FOR R.H.S. OF EQN.V. $\theta = \pi + 2\pi\lambda$
b. FOR R.H.S. OF EQN.V. $\theta = 0 + 2\pi\lambda$

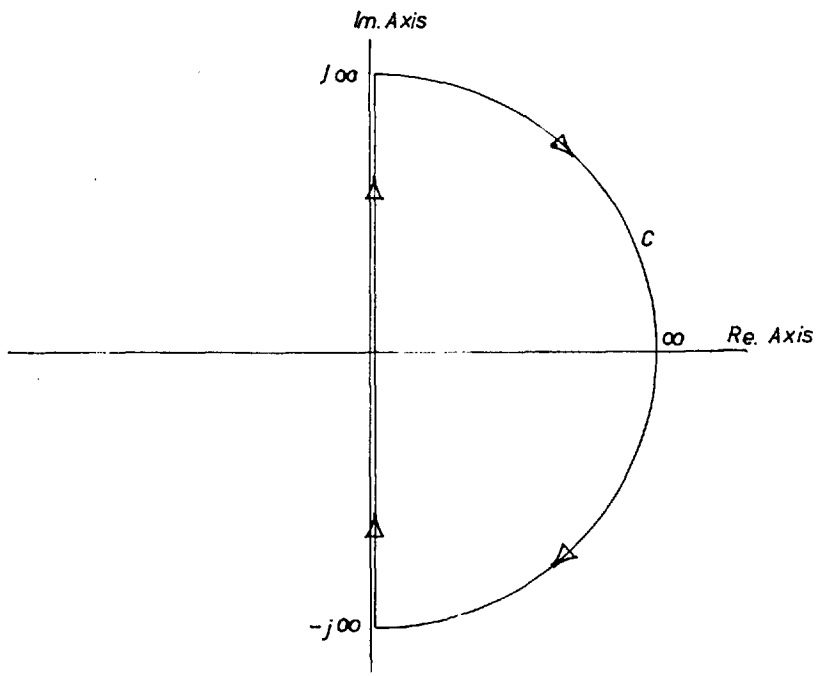

FIG.V.4._ NYQUIST CONTOUR.

V.1.3.5 Zero Angle Conditionn

In general the angle condition is given by Eqn. (V.8). If R is negative the right hand side of Eqn. (V.8) becomes $0 + 2\pi\lambda$. R could be negative under positive feedback conditions or when the highest coefficient of N(p) or D(p) becomes negative. The rule in Sect. V.1.3.4 correspondingly stands modified (because of the change in Eqn. V.8), and is demonstrated by an illustration in Fig. V.3b, showing the branches of a typical root-locus on the real-axis for the same pole-zero configuration as in Fig. V.3a.

V.1.3.6. Intersection With the $j\omega$ -axis

The intersections of the root-locus with the $j\omega$-axis establish pure oscillatory roots of the characteristic equation, and determine the natural frequency of the closed-loop system. The conditions for obtaining purely imaginary roots of the characteristic equation are discussed in Sect. V.2.1.

V.1.3.7 Asymptotes

In Sect. V.1.3.3 it is mentioned that m-n roots approach to infinity. These roots approach to infinity asymptotically. For a point remote from the open-loop

poles and zeros, the effect is the same as if they were all located at the centre of gravity determined from the arithmetic mean

$$p_m = \frac{(p_1+p_2\ldots p_m)-(z_1+z_2\ldots z_n)}{m-n}$$

All the roots approaching infinity to asymptotically converge if extended backwards to the centre of gravity determined in this way.

V.1.4 Inverse Root-Locus

The root-locus in the inverse form can be of great use when the roots of the characteristic equation increase in magnitude very rapidly and change over from the L.H. plane to the R.H. plane. Such a change causes difficulty in assessing the limit of stability. It can be overcome by plotting the inverse root-locus. The inversion brings the points at infinity to the origin and the convergence of loci at infinity can be more readily verified. The 'Angle' and 'Magnitude' conditions and other rules mentioned in Sect. V.1.3 are unchanged. The inversion is carried out as follows:

Take a general transfer function

$$\frac{a_3p^3+a_2p^2+a_1p+a_o}{d_4p^4+d_3p^3+d_2p^2+d_1p+d_o}$$

Using the transformation $W = \frac{1}{p}$
the transfer function in the W-plane becomes:

$$\frac{a_3W+a_2W^2+a_1W^3+a_oW^4}{d_4+d_3W+d_2W^2+d_1W^3+d_oW^4}$$

Instead of dealing with the system in the p-plane it can now be dealt with in the W-plane. Each root of the p-plane appears as its inverse in the W-plane. This technique is used in Sect. 2.3.4 (see Fig. 2.9).

V.2 Routh Criterion

The Routh criterion in algebraic and graphical form is discussed below.

V.2.1 Algebraic form

The characteristic equation of the system can be written in the following form

$$C_np^n + C_{n-1}p^{n-1} + \ldots\ldots + C_o = 0 \qquad (V.10)$$

For all the roots of the characteristic equation to be in the L.H. p-plane, it is necessary that all the coefficients C_n , C_{n-1} ..... C_o must be positive. But this condition is not sufficient. To meet the necessary and sufficient conditions the coefficients of the characteristic equation are arranged in the following array.

p^n	C_n	C_{n-2}	C_{n-4}	....	....
p^{n-1}	C_{n-1}	C_{n-3}	C_{n-5}	....	.....

The coefficients of the third row are obtained by cross multiplication as follows:

$$p^{n-2} \qquad \frac{C_{n-1}.C_{n-2}-C_nC_{n-3}}{C_{n-1}} \quad \frac{C_{n-1}.C_{n-4}-C_n.C_{n-5}}{C_{n-1}} \quad \ldots$$

The coefficients of the fourth row are obtained again by cross multiplication, using the second and third row and so forth until $n+1$ rows are obtained.

The number of changes in sign of the coefficients in the first column of the above array is equal to the roots of the characteristic equation in the R.H. p-plane, i.e., the roots with positive real parts. For a third

order system the Routh array becomes:

$$\begin{array}{lll} p^3 : & C_3 & C_1 \\ p^2 : & C_2 & C_o \\ p^1 : & \dfrac{C_2C_1 - C_3C_o}{C_2} & 0 \\ p^o : & C_o & 0 \end{array} \qquad (V.11)$$

This leads to the conditions of Eqn. (2.33).

If in the Routh array all the coefficients in a row are zero, this indicates that there are two equal and opposite roots, in particular, two imaginary conjugate roots. For a third order system to have purely imaginary conjugate roots coefficients in the p^1 row of array (V.11) must be zero. This leads to the following condition

$$C_2C_1 - C_3C_o = 0 \qquad (V.12)$$

The imaginary conjugate roots determine the natural frequency of the closed-loop system. The oscillatory mode is determined from an auxiliary equation established from the coefficients of a row just above the zero

coefficient row. For a third order system the auxiliary equation is

$$C_2 p^2 + C_o = 0 \qquad (V.13)$$

This technique is used in Sect. 2.3.3 for finding the natural frequency of the closed-loop system.

V.2.2 Graphical form

In the characteristic equation (V.10) some of the coefficients C_n , C_{n-1} , contain the gain constant term R . This makes the Routh stability coefficients dependent on the gain R . For stability at any gain level R all the Routh stability coefficients must be positive. If the Routh stability coefficients are plotted against the gain R , the stable and unstable zones can easily be demarcated. Fig. 2.10 shows such plots, see Sect. 2.3.4.

V.3 Nyquist Criterion

The Nyquist criterion uses an open-loop frequency response plot to determine the stability of the close-loop. It states that the closed-loop system is stable, if its open-loop frequency response locus encloses the

$(-1,0)$ point counter clockwise a number of times equal to the unstable poles of the open-loop transfer function.

The above criterion stems from the consideration that if a closed curve C in Fig. V.4 which consists of: (a) a line parallel to the $j\omega$-axis and at infinitesimal distance to the right of it, (b) a semicircle of infinite radius in the right hand plane is traced clockwise and a corresponding locus plotted on a complex plane of a function $F(p)$, the $F(j\omega)$ locus can be shown to encircle the $(0,0)$ point as many number of times clockwise as there are roots of $F(p) = 0$ in the R.H. p-plane. This concept is extended to a general transfer function $\frac{N(p)}{D(p)}$. If it has Z zeros and P poles in the R.H. p-plane then the locus $\frac{N(j\omega)}{D(j\omega)}$ will encircle the $(0,0)$ point counter clockwise $(P-z)$ times. This concept when extended to $1 + \frac{N(j\omega)}{D(j\omega)}$ leads to the closed-loop stability criterion mentioned above.

Table No.1

The Direct-axis Regulation Machine Parameters[1]

The michro-machine stator NO 334818

The michro-machine rotor NO 334828

Machine Rating	2KVA	
Unit Voltampere	1825VA	
Unit Voltage	186V (Line to line)	
Unit Current	5.66A	
Parameter	Parameter value	Remarks
X_d	2.321 p.u.	All the machine parameters include X_c
X_q	1.91 p.u.	
T'_{do}	4.75 sec.	
X'_d	0.544 p.u.	
T'_d	1.11 sec.	
X_c	.321 p.u.	
X_a	.431 p.u.	
r_a	0.0384 p.u.	
r_{fd}	0.001425 p.u.	
J	0.0318 p.u.	

Since damping is neglected in the computations, therefore, all such parameters as a consequence of damping are not included in the table above.

Table No. II

The Quadrature-axis Regulation Machine Parameters

The micro-machine stator NO 334818

The micro-machine rotor NO 334835

Machine Rating 2KVA

Unit Voltampere 1825VA

Unit Voltage 186V (Line to line)

Unit Current 5.66A

P.U. Quadrature field voltage - 646 volts

P.U. Quadrature field impedance - 418 ohms

Parameter	Parameter value	Remarks
X_d	2.471 p.u.	measured from equilibrium diagrams at 0,2 p.u. power over a range of vars
X_q	1.93 p.u.	
X'_d	0.91 p.u.	measured from variable frequency response static impedance test
X'_q	0.615 p.u	
T'_{do}	1.2 sec.	measured from sudden short circuit of the field winding, with alternator open-circuited
T'_{qo}	1.1 sec.	
T'_d	.442 sec.	calculated from T'_{do} and X'_d
T'_q	.35 sec.	calculated from T'_{qo} and X'_q
r_{fq}	.00482 p.u.	d.c. measurement

All the machine parameters include X_c.

X_c, X_a, r_a are the same as in table 1.

The system inertia J is also the same as in table 1, because the major part of inertia is contributed

by the flywheel and interchange of similar rotors is considered not to affect it.

REFERENCES

1. Jacovides, L.J., Adkins, B.: Effect of Excitation Regulation on Synchronous Machine Stability, Proc. IEE, 1966, 113, (6), p.1021.

2. Kron, G.: A Super Regulator, Matrix and Tensor Quarterly, 1955, 5, p.71.

3. Aldred, A.S., and Shackshaft, G.: The Effect of Voltage Regulator on the Steady State and Transient Stability of Synchronous Generator, Proc. IEE, 1958, 105A, p.420.

4. Aldred, A.S., and Shackshaft, G.: A Frequency Response Method for the Predetermination of Synchronous Machine Stability, ibid., 1960, 107C, p.2.

5. Gove, R.M.: Geometric Construction of Stability Limits of Synchronous Machines, ibid., 1965, 112 (5), p.977.

6. Messerle, H.K., and Bruck, R.W.: Steady State Stability of Synchronous Generators as affected by Regulators and Governors, ibid., 1956, 103(c), p.24.

7. Concordia, C.: Steady State Stability of Synchronous Machine as affected by Voltage Regulator Characteristics, Trans. A.I.E.E., 1944, 63, p.215.

8. Venikov, V.A., and Litkens, I.V.: Experimental and Analytical Investigation of Power System Stability with Automatically Regulated Generator Excitation, C I G R E , 1956, paper 324.

9. Stapleton, C.A.: Root-Locus Study of Synchronous Machines Regulation, Proc. IEE, 1964, III, (4), p.761.

10. Concordia, C.: Steady State Stability of Synchronous Machine as affected by Angle Regulator Characteristics, Trans. A.I.E.E., 1948, 67, p.687.

11. Hamdi-Sepen, C.: Process for Increasing the Transient Stability Power Limits on A.C. Transmission Systems, CIGRE, 1962, Paper 305.

12. Nicholson, H.: Integrated Control of Non-linear Turbo-alternator Model Under Fault conditions, Proc. IEE, 1967, 114 (6), p.834.

13. Soper, J.A.: A Method of Improving the Stability and Reactive Capability of Alternators and Motors, Research Report No. 14/65.

14. Laughton, M.A.: Matrix Analysis of Dynamic Stability in Synchronous Multi-machine System, Proc. IEE, 1966, 113 (2), p.325.

15. Dromey, G.: Turbogenerator Control System Analysis and Synthesis Using a Digital Computer, Ph.D. Thesis, Welsh College of Advanced Technology, July 1966.

16. Adkins, B.: The General Theory of Electrical Machines (book), Chapman and Hall, London, 1957.

17. Crary, S.B.: Power System Stability Vol. II (book), John Wiley, N.Y., 1947.

18. Gille, J.C.: Pelegrin, M.J. and Decaulne P.: Control Systems Engineering (book), McGraw-Hill, N.Y., 1959.

19. Truxal, J.C.: Automatic Control System Synthesis (book), McGraw-Hill, N.Y., 1955.

20. Brown, G. and Campbell, D.: Principle of Servo-mechanism (book), John Wiley, N.Y. 1948.

21. Bharali, P., and Adkins, B.: Operational Impedance of Turbogenerator with Solid Rotors, Proc. IEE, 1963, 110, p.2185

22. Jacovides, L.J.: The Effect of Regulation of Excitation on the Stability of Synchronous Machines, Ph.D. thesis, University of London, 1965.

23. A.I.E.E. Test Code for Synchronous Machines, A.I.E.E. Publication No. 503, June 1945.

24. Alford, R.J.: The Micro-machine Exciter System and Time Constant Regulator, Imperial College, London, Department of Elect. Engg., Power Systems Report No. 49, Nov. 1963.

25. Robert, R.: Micro-Machine and Micro Research Study of Problems of Transient Stability by use of Models Similar Electromechanically to Existing Machines and Systems CIGRE 1950, paper 338.

26. Moe Wind, (Editor): Handbook of Electronic Measurements Vol. II (book), 1959, Polytechnique Institute of Brooklyn Publication, N.Y., p.1-48.

27. Terman and Pettit: Electronic Measurements (book), 1952, McGraw--Hill, N.Y., p.273.

28. U.S. Department of Army: Basic Theory and Application of Transistors (book), 1959, Dover Publication, N.Y., p.133.

29. Fifer, S.: Analogue Computation Vol. II (book), 1961 McGraw-Hill, N.Y., p.493.

30. Blackman, P.F.: The Pole-Zero Approach to Systems Analysis, Morgan Brothers (Publishers) Ltd.

31. Korn and Korn: Electronic Analogue and Hybrid Computers (book), 1964, McGraw-Hill, N.Y., p I-16.

32. Zadeh, L.A. and Desoer, C.A.: Linear System Theory (book), McGraw-Hill, N.Y., 1963.

33. Gupta, C.S.: Transform and State Variable Methods in Linear Systems (book), John Wiley, N.Y., 1966.

34. Mac-Farlane, A .G.J.: Engineering System Analysis (book), George G. Harrap, London, 1964.

35. Park, P.C.: A New Proof of the Routh-Horwitz Stability Criterion using Second Method of Lyapunov, Proc. Camb. Phil. Soc., 1962, 58, pt. IV, p.694.

36. Fallside, F. and Patel, M.R.: On the Application of the Lyapunov Method to Synchronous Machine Stability, Int. J. Control, 1966, 4, (6), p.501.

37. Gless, G.E.: Direct Method of Lyapunov Applied to transient Power System Stability, Trans. A.I.E.E., 1966, 58, pt.3, p.159.

38. El. Abiad, A.H., and Naggapan, K.: Transient Stability regions of Multimachine Power System, ibid, p.169.